To the Graduate Council:

I am submitting herewith a dissertation written by Bruce W. McNeill entitled "Methods and Formulas for Determining the Integral Nonlinearity of Solid-State Amplifiers." I recommend that it be accepted in partial fulfillment of the requirements for the degree of Doctor of Philosophy, with a major in Electrical Engineering.

J. Frank Pierce

J. Frank Pierce, Major Professor

We have this dissertation
and recommend its acceptance:

James C. Hung

T. V. Blalock

N. C. Simpson

Accepted for the Council:

L. Evans Roth

Vice Chancellor
Graduate Studies and Research

METHODS AND FORMULAS FOR DETERMINING THE INTEGRAL NONLINEARITY OF SOLID-STATE AMPLIFIERS

A Dissertation

Presented for the

Doctor of Philosophy

Degree

The University of Tennessee, Knoxville

Bruce W. McNeill

December 1980

DEDICATION

This dissertation is dedicated to Dianne, who suffered greatly with me throughout the entire ordeal.

ACKNOWLEDGEMENTS

The author is indebted to Dr. J. Frank Pierce, the thesis supervisor, for the immense amount of his time and effort that were freely given in the development of this work.

The author would also like to thank Dr. J.C. Hung and Dr. T.V. Blalock for their encouragement and fatherly advice during the course of the study. Special thanks are due to James Barnes and Lendon L. Adkins for helping to secure vital parts that were needed in the test arrangements used in this work.

ABSTRACT

Analytical and computer simulation techniques were developed in this study to determine the integral nonlinearity of solid-state amplifiers. The three analytical techniques developed include an exact analysis and two approximations. Each of the three techniques was used to evaluate the integral nonlinearity of several single-stage bipolar transistor and JFET amplifiers. In evaluating the nonlinearity of these single-stage amplifiers, the exact analysis proved to be cumbersome and produced results that were difficult to evaluate. The two approximations were less cumbersome and produced results that were easier to evaluate. One of the two approximations was particularly accurate and predicted values of nonlinearity that were nearly equal, over large dynamic ranges, to the values of nonlinearity determined by the exact analysis.

Two computer simulation techniques were developed for determining the closed-loop nonlinearity for nonperiodic signals in negative feedback amplifiers with memory. Both of these techniques use computer time efficiently. One of the two computer techniques linearizes the feedback loop which allows closed-loop nonlinearity to be evaluated analytically. This linearized model can be used to empirically understand closed-loop linearity performance. The other simulation technique is slightly more accurate. Both of the simulation techniques use first-order approximations and the accuracy of these models depends on the magnitude of the nonlinearity. The fractional value of the error in simulating the

nonlinearity is generally less than the fractional value of the open-loop nonlinearity.

The computer simulation techniques were used to find the integral nonlinearity of several negative feedback amplifiers, each of which had an integrating element in the forward plant. This type of feedback amplifier closely approximates most operational amplifiers. The results of several simulations indicate that the closed-loop nonlinearity at the output of such feedback amplifiers is differentiated with respect to time. For spectroscopy type pulses, the nonlinearity is going through zero at approximately the time that the pulse peaks.

TABLE OF CONTENTS

LIST OF TABLES

TABLE PAGE

TABLE PAGE

LIST OF FIGURES

FIGURE PAGE

FIGURE PAGE

CHAPTER I

INTRODUCTION, BACKGROUND, AND OUTLINE TO DISSERTATION

I. INTRODUCTION

An imperfection inherent in all solid-state amplifiers is nonlinearity. This imperfection can be quantified by parameters such as total harmonic distortion, integral nonlinearity, or differential nonlinearity. Integral nonlinearity is a time-domain measurement of nonlinearity. This quantity is different from total harmonic distortion which is a frequency-domain analysis. Total harmonic distortion is generally used to quantify the nonlinearity of instruments whose signals may be approximated by sinusoids, such as in audio or communications equipment. Integral nonlinearity is generally used to quantify the nonlinearity produced in instruments with nonsinusoidal signals, such as pulse amplifiers or linear sweeps. In this study, the integral nonlinearity of linear solid-state amplifiers is investigated.

Although strongly related, total harmonic distortion and integral nonlinearity are not the same. When comparing two amplifiers, the amplifier with the smallest value of harmonic distortion may or may not have the smallest value of integral nonlinearity.

Many works have been published on the total harmonic distortion of amplifiers, and the analysis is quite advanced. Very little material has been published on the integral nonlinearity of solid-state amplifiers.

The major objective of this dissertation is to develop methods that can be used to predict the integral-nonlinearity performance of solid-state amplifiers. Among the tools developed are: 1) procedures for calculating the integral nonlinearity of arbitrary functions, 2) tables of the nonlinear parameters of polynomial functions, 3) definition of and techniques used to predict the spectral effects on the nonlinearity of pulses, and 4) methods for predicting the integral nonlinearity of negative feedback amplifiers. Both analytical and computer simulation techniques for determining integral nonlinearity are included in this study. While this analysis is particularly useful to designers of pulse spectroscopy instruments, much of the work is applicable to related areas.

A secondary objective of this work is to generate useful formulas that may be applied to the determination of the nonlinearity of solid-state amplifiers. Therefore, the techniques developed in this study are applied in detail to a few major sources of nonlinearity of some single-stage solid-state amplifiers. By investigating a few sources in detail, the relative merits of related techniques can be compared. These results are carefully tabulated for easy reference.

II. BACKGROUND

The majority of background material given here is not on the integral nonlinearity of solid-state amplifiers but is from related areas. Little information on the integral nonlinearity of amplifiers is available in the literature.

Integral Nonlinearity of Solid-State Amplifiers

The integral nonlinearity of an emitter-follower amplifier in a feedback loop is evaluated in the appendix of a paper by B. Gilbert [1]. The source of nonlinearity considered is the exponential characteristic of the base-emitter diode junction of the device. Rather than make a Taylor series expansion to approximate the nonlinearity of the amplifier, the nonlinearity is evaluated using the transcendental function of the base-emitter junction. However, the results that Gilbert obtains are highly specialized and cannot be applied easily to a more general case. This paper was the only one the author found in the literature which specifically treats the integral nonlinearity of a solid-state amplifier.

Nonlinearity of Linear Sweeps

The nonlinearity of linear sweeps is generally quantified by integral nonlinearity. A representative work by Nambiar and Boothroyd evaluates the nonlinearity of a linear voltage sweep with bootstrap feedback [2]. The approach used to evaluate the integral nonlinearity of the circuit was to take the Maclaurin series expansion of the RC exponential charging curve. The nonlinearity was then estimated to be due to the second-order term alone since higher order terms are generally much smaller for a nearly linear voltage sweep.

The design of a voltage-to-frequency converter by Shapiro combined a linear ramp circuit, which consisted of a capacitor in the feedback loop of an operational amplifier, with a comparator driving a reset circuit [3]. The nonlinearity found at low frequencies is due mainly to the finite RC time constant of the exponential charging curve. This nonlinearity is evaluated with the same technique used in the paper by Nambiar and Boothroyd. Shapiro also includes the nonlinearity at high frequencies of the voltage-to-frequency converter due to the finite time delay through the amplifier.

Harmonic Distortion of Solid-State Amplifiers

The majority of information on the nonlinearity of solid-state amplifiers uses harmonic distortion analysis.

A classical work on the distortion of bipolar transistor amplifiers was written by D.R. Fewer [4]. Using the Ebers-Moll model for the bipolar transistor, Fewer evaluates the distortion of a common-emitter amplifier due to the nonlinear exponential relation between the base-to-emitter voltage and the emitter current of the transistor. In addition, Fewer analyzes the nonlinearity due to the variation of the current gain of the transistor with collector current. These two distortions are complementary, and Fewer indicates that with proper design, the second harmonics of these two distortions will cancel. The topic of distortion reduction by complementary distortion itself is covered by J.R. MacDonald [5,6].

Other articles have appeared which have some improvements of the Ebers-Moll model such that the low-frequency distortion of the bipolar transistor could be more accurately calculated. A second article by Fewer [7] evaluates the nonlinearity due to the drop in emitter efficiency at higher current levels (the Webster effect). An article by G.M. Riva, P.J. Beneteau, the E.D. Volta [8] evaluates the nonlinearity due to avalanching in the break-down region of the transistor. Also introduced in this article is an important empirical equation which relates current gain to collector current.

Other work on harmonic distortion includes the calculation of intermodulation distortion using the Volterra-series approach [9,10,11]. This topic is not important for time-domain analysis.

Bipolar Transistor Modeling

In addition to the Ebers-Moll model of the bipolar transistor, a charge-control model of the transistor was introduced by R. Beaufoy, and J.J. Sparkes [12]. This model of the bipolar transistor is compared to the Ebers-Moll model in a paper written by D.J. Hamilton, F.A. Lindholm and J.A. Narud [13]. According to their comparison, the charge-control model gives the same numerical results as the Ebers-Moll model, but the Ebers-Moll model is more convenient to use for analytical work. These two models of the bipolar transistor are united in an integral charge control model in a paper presented by H.K. Gummel and H.C. Poon [14]. This model uses 21 different parameters and is suitable for computer simulations. This particular model is referenced often in current literature, and has apparently found wide acceptance.

JFET Modeling

The analytical modeling of the JFET does not seem as accurate as that of the bipolar transistor. Despite numerous articles on the physics of the operation of the JFET, this author did not find any improvement over the empirical, square-law approximation of the low-frequency characteristics of the device. This square-law model of the JFET is introduced in a pair of letters to the IEEE Proceedings from I. Richer and R.D. Middlebrook [15,16].

Two early landmark papers on the field-effect transistor are W. Shockley's article [17], and G.C. Dacey and I.M. Ross's work [18]. Shockley introduces his invention of the junction field-effect transistor in his paper and gives an approximation of the anticipated characteristics of the device. Dacey and Ross improve on Shockley's model by including the dependence of the mobility of the carriers on the electric field intensity. In both of these papers, the depletion approximation for the junction diode is used. The channel of the JFET is "pinched off," or totally void of carriers, when the drain current reaches its maximum value. This condition is a contradiction of the physics used in the modeling. Despite the approximations used in these two papers and the apparent contradiction in the physics, the analytical expressions derived in these papers are still used in the literature today to approximate the JFET equations.

Certain refinements of the analytical JFET model have been proposed in a paper by A.B. Grebene and S.K. Ghandhi [19] and also by K. Lehovec and R. Zuleeg [20]. Grebene and Ghandhi propose a small undepleted channel in the center of the JFET to account for the saturation current of the device. Lehovec and Zuleeg combine this model with an equation describing the drift velocity of the carriers in the channel as a function of the electric field. In both of these papers, the analysis is used to predict the small-signal parameters of the device as functions of the geometrical and physical device parameters. The analytical expressions derived in these two papers are not useful for large signal analysis of the JFET.

In a recent letter to the IEEE Journal of Solid State Circuits, T. Taki introduces an empirical large-signal model of the JFET [21]. This model is a modification of the square-law model, and represents the drain current as a hyperbolic tangent function of the drain-to-source voltage. This author was not able to match accurately this empirical model to the devices that were used in this study.

An important work in understanding the operation of the JFET is the "Computer Aided Two-Dimensional Analysis of the Junction Field-Effect Transistor" given by D.P. Kennedy, and R.R. O'Brien [22]. In this often-referenced paper, Kennedy and O'Brien solved the boundary value problems of the two dimensional JFET using the six basic field equations and a finite differences analysis method on a digital computer. The carrier distributions, electron flux distributions, and electrostatic charge distributions were analyzed for wide, narrow, and very narrow-gate devices. The results are given in two-dimensional graphical form intended for empirical understanding of the physics of the device. No analytical equations are given in this paper.

Reduction of Nonlinearity with Negative Feedback

In H.S. Black's 1934 paper describing his invention, the negative feedback electronic amplier, Black found it "possible to effect extraordinary improvement in ... freedom from non-linearity" [23]. Experimental data included in this paper showed that harmonic distortion was reduced by a factor nearly equal to the magnitude of the loop transmission of the amplifier. C.A. Desoer lists several references in which the authors show that the midband distortion in a negative feedback amplifier is reduced by a factor approximately equal to the loop transmission plus one [24].

A much more detailed analysis of the harmonic distortion of negative feedback amplifiers is given by Ketchledge [25]. In this detailed analysis, distortion is analyzed for the case where the magnitude and phase of the loop transmission varies with frequency. Included in this analysis is the mixing of harmonic frequencies which are fedback to the summing junction with the input signal; this action generates higher-frequency harmonics.

G. Zames describes a technique for giving an upper bound on the nonlinearity of a band-limited signal using functional analysis [26]. An iterative technique is used to solve for the system response to the input signal. This technique can be applied to nonsinusoidal signals and there are no restrictions on the magnitude of the nonlinearities. The analysis is very advanced.

III. OUTLINE OF DISSERTATION

CHAPTER II contains the basic definitions, properties, and equations of integral nonlinearity which are used in the remainder of this study.

Several definitions of integral nonlinearity are found in the literature. A few definitions are given in Strauss [27], and these same definitions are repeated in Millman and Taub [28].

The definition of integral nonlinearity used in this study is one taken from these two references, and this definition is given in CHAPTER II. From this definition of integral nonlinearity, a procedure is developed for calculating the integral nonlinearity of any function which has a monotonic first derivative. This procedure is used for calculating the integral nonlinearity of bipolar transistor amplifiers in CHAPTER III, and for calculating the integral nonlinearity of JFET amplifiers in CHAPTER IV.

Normalized nonlinearities from several sources may be summed to approximate the total nonlinearity of an instrument. The justification of this property is given in CHAPTER II.

A Taylor series expansion of a complex function may be used to obtain a quick approximation of the nonlinearity of that function. Therefore, important nonlinearity parameters such as integral gain, point at which maximum deviation occurs, and integral nonlinearity are derived for two-term polynomial functions of arbitrary order. Results for the second-order polynomial and the third-order polynomial cases are summarized in tables for easy reference.

In the last section of CHAPTER II, the closed-loop nonlinearity is shown to be approximately equal to the open-loop nonlinearity of the instrument divided by the loop transmission plus one. An important finding of this derivation is that the loop transmission of the nonlinear feedback system should be calculated from the integral gain of the system rather than from the small-signal gain.

In CHAPTER III, nonlinearities due to the exponential characteristic of the base-emitter junction of the bipolar transistor are examined in detail. The nonlinearity of several single-stage amplifier configurations are evaluated from their transcendental functions rather than Taylor series expansions of these functions. The results from these analyses are accurate over large dynamic ranges. Important parameters such as integral gain and normalized nonlinearity are tabulated in this chapter for easy reference. Extensive test measurements are used to verify the accuracy of the analysis.

In addition to the more exact analysis, the exponential nonlinearity of the bipolar transistor amplifiers is approximated from two-term polynomial expansions of their transcendental functions. These polynomial approximations are easier to evaluate than the more exact analysis and are useful for comparing nonlinearities of different functions.

The nonlinearity due to variations of the DC current gain of a bipolar transistor is approximated for the common-emitter amplifier configuration. This approximation uses a Taylor series expansion of an empirical formula that relates DC current gain to the collector current of a bipolar transistor.

In CHAPTER IV, the nonlinearities of several single-stage JFET amplifier configurations are examined in detail. The square-law approximation of the low-frequency transfer function of the JFET is used for this analysis. The results of the nonlinearity analysis are tabulated for several single-stage amplifier configurations, and extensive tests are used to verify the accuracy of this analysis. Simpler, but less accurate, expressions of the nonlinearity parameters are derived from two-term polynomial approximations of the more exact transfer functions.

The low-frequency nonlinearities of similar type amplifier stages are compared in CHAPTER V.

The nonlinearity of a pulse changes when the pulse passes through a frequency-dependent transfer function. In CHAPTER VI, a procedure for calculating the magnitude of the change in nonlinearity is given for second-order and third-order two-term polynomial nonlinearities. This procedure is illustrated with three example waveforms. A computer simulation technique is detailed for finding the change in the magnitude of the nonlinearity of a pulse due to these spectral changes. This simulation technique may be used for pulses with more complex nonlinearities than two-term polynomials. Simulation results are compared to the hand analysis results for the three example waveforms.

A technique is presented for estimating the change in nonlinearity of a pulse which has complex nonlinearities by using the results from the two-term polynomial hand analysis. The accuracy of this technique is verified by computer simulations.

In CHAPTER VII, two computer models are given which are used to find the closed-loop nonlinearity of a feedback system with memory. These two computer models give the nonlinearity of a system as a function of time. One of these two models is used to simulate the closed-loop nonlinearity of some example nonlinear systems. Loop transmission and phase margin of the systems are varied to determine their effects on the nonlinearity.

CHAPTER II

BASIC DEFINITIONS AND EQUATIONS

I. INTRODUCTION

This chapter provides reference materials which are to be used throughout the remainder of this dissertation. First, the definition of integral nonlinearity that is used in this dissertation is introduced. Next, the justification that normalized nonlinearities from several sources may be summed to approximate the normalized nonlinearity of the complete system is given. Formulas for the nonlinearity of two-term polynomial functions are derived, and a formula to approximate the nonlinearity of a polynomial function with more than two terms is derived. Finally, the closed-loop normalized nonlinearity of a negative feedback amplifier at midband is shown to be approximately equal to the open-loop normalized nonlinearity divided by the loop transmission plus one.

II. DEFINITION OF INTEGRAL NONLINEARITY

Although there are several different definitions of integral nonlinearity, only one definition is used in this thesis, and this definition is illustrated in Figure 2.1. This method for defining integral nonlinearity is the IEEE standard for nuclear instrumentation [29] and has been used to characterize the integral nonlinearlity of linear ramps [27], digital-to-analog converters

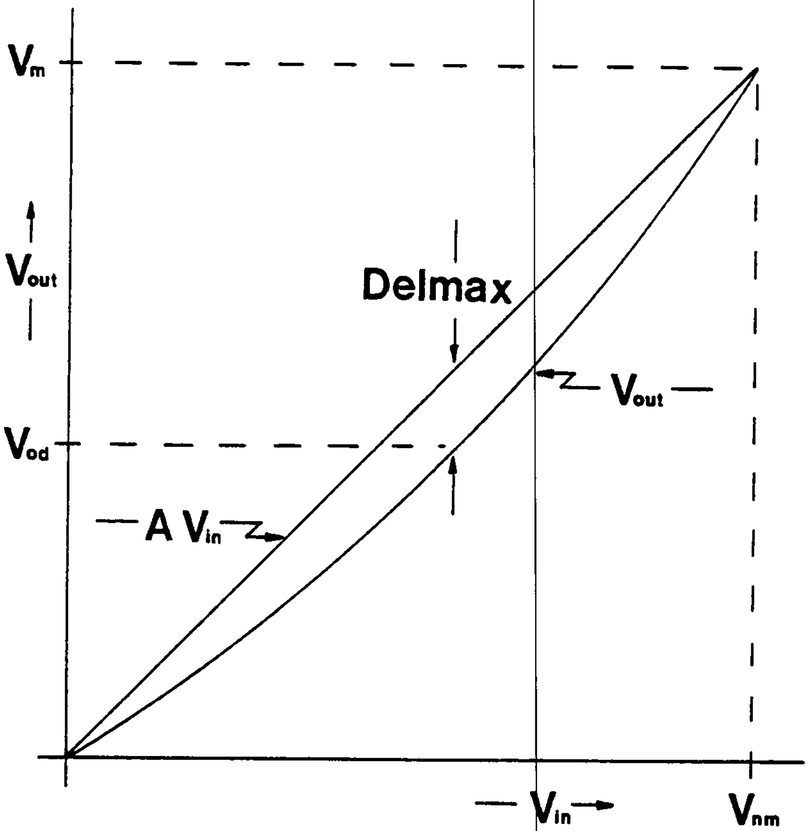

Figure 2.1. Curve illustrating the integral gain, A, of a nonlinear function, and showing the maximum deviation, Delmax, occurring at an output, V_{od}.

[30], and voltage-to-frequency converters [11]. The full-scale value of the transfer function intersects the ideal linear curve, a straight line from the origin, as shown in Figure 2.1. The maximum deviation of the nonlinear function from this straight line is the integral nonlinearity. This number is generally normalized by dividing it by the full-scale output.

The nonlinear function shown in Figure 2.1 has a monotonically increasing slope. For this case, the nonlinear-function curve always lies below the integral-gain curve (except at the end points), and the deviation from the integral-gain curve has a positive value. If a nonlinear function has a monotonically decreasing slope, then the nonlinear-function curve always lies above the integral-gain curve (except at the end points), and the deviation from the integral-gain curve has a negative value. When a function has neither a monotonically increasing nor monotonically decreasing slope, then the nonlinear-function curve may lie both above and below the integral-gain curve. For this case, the nonlinearity is determined by the deviation with the greatest magnitude.

III. PROCEDURE FOR CALCULATING NONLINEARITY WHERE THE INPUT IS REPRESENTED AS A FUNCTION OF THE OUTPUT

The procedure for finding the integral nonlinearity used in this study requires that the input must be given as a function of the output. The reason for choosing this procedure is that the input voltage of certain single-stage bipolar transistor amplifiers can be determined as a function of the output voltage, but the output can not be given as a function of the input in a closed form.

This procedure for calculating integral nonlinearity is based on Figure 2.1. A given maximum output, V_m, has a corresponding maximum input, V_{nm}. The integral gain is defined by

$$A \equiv V_m/V_{nm}. \tag{2.1}$$

The difference, Del, between the linear curve and the actual output is then

$$\mathrm{Del} = A \cdot V_{in} - V_{out}, \tag{2.2}$$

where V_{in} is the input and V_{out} is the output. If V_{in} is expressed as a function of V_{out}, the output at which the variation is a maximum, V_{od}, can be obtained by setting the derivative of Equation (2.2) with respect to V_{out},

$$\frac{d\mathrm{Del}}{dV_{out}} = A \cdot \frac{dV_{in}(V_{out})}{dV_{out}} - 1, \tag{2.3}$$

equal to zero. The normalized integral nonlinearity, NL, is then

$$\mathrm{NL} = \frac{A \cdot V_{in}(V_{od}) - V_{od}}{V_m}. \tag{2.4}$$

This process is conceptually simple enough, but the algebra involved is generally awkward.

IV. SUMMING NONLINEARITIES FROM SEVERAL SOURCES

The total normalized nonlinearity of a system consisting of two cascaded nonlinear stages is approximately the sum of the normlaized nonlinearities of the individual stages. This property is justified in this section with the help of Figure 2.2.

With an input, V_{in}, the output of the first stage is

$$V_{out1} = A \cdot V_{in} + Del_1 \tag{2.5}$$

where A is the integral gain of the first stage, and Del_1 is the nonlinear variation from that integral gain. The output of the second stage is

$$V_{out2} = B \cdot (A \cdot V_{in} + Del_1) + Del_2 \tag{2.6}$$

where B is the integral gain of the second stage, and Del_2 is the nonlinear deviation of the second stage from its integral gain. When the input voltage is at the maximum value, V_{nm}, the two deviations, Del_1 and Del_2, are zero and the full-scale output of the first and second stages are $A \cdot V_{nm}$, and $A \cdot B \cdot V_{nm}$ respectively.

If the deviations of the first and second stages are approximately equal to their maximum values when the peak deviation of the total system occurs, the normalized nonlinearity of the total system is approximately

$$NL_{total} \cong \frac{B \cdot Delmax_1 + Delmax_2}{A \cdot B \cdot V_{nm}}, \tag{2.7}$$

where $Delmax_1$ is the maximum deviation of the first stage, and $Delmax_2$ is the maximum deviation of the second stage. The normalized nonlinearity of the first stage is

$$NL_1 = \frac{Delmax_1}{A \cdot V_{nm}}, \tag{2.8}$$

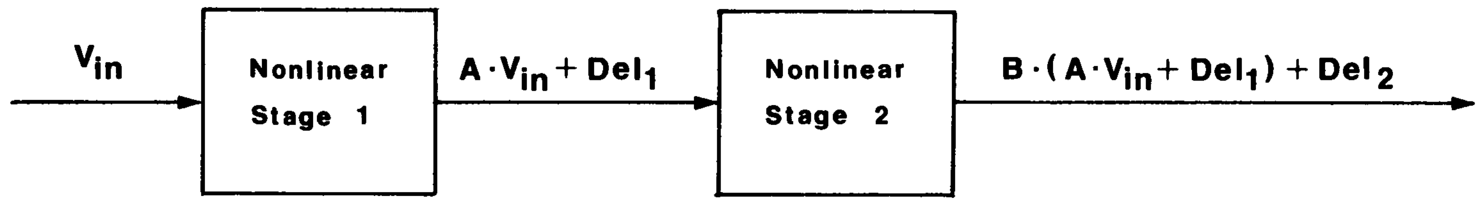

Figure 2.2. Block diagram of two cascaded nonlinear stages used to illustrate that the normalized nonlinearities of cased stages may be summed to approximate the total normalized nonlinearity of the complete system.

and the normalized nonlinearity of the second stage is

$$NL_2 = \frac{Delmax_2}{A \cdot B \cdot V_{nm}}. \tag{2.9}$$

Combining Equations (2.7), (2.8), and (2.9) gives the justification to

$$NL_{total} \cong NL_1 + NL_2. \tag{2.10}$$

This procedure is easily extended to show that the normalized nonlinearities of several cascaded nonlinear stages may be summed to approximate the total normalized nonlinearity of the complete system.

V. NONLINEARITY OF A TWO-TERM POLYNOMIAL

With the Output Represented as a Function of the Input

The integral nonlinearity of a system is evaluated in this section using a two-term polynomial approximation for the nonlinear function. This polynomial can be obtained from a Taylor series expansion of the nonlinear function,

$$V_{out}(V_{in}) = a_1 V_{in} + a_2 V_{in}^{\ 2} + a_3 V_{in}^{\ 3} + \ldots \tag{2.11}$$

The constant term, a_o, has been ommitted in the above expansion since constant offset values are generally considered separately from other nonlinear terms. Taking the linear term, and the lowest order, nonzero, nonlinear term of the Taylor expansion gives the two-term polynomial

$$V_{out}(Vin) \cong a_1 V_{in} + a_n V_{in}^{\ n} \tag{2.12}$$

to approximate the nonlinear function. The integral gain and integral nonlinearity of a function can be represented as functions of the peak input and the coefficients a_1 and a_n by using this approximation.

The integral nonlinearity of the polynomial can be evaluated using Figure 2.1. The definition of the integral gain of the function is

$$A \equiv V_m / V_{nm} \tag{2.13}$$

where V_m is the maximum output, and V_{nm} is the maximum input. This gain is

$$A = a_1 + a_n V_{nm}^{(n-1)} \tag{2.14}$$

for the nonlinear function described by Equation (2.12). The function deviation, Del, from this integral gain curve is

$$\text{Del} = A \cdot V_{in} - (a_1 V_{in} + a_n V_{in}^{\;n}). \tag{2.15}$$

Setting the derivative of Del with respect to V_{in} equal to zero gives the input at which the maximum deviation occurs,

$$V_{in}\Big|_{\text{Delmax}} = V_{nm}\, n^{\left(\frac{1}{1-n}\right)}, \tag{2.16}$$

and placing this value of input into Equation (2.15) gives the maximum deviation,

$$\text{Delmax} = a_n V_{nm}^{\;n}\,(n-1)\, n^{\left(\frac{n}{1-n}\right)}. \tag{2.17}$$

The normalized nonlinearity of the system, which is the peak deviation divided by the maximum output, is then

$$NL = \frac{a_n V_{nm}^{(n-1)}}{(a_1 + a_n V_{nm}^{(n-1)})} (n-1)\, n^{\left(\frac{n}{1-n}\right)} . \tag{2.18}$$

The nonlinearity expression given in Equation (2.18) is a function of the input. This expression can be used to give an approximation of the nonlinearity as a function of the output. First, Equation (2.18) must be rewritten in the form

$$NL = \frac{a_n V_m^{(n-1)}}{A^n} (n-1)\, n^{\left(\frac{n}{1-n}\right)} . \tag{2.19}$$

Then, by using the approximation

$$A = a_1 + a_n \left(\frac{V_m}{a_1}\right)^{(n-1)} , \tag{2.20}$$

the normalized nonlinearity is approximately

$$NL = \frac{a_n V_m^{(n-1)}}{\left[a_1 + a_n \left(\frac{V_m}{a_1}\right)^{(n-1)}\right]^n} \cdot (n-1)\, n^{\left(\frac{n}{1-n}\right)} . \tag{2.21}$$

With the Input Represented as a Function of the Output

The nonlinearity of a system can also be calculated when the input to the system is represented as a function of the output. The Taylor series expansion of such a function can be written

$$V_{in}(V_{out}) = b_1 V_{out} + b_2 V_{out}^2 + b_3 V_{out}^3 \cdot \cdot \cdot . \tag{2.22}$$

This function may then be approximated by the two-term polynomial

$$V_{in}(V_{out}) \tilde{=} b_1 V_{out} + b_n V_{out}{}^n \tag{2.23}$$

where b_n is the lowest order, nonzero coefficient of the nonlinear terms.

The integral gain of the nonlinear function is

$$A = \frac{1}{b_1 + b_n V_m{}^{(n-1)}}, \tag{2.24}$$

and the function's deviation, Del, from this integral gain is given by

$$\text{Del} = A(b_1 V_{out} + b_n V_{out}{}^n) - V_{out}. \tag{2.25}$$

The output for which the above deviation is maximum is given by

$$V_{out}\Big|_{\text{Delmax}} = V_m \, n^{\left(\frac{1}{1-n}\right)}, \tag{2.26}$$

and the magnitude of this deviation is

$$\text{Delmax} = \frac{b_n V_m{}^n \, (1-n) \, n^{\left(\frac{1}{1-n}\right)}}{b_1 + b_n V_m{}^{(n-1)}}. \tag{2.27}$$

When normalized with the peak value of the output, the nonlinearity is

$$NL = \frac{b_n V_m{}^{(n-1)} \, (1-n) \, n^{\left(\frac{n}{1-n}\right)}}{b_1 + b_n V_m{}^{(n-1)}}. \tag{2.28}$$

The nonlinearity of the function can be estimated from the peak input by using the approximation

$$A \cong \frac{1}{b_1 + b_n \left(\frac{V_{nm}}{b_1}\right)^{n-1}}. \tag{2.29}$$

Then the normalized nonlinearity is approximately

$$NL \cong \frac{b_n V_{nm}^{(n-1)} (1-n)\, n^{\left(\frac{n}{1-n}\right)}}{\left[b_1 + b_n \left(\frac{V_{nm}}{b_1}\right)^{(n-1)}\right]^n}. \tag{2.30}$$

Results for Second-Order and Third-Order Polynomials

The equations developed in this section predicting the nonlinear characteristics of two-term polynomials are given for arbitrary orders of the nonlinear term. However, the second-order and third-order polynomials are by far the most useful. Therefore, the salient points of the nonlinearity analysis are tabulated in this section for these two cases.

The salient points of the analysis are given in Table 2.1 with the output of the nonlinear function represented as a function of the input by Equation (2.12). The input at which the maximum deviation occurs, the integral gain, and the normalized nonlinearity are given as functions of the peak input voltage, V_{nm}. Also included in this table are approximations of the integral gain and normalized nonlinearity as functions of the peak output voltage, V_m.

The salient points of the analysis are given in Table 2.2 for the nonlinear function represented with the input given as a function of the output by Equation (2.23). The output at which the maximum deviation occurs, the integral gain, and the normalized

Table 2.1. Nonlinear characteristics of a two-term polynomial with the output represented as a function of the input for second-order and third-order polynomials.

Characteristic	Second-order $n = 2$	Third-order $n = 3$
Input at which the maximum deviation occurs.	$\frac{V_{nm}}{2}$	$\frac{V_{nm}}{\sqrt{3}}$
Integral gain, A	$a_1 + a_2 V_{nm}$	$a_1 + a_3 V_{nm}^{2}$
Normalized non-linearity, NL	$\frac{a_2 V_{nm}}{4\,(a_1 + a_2 V_{nm})}$	$\frac{3\, V_{nm}^{2}}{\frac{3\sqrt{3}}{2}\,(a_1 + a_3 V_{nm}^{2})}$
Approximate integral gain	$a_1 + a_2 \left(\frac{V_m}{a_1}\right)$	$a_1 + a_3 \left(\frac{V_m}{a_1}\right)^2$
Approximate	$\frac{a_2 V_m}{4 \left[a_1 + a_2 \left(\frac{V_m}{a_1}\right)\right]^2}$	$\frac{a_3 V_m}{\frac{3\sqrt{3}}{2} \left[a_1 + a_3 \left(\frac{V_m}{a_1}\right)^2\right]^3}$

Table 2.2. Nonlinear characteristics of a two-term polynomial with the input represented as a function of the output for second-order and third-order polynomials.

Characteristic	Second-order $n = 2$	Third-order $n = 3$
Output at which the maximum deviation occurs.	$\frac{V_m}{2}$	$\frac{V_m}{\sqrt{3}}$
Integral gain, A	$\frac{1}{b_1 + b_2 V_m}$	$\frac{1}{b_1 + b_3 V_m^2}$
Normalized nonlinearity, NL	$\frac{-b_2 V_m}{4 (b_1 + b_2 V_m)}$	$\frac{-b_3 V_m^2}{\frac{3\sqrt{3}}{2} (b_1 + b_3 V_m^2)}$
Approximate integral gain	$\frac{1}{b_1 + b_2 \left(\frac{V_{nm}}{b_1}\right)}$	$\frac{1}{b_1 + b_3 \left(\frac{V_{nm}}{b_1}\right)^2}$
Approximate normalized nonlinearity	$\frac{-b_n V_{nm}}{4 \left[b_1 + b_2 \left(\frac{V_m}{b_1}\right)\right]^2}$	$\frac{-b_3 V_{nm}^2}{\frac{3\sqrt{3}}{2} \left[b_1 + b_3 \left(\frac{V_{nm}}{b_1}\right)^2\right]^3}$

nonlinearity are given as functions of the peak output voltage V_m. Also included in this table are approximations of the integral gain and normalized nonlinearity as functions of the peak input voltage, V_{nm}.

The formulas given in Tables 2.1 and 2.2 are useful for estimating the nonlinearity of a function for which the Taylor series expansion is known, and when the magnitude of the non-linearity is relatively small. Examples of their application are given in CHAPTER III for several bipolar transistor amplifier configurations, and more examples are given in CHAPTER IV for several JFET amplifier configurations.

VI. MIDPOINT APPROXIMATION APPLIED TO A POLYNOMIAL EXPANSION

The nonlinearity of a polynomial with three or more significant terms may be approximated by applying the midpoint approximation to the polynomial. The midpoint approximation for determining the nonlinearity of a function assumes that the value of the deviation of the function from the integral gain curve is near the peak value of the deviation when the signal is at midscale. For the polynomial given by Equation (2.11) (page 20), the deviation is assumed to be near its maximum value when the input voltage is half of its maximum value, or $V_{nm}/2$. The ratio of the deviation to the peak output voltage for this input level is

$$NL \cong \frac{\sum_{n=2}^{\infty} (\frac{1}{2} - 2^{-n})\ a_n V_{nm}^{(n-1)}}{\sum_{n=1}^{\infty} a_n V_{nm}^{(n-1)}}$$

$$= \frac{\frac{1}{4} a_2 V_{nm} + \frac{3}{8} a_3 V_{nm}^2 + \frac{7}{16} a_4 V_{nm}^3 + \ldots}{a_1 + a_2 V_{nm} + a_3 V_{nm}^2 + \ldots} \tag{2.31}$$

which is an approximation for the normalized nonlinearity of the function.

The second-order two-term polynomial is a special case for the approximation given by Equation (2.31) where all the coefficients of the polynomial are zero except a_1 and a_2. For this case, the normalized nonlinearity from the midpoint approximation is

$$NL = \frac{a_2 V_{nm}}{4\ (a_1 + a_2 V_{nm})} \tag{2.32}$$

which is the same as the results given in Table 2.1 (page 23) for the second-order two-term polynomial. The third-order two-term polynomial is another special case for the approximation given by Equation (2.31); all coefficients of the polynomial are zero except a_1 and a_3. For this case, the normalized nonlinearity from the midpoint approximation is

$$NL = \frac{3}{8} \cdot \frac{a_3 V_{nm}^2}{(a_1 + a_3 V_{nm}^2)}, \tag{2.33}$$

which is within 2.6% of the nonlinearity calculated for the third-order two-term polynomial given in Table 2.1 (page 23).

For the polynomial given by Equation (2.22) (page 20), the deviation is assumed to be near its maximum value when the output voltage is at half the maximum value, or $V_m/2$. The normalized nonlinearity for this polynomial is then approximately

$$NL = \frac{-\sum_{n=2}^{\infty}\left(\frac{1}{2} - 2^{-n}\right) b_n V_m^{(n-1)}}{\sum_{n=1}^{\infty} b_n V_m^{(n-1)}}$$

$$= \frac{-(\frac{1}{4} b_2 V_m + \frac{3}{8} b_3 V_m^2 + \frac{7}{16} b_4 V_m^3 + \ldots)}{b_1 + b_2 V_m + b_3 V_m^2 + \ldots}. \qquad (2.34)$$

The midpoint approximation is useful for nonlinear functions for which the Taylor series has two or more nonlinear terms of approximately equal value. The nonlinear function which describes the current gain of a bipolar transistor is a good example. The coefficients of the second-order and third-order terms of the Taylor series expansion are derived in CHAPTER III for this nonlinear function. Each of the two coefficients is zero at different values of bias current. Therefore, the midpoint approximation is useful in describing the nonlinearity of this function.

VII. REDUCTION OF OPEN-LOOP NONLINEARITY BY NEGATIVE FEEDBACK AT MIDBAND

Closed-loop nonlinearity has been shown to be equal to the open-loop nonlinearity divided by the value of the loop-transmission plus one [24]. This relation is shown in this section to be true specifically for integral nonlinearity.

The nonlinear function of the feedback system shown in Figure 2.3 is described by

$$V_{out} = A \cdot V_1 + \mathrm{Del}(V_{out}) \tag{2.35}$$

Although the deviation, $\mathrm{Del}(V_{out})$, is given here as a function of the output voltage of the nonlinear block, representing the deviation as a function of the input voltage to the block, V_1, is equally correct.

Since the nonlinear term, $\mathrm{Del}(V_{out})$, is defined as the deviation from the integral-gain curve, the variable A in Equation (2.35) must be equal to the integral gain of the nonlinear function. This point is very important because the integral gain and the small-signal gain of a function can differ significantly.

Substituting

$$V_1 = V_{in} - H \cdot V_{out} \tag{2.36}$$

into the Equation (2.35) eliminates V_1 from the expression for the output voltage,

$$V_{out} = \frac{1}{H}\left[\frac{H \cdot A}{H \cdot A + 1}\right] V_{in} + \frac{\mathrm{Del}(V_{out})}{H \cdot A + 1}. \tag{2.37}$$

For a given value of output, V_{out}, the nonlinear term is reduced by a factor of the loop transmission plus one.

The value of the loop transmission calculated from the integral gain of a feedback amplifier can be used to calculate other closed-loop parameters. Repeated laboratory experiments have shown that values of loop transmission calculated from integral gain give more

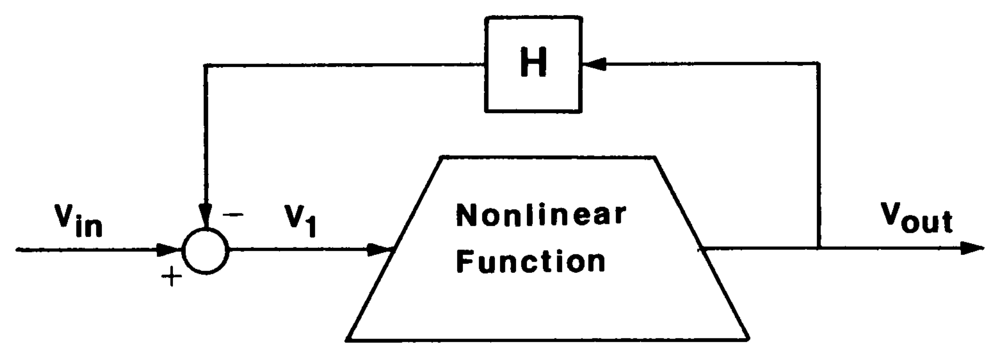

Figure 2.3. Simple feedback arrangement used to show that the closed-loop nonlinearity is equal to the open-loop nonlinearity divided by the loop-transmission plus one.

accurate predictions for closed-loop output impedance and closed-loop rise times than predictions using values of loop transmission calculated from a small-signal model.

CHAPTER III

NONLINEARITY OF SEVERAL SINGLE-STAGE BIPOLAR TRANSISTOR AMPLIFIERS

I. INTRODUCTION

The low-frequency nonlinearity of several single-stage bipolar transistor amplifiers is investigated in detail in this chapter. The Ebers-Moll model is used to evaluate the nonlinearity due to the exponential characteristic of the base-emitter junction [31]. Using this model, the input voltage is found as a transcendental function of the output voltage for the common-emitter, common-base, emitter-follower, bipolar complementary, and bipolar differential amplifier configurations. The nonlinearity of these amplifier configurations is then calculated from these equations using a procedure outlined in CHAPTER II (page 14), and the results are tabulated. These results are accurate over large dynamic ranges, but the expressions are rather complex.

Two methods of approximating the nonlinearity of the amplifier configurations are also introduced. A two-term polynomial approximation of the more complex transcendental equations is obtained by retaining the first two terms from the Taylor series expansion. Using this two-term polynomial and the formulas listed in Table 2.2 (page 24), approximations for the nonlinearity parameters of all five amplifier configurations are derived and tabulated. These results are most useful for comparing relative values of nonlinearity between similar type amplifiers, and for gaining insights into where maximum deviations occur. These expressions for nonlinearity are simple and easy to evaluate, but the expressions are inaccurate for large signal swings.

The midpoint approximation assumes that the maximum deviation of the amplifier occurs at midscale. Using this approximation, nonlinearity expressions were obtained for a couple of amplifier configurations. These expressions are more complex than the expressions obtained from the polynomial approximation. However, a comparison shows that the midpoint approximation is more accurate than the two-term polynomial approximation.

The nonlinearity due to the variation of the D.C. current gain is evaluated for the common-emitter configuration only. Using an empirical equation relating current gain to collector current, the input current is found as a three-term polynomial function of the output current. The nonlinearity of the amplifier can then be approximated from the polynomial nonlinearity expressions developed in CHAPTER II (page 27).

Experimental results are included to illustrate the accuracy of the nonlinearity expressions derived in this chapter. These experiments and their results are carefully documented. Most of the nonlinearity measurements were within 5% of the calculated values, and all nonlinearity measurements were within 10% of the calculated values.

II. NONLINEARITY DUE TO EXPONENTIAL BEHAVIOR OF BASE-EMITTER DIODE JUNCTION

The nonlinearity of several single-stage bipolar amplifiers due to the exponential characteristic of the base-emitter junction is calculated in this section. Unlike other nonlinear analyses, Taylor series expansions of the transcendental functions are not used. Instead, the nonlinearities are given as transcendental functions of the output voltage and current. The analyses are accurate over large dynamic ranges, which is often important for the calculation of the nonlinearity of the output stages of amplifiers.

Ebers-Moll Model

The voltage-to-current transfer function for a normally biased npn bipolar transistor (collector reverse biased) can be represented by the Ebers-Moll equations as follows:

$$I_e = \frac{I_{eo}}{(1 - \alpha_n \alpha_i)} \left(e^{\frac{qV}{kT}} - 1 \right) + \frac{\alpha_i I_{co}}{1 - \alpha_n \alpha_i} \tag{3.1}$$

and

$$I_c = \frac{\alpha_n I_{eo}}{(1 - \alpha_n \alpha_i)} \left(e^{\frac{qV}{kT}} - 1 \right) + \frac{I_{co}}{(1 - \alpha_n \alpha_i)} \tag{3.2}$$

where I_e is the current leaving the emitter, I_c is the current entering the collector, I_{eo} is the reverse saturation current of the emitter junction, I_{co} is the reverse saturation current of the collector junction, α_n is the emitter-to-collector gain (or normal alpha), α_i is the collector-to-emitter current gain when the emitter is reverse biased and the collector forward biased (or inverted alpha), V is the base-to-emitter voltage, q is the charge on an electron, T is the absolute temperature, and k is Boltzmann's constant. The two alphas in the above equations are assumed to be constant.

In general, the second terms in Equations (3.1) and (3.2) are much smaller than the first terms. In addition, the exponential in both equations is generally much greater than unity. Thus, the Ebers-Moll equations can be simplified to

$$I_e \cong I_s \, e^{\frac{qV}{kT}} \tag{3.3}$$

and

$$I_c \cong \alpha_n \, I_s \, e^{\frac{qV}{kT}} \tag{3.4}$$

where I_s is a pseudo saturation current for the emitter junction given by

$$I_s = I_{eo}/(1 - \alpha_n \alpha_i). \tag{3.5}$$

Input Voltage Represented as a Function of the Output Voltage for Several Amplifiers

When determining the nonlinearity of amplifier stages using the procedure outlined in CHAPTER II (page 14), the input voltage must be given as a function of the output voltage. These functions are derived in this section for the common-emitter, common-base, emitter-follower, bipolar complementary, and bipolar differential amplifiers.

i) Common-Emitter and Common-Base Amplifiers. The output voltage of a common-emitter amplifier is the deviation of the collector voltage from a D.C. bias level. The input voltage to a common-emitter amplifier causes the D.C. level of the base-to-emitter voltage to change. The change from the D.C. collector voltage, V_{out}, for a given base-to-emitter voltage change, V_{in}, is

$$V_{out} = -I_{oc} R_L \left(e^{\frac{qV_{in}}{kT}} - 1 \right) \tag{3.6}$$

where I_{oc} is the initial bias current entering the collector. By rearranging Equation (3.6), the necessary expression for input voltage as a function of the output voltage is

$$V_{in} (V_{out}) = \frac{kT}{q} \ln \left(\frac{I_{oc} R_L - V_{out}}{I_{oc} R_L} \right). \tag{3.7}$$

For a common-base amplifier, the polarity of the above function is reversed.

ii) Emitter-Follower Amplifier. The output voltage of an emitter-follower amplifier is the change in the emitter voltage from a D.C. bias level. For a given change in the emitter voltage, V_{out}, the corresponding change in the base-to-emitter voltage is

$$\Delta V_{be} = \frac{kT}{q} \ln \left(\frac{I_{oe} R_L + V_{out}}{I_{oe} R_L} \right), \tag{3.8}$$

where I_{oe} is the initial bias current leaving the emitter of the transistor. The input voltage to the emitter-follower amplifier as a function of the output voltage is the base-to-emitter voltage change plus the output voltage or

$$V_{in}\ (V_{out}) = V_{out} + \frac{kT}{q} \ln\left(\frac{I_{oe}\ R_L + V_{out}}{I_{oe}\ R_L}\right). \tag{3.9}$$

iii) Bipolar Complementary Amplifier. The model used to find the transfer function for the complementary amplifier stage is shown in Figure 3.1. The change in the base-to-emitter voltage of the two transistors as a function of output voltage is shown in Appendix I to be

$$\Delta V_{be} = \frac{kT}{q} \sinh^{-1}\left(\frac{V_{out}}{2\ I_{oe}\ R_L}\right) \tag{3.10}$$

where I_{oe} is the initial bias current leaving the emitter of Q_1 and entering the emitter of Q_2. The input voltage to the complementary amplifier as a function of the output voltage is

$$V_{in}\ (V_{out}) = V_{out} + \frac{kT}{q} \sinh^{-1}\left(\frac{V_{out}}{2\ I_{oe}\ R_L}\right). \tag{3.11}$$

iv) Bipolar Differential Amplifier. The model used to find the transfer function of the balanced bipolar differential amplifier is shown in Figure 3.2. The bias current, I_o, of the amplifier is defined as the sum of the two emitter currents. Without loss of generality, the voltage at the base of Q_2 is arbitrarily set at zero volts and the differential input voltage is given as V_{in}. In Appendix I, the output voltage at the collector of Q_1 is shown to be

$$V_{out1} = -\frac{I_o\ \alpha_1\ R_L}{2} \tanh\left(\frac{qV_{in}}{2kT}\right), \tag{3.12}$$

and the output at the collector of Q_2 is shown to be

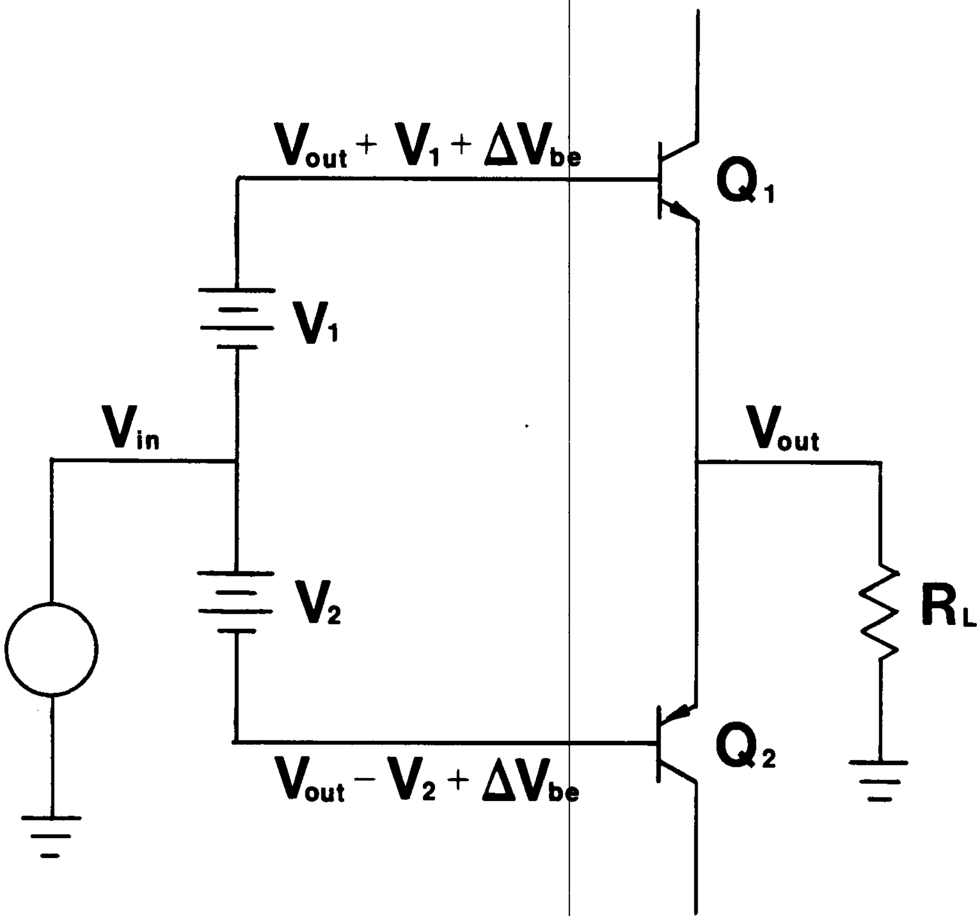

Figure 3.1. Model of a bipolar complementary amplifier where ΔV_{be} is the change in base-to-emitter voltages of transistors Q, and Q_2, V_{out} is the output voltage, V_{in} is the input voltage, V_1 is the initial base-to-emitter voltage for Q_1 and V_2 is the initial base-to-emitter voltage for Q_2.

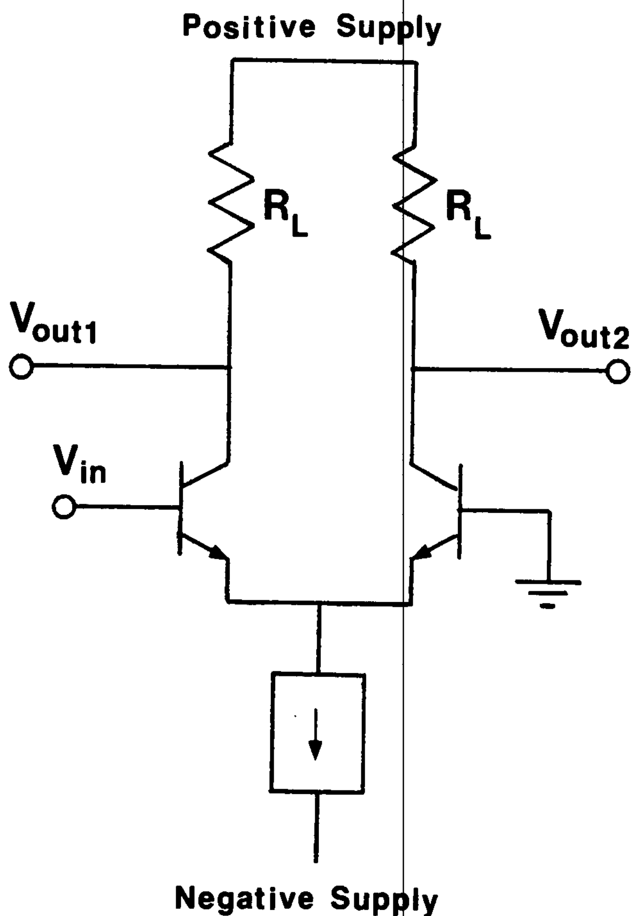

Figure 3.2. Model used to develop the low-frequency transfer function of the bipolar differential amplifier.

$$V_{out2} = \frac{I_o \alpha_2 R_L}{2} \tanh\left(\frac{qV_{in}}{2kT}\right), \tag{3.13}$$

where α_1 and α_2 are the emitter-to-collector current gains of Q_1 and Q_2 respectively.

Using the output voltage at the collector of Q_2 as the independent variable, the input voltage is given by

$$V_{in}\ (V_{out2}) = \frac{2kT}{q} \tanh^{-1}\left(\frac{2\ V_{out2}}{\alpha_2\ I_o\ R_L}\right). \tag{3.14}$$

The input voltage could also be written as a function of V_{out1}, or as a function of the differential output $(V_{out1} - V_{out2})$. However, neither is used in this study since a conversion to either of these two variables is trivial.

Evaluation of Bipolar Transistor Exponential-Characteristic Nonlinearity and Tabulation of Results

The functions given by Equations (3.7), (3.9), (3.11), and (3.14) were used to evaluate the nonlinearities of their respective amplifier configurations, using the procedure outlined in CHAPTER II (page 14). The development is straight forward but overburdened with detail. Therefore, only the salient points of the analysis are given here in Table 3.1. The table includes the integral gain, the output voltage at which the maximum deviation occurs, and the integral nonlinearity of the amplifier configurations. The variable X, which is defined as the ratio of the peak signal current to the initial bias current, has been introduced to simplify the equations given in Table 3.1.

Table 3.1 Salient points of the integral nonlinearity analysis of six single-stage bipolar transitor amplifiers. The variable $X = (V_m/I_oR_L)$ is introduced to simplify the expressions.

Amplifier configuration	Integral gain	Output at which the maximum deviation occurs	Normalized integral nonlinearity
Common-emitter	$\frac{V_m}{\frac{kT}{q}\ln(1-X)}$	$V_m\left[\frac{1}{\ln(1-X)}+\frac{1}{X}\right]$	$\frac{\ln\left[\frac{-X}{\ln(1-X)}\right]-1}{\ln(1-X)}-\frac{1}{X}$
Common-base	$\frac{-V_m}{\frac{kT}{q}\ln(1-X)}$	$V_m\left[\frac{1}{\ln(1-X)}+\frac{1}{X}\right]$	$\frac{\ln\left[\frac{X}{\ln(1-X)}\right]-1}{\ln(1-X)}-\frac{1}{X}$
Emitter-follower	$\frac{V_m}{V_m+\frac{kT}{q}\ln(1+X)}$	$V_m\left[\frac{1}{\ln(1+X)}-\frac{1}{X}\right]$	$\frac{(\frac{kT}{q})\ln(1+X)}{V_m+(\frac{kT}{q})\ln(1+X)}\cdot\left\{\frac{\ln\left[\frac{X}{\ln(1+X)}\right]-1}{\ln(1+X)}+\frac{1}{X}\right\}$
Bipolar complementary	$\frac{V_m}{V_m+\frac{kT}{q}\sinh^{-1}(\frac{X}{2})}$	$V_m\sqrt{\left(\frac{1}{\sinh^{-1}\frac{X}{2}}\right)^2-\left(\frac{2}{X}\right)^2}$	$\frac{(\frac{kT}{q})}{V_m+(\frac{kT}{q})\sinh^{-1}\frac{X}{2}}\cdot\left\{\cosh^{-1}\left[\frac{\frac{X}{2}}{\sinh^{-1}(\frac{X}{2})}\right]-\sqrt{1-\left[\frac{X}{2}\sinh^{-1}(\frac{X}{2})\right]^2}\right\}$
Bipolar differential	$\frac{V_m}{\frac{2kT}{q}\tanh^{-1}(2X)}$	$V_m\sqrt{\frac{1}{2X\tanh^{-1}(2X)}-\frac{1}{4X^2}}$	$\frac{\tanh^{-1}\left[2X\sqrt{\frac{1}{2X\tanh^{-1}(2X)}-\frac{1}{4X^2}}\right]}{\tanh^{-1}(2X)}-\sqrt{\frac{1}{2X\tanh^{-1}(2X)}-\frac{1}{4X^2}}$
Common-emitter with an unbypassed emitter resistor	$\frac{V_m}{\frac{-V_mR_E}{\alpha R_L}+\frac{kT}{q}\ln(1-X)}$	$V_m\left[\frac{1}{\ln(1-X)}+\frac{1}{X}\right]$	$\frac{\frac{kT}{q}\ln(1-X)}{-V_m\left(\frac{R_E}{\alpha R_L}\right)+\frac{kT}{q}\ln(1-X)}\left\{\frac{\ln\left[\frac{-X}{\ln(1-X)}\right]-1}{\ln(1-X)}-\frac{1}{X}\right\}$

Effect of Unbypassed Emitter Resistance

The nonlinearity equation of the emitter-follower amplifier can be extended to give the integral nonlinearity equation for a common-emitter amplifier with an unbypassed emitter resistor. Since the emitter-to-collector current gain is constant for the Ebers-Moll model, the normalized nonlinearity of the output voltage at the collector terminal will be equal to the normalized nonlinearity of the voltage across the unbypassed emitter resistor. Therefore, the nonlinearity equation for the common-emitter amplifier with an unbypassed emitter resistor can be derived by 1) representing the change in the emitter voltage as a function of the change in the collector voltage, 2) representing the emitter bias current in terms of the collector bias current, 3) placing these two changes in the nonlinearity equation for the emitter-follower amplifiers. The nonlinearity equation for a common-emitter amplifier with an unbypassed emitter resistor given in Table 3.1 was obtained by this method. The change of emitter voltage as a function of the change of collector voltage is

$$V_e = - \frac{R_E}{R_L} \cdot \frac{V_{out}}{\alpha_n} \tag{3.15}$$

where R_L is the resistance at the collector, R_E is the unbypassed emitter resistor, and V_{out} is the output voltage at the collector.

Effect of Generator and Base-Spreading Resistances

The effect of the generator resistance, R_g, in the base circuit, and the base-spreading resistance of the transistor, R_b, can be accounted for in bipolar transistor amplifiers with an equivalent unbypassed emitter resistor whose value is

$$R_E' = \frac{R_b + R_g}{\beta + 1} \tag{3.16}$$

where β is the base-to-collector current gain of the transistor. This equivalent emitter resistor can have a significant effect on the integral nonlinearity produced by some amplifier configurations.

III. APPROXIMATIONS OF THE TRANSFER FUNCTIONS AND NONLINEARITY DUE TO EXPONENTIAL BEHAVIOR OF BASE-EMITTER DIODE JUNCTION

Two-Term Polynomial Approximations

Two-term polynomials approximating the low-frequency transfer functions of several single-stage bipolar transistor amplifiers are given in this section. The integral gain and integral nonlinearity of these amplifiers are then estimated from the equations derived in CHAPTER II for two-term polynomial functions (Tables 2.1 and 2.2 on pages 23-24). These expressions for nonlinearity are not as accurate as the transcendental equations given in Table 3.1 (page 40), but they are simpler and easier to use. These simplified expressions allow the linearity of certain amplifiers to be compared in a later chapter of this dissertation.

In Table 3.2, the input voltages of five amplifiers are given as two-term polynomial functions of their output voltages. These polynomials were derived from the equations given earlier in this chapter describing input voltages as functions of output voltages (pages 34-39). The polynomials are the first two, nonzero terms

Table 3.2. The input represented as a two-term polynomial function of the output voltage for several single-stage bipolar transistor amplifiers, and the integral gain and integral nonlinearity calculated from the polynomials. The variable $X = (V_m/I_oR_L)$ is introduced to simplify the expressions.

Amplifier	Two-Term Polynomial	Integral Gain	Integral Nonlinearity
Common-emitter	$V_{in} = \left(\frac{-kT}{qI_oR_L}\right) V_{out} + \left(\frac{-kT}{2q}\right)\left(\frac{1}{I_oR_L}\right)^2 V_{out}^2$	$\dfrac{-\left(\alpha \frac{R_L}{r_e}\right)}{1 + \frac{X}{2}}$	$\dfrac{-(\frac{X}{8})}{1 + \frac{X}{2}}$
Common-base	$V_{in} = \left(\frac{kT}{qI_oR_L}\right) V_{out} + \frac{kT}{2q}\left(\frac{1}{I_oR_L}\right)^2 V_{out}^2$	$\dfrac{\left(\alpha \frac{R_L}{r_e}\right)}{1 + X/2}$	$\dfrac{-(\frac{X}{8})}{1 + \frac{X}{2}}$
Emitter-follower	$V_{in} = \left(\frac{R_L + r_e}{R_L}\right) V_{out} + \left(\frac{-r_e}{2R_L}\right)\frac{1}{I_oR_L} V_{out}^2$	$\dfrac{R_L}{R_L + \left(1 - \frac{X}{2}\right)r_e}$	$\dfrac{(\frac{X}{8})r_e}{R_L + \left(1 - \frac{X}{2}\right)r_e}$
Bipolar complementary	$V_{in} = \left[\frac{R_L + (\frac{r_e}{2})}{R_L}\right] V_{out} + \left(\frac{-r_e}{12R_L}\right)\left(\frac{1}{2I_oR_L}\right)^2 V_{out}^3$	$\dfrac{R_L}{R_L + \left(1 - \frac{X^2}{24}\right)(\frac{r_e}{2})}$	$\dfrac{\left(\frac{X^2}{72\sqrt{3}}\right)r_e}{R_L + \left(1 - \frac{X^2}{24}\right)(\frac{r_e}{2})}$
Balanced bipolar differential	$V_{in} = \left(\frac{2r_e}{\alpha R_L}\right) V_{out} + \left(\frac{+4r_e}{3\alpha R_L}\right)\left(\frac{1}{\alpha I_oR_L}\right)^2 V_{out}^3$	$\dfrac{\frac{\alpha R_L}{2r_e}}{1 + \frac{2}{3}\left(\frac{X}{\alpha}\right)^2}$	$\dfrac{\frac{4\sqrt{3}}{27}\left(\frac{X}{\alpha}\right)^2}{\left[1 + \frac{2}{3}\left(\frac{X}{\alpha}\right)^2\right]}$

from the familiar Maclaurin series expansion,

$$f(X) = f(0) + f'(0)X + \frac{1}{2} f''(0)X^2 + \cdot \cdot \cdot \cdot$$

$$+ \frac{1}{n!} f^n(0)X^n + \cdot \cdot \cdot, \qquad (3.17)$$

of the equations.

In Table 3.3, the output voltages of the five amplfiers are given as two-term ploynomial functions of their input voltages. For some of these amplifiers, equations were available which give the output voltage of the amplifier as a function of the input voltage, and the Maclaurin series were developed for these amplifiers in a straightforward manner. For the other amplifiers, the Maclaurin series had to be developed using the equations which describe the output voltage of the amplifier as a function of the input voltage. For the arbitrary function,

$$V_{out} = f(V_{in}), \qquad (3.18)$$

the first derivative of the input voltage with respect to the output voltage,

$$\frac{dV_{in}}{dV_{out}} = \frac{1}{\frac{d}{dV_{in}}\left[f(V_{in})\right]}, \qquad (3.19)$$

can be found be implicit differentiation. The second derivative,

$$\frac{d^2V_{in}}{dV_{out}^{\;2}} = \frac{d}{dV_{in}}\left[\frac{dV_{in}}{dV_{out}}\right] \cdot \frac{dV_{in}}{dV_{out}}, \qquad (3.20)$$

Table 3.3. The output voltage represented as a two-term polynomial function of the input voltage for several single-stage bipolar transistor amplifiers, and the integral gain and integral nonlinearity calculated from the polynomials.

Amplifier	Two-term polynomial	Integral gain	Integral nonlinearity
Common-emitter	$V_{out} = \left(\frac{-R_L}{r_e}\right) V_{in} + \left(\frac{-R_L}{2r_e}\right)\frac{q}{kT}\ V_{in}^{\ 2}$	$\frac{-R_L}{r_e} + \left(\frac{-R_L qV_{nm}}{2r_e kT}\right)$	$\dfrac{\frac{qV_{nm}}{8kT}}{\left(1 + \frac{qV_{nm}}{2kT}\right)}$
Common-base	$V_{out} = \left(\frac{R_L}{r_e}\right) V_{in} + \left(\frac{R_L}{2r_e}\right)\frac{q}{kT}\ V_{in}^{\ 2}$	$\frac{R_L}{r_e} + \left(\frac{R_L qV_{nm}}{2\ r_e kT}\right)$	$\dfrac{\frac{-qV_{nm}}{8kT}}{\left(1 - \frac{qV_{nm}}{2kT}\right)}$
Emitter-follower	$V_{out} = \left(\frac{R_L}{R_L + r_e}\right) V_{in} + \left(\frac{r_e R_L}{2I_o}\right)\left[\frac{1}{R_L + r_e}\right]^3 V_{in}^{\ 2}$	$\left(\frac{R_L}{R_L + r_e}\right) + \left[\frac{r_e^{\ 2} R_L}{R_L + r_e^{\ 3}}\right]\frac{qV_{nm}}{2kT}$	$\dfrac{r_e^{\ 2}\left(\frac{qV_{nm}}{8kT}\right)}{(R_L + r_e)^2 + r_e^{\ 2}\left(\frac{qV_{nm}}{2kT}\right)}$
Bipolar complementary	$V_{out} = \left(\frac{R_L}{R_L + \frac{r_e}{2}}\right)V_{in} + \left[\frac{R_L}{R_L + \frac{r_e}{2}}\right]^4\left(\frac{1}{2I_o R_L}\right)^2\left(\frac{r_e}{12R_L}\right)V_{in}^{\ 3}$	$\left(\frac{R_L}{R_L + \frac{r_e}{2}}\right) + \frac{1}{12}\left[\frac{R_L}{R_L + \frac{r_e}{2}}\right]^4\left(\frac{r_e}{R_L}\right)^3\left(\frac{qV_{nm}}{2kT}\right)^2$	$\dfrac{\frac{4\sqrt{3}}{54}\left[\frac{r_e}{R_L + \frac{r_e}{2}}\right]^3\left(\frac{qV_{nm}}{2kT}\right)^2}{\left\{1 + \frac{1}{6}\left[\frac{r_e}{R_L + \frac{r_e}{2}}\right]^3\left(\frac{qV_{nm}}{2kT}\right)^2\right\}}$
Balanced bipolar differential	$V_{out} = \left(\frac{\alpha R_L}{2r_e}\right) V_{in} + \left(\frac{-\alpha R_L}{6r_e}\right)\left(\frac{q}{kT}\right)^2 V_{in}^{\ 3}$	$\frac{\alpha R_L}{2r_e} + \left(\frac{-\alpha R_L}{6r_e}\right)\left(\frac{qV_{nm}}{2kT}\right)^2$	$\dfrac{-\frac{2\sqrt{3}}{27}\left(\frac{qV_{nm}}{2kT}\right)^2}{1 - \frac{1}{3}\left(\frac{qV_{nm}}{kT}\right)^2}$

and higher order derivatives are found by the chain rule of differential calculus. The coefficients of the Macluarin series can then be determined by evaluting these derivatives at V_{in} equal to zero, since V_{in} is zero when V_{out} is zero.

Midpoint Approximations of Nonlinearity

The nonlinearity of several amplifier stages was estimated from two-term polynomial approximations in the previous section. These approximations simplified the expressions for the nonlinearity, but they are not very accurate for large values of the variable X, which is the ratio of the peak signal current to the initial bias current. In this section, a technique for approximating the nonlinearity of amplifiers is introduced which also gives simplified expressions for the nonlinearity of amplifiers, but without a serious loss of accuracy over a wide range of values of the variable X. The procedure and its accuracy are demonstrated for the common-emitter and emitter-follower amplifiers.

The peak deviation of an amplifier typically occurs near midscale. The nonlinearity of an amplifier can therefore be estimated by calculating the deviation of the amplifier at mid-scale. Using the deviation of the common-emitter amplifier when the input voltage is at half of its maximum value results in the approximation

$$NL_{ce} = \frac{1}{2} + \frac{\sqrt{1-X}}{X} - \frac{1}{X} \tag{3.21}$$

for the normalized nonlinearity of the amplifier. This approximation and the approximation obtained from the two-term polynomial are compared in Table 3.4 for several values of the variable X to the nonlinearity calculated from the more accurate expression given in Table 3.1 (page 40). The approximation given by Equation (3.21) is much more accurate than the two-term polynomial approximation, and is within 4% of the nonlinearity predicted by the more exact analysis for values of X from -0.9 to 10.0.

The midpoint approximation for the emitter-follower amplifier is not so straightforward. Two approximations are given here.

The magnitude of the deviation of the output from the integral gain is

$$\mathrm{Del} = \frac{kT}{q} \ln\left(1 + \frac{V_{out}}{I_o R_L}\right) - \frac{kT}{2q} \ln(1 + X) \tag{3.22}$$

when the magnitude of the input voltage to the emitter-follower amplifier is half of its maximum amplitude. Since the output voltage of an emitter-follower amplifier cannot be determined directly from the input voltage in a closed form, this expression cannot be reduced further without some approximation. By assuming that the magnitude of the output voltage is approximately one-half of its maximum amplitude, the nonlinearity of the emitter-follower is approximately

$$NL_{ef} \simeq \frac{kT}{qV_m} \left[\ln\left(1 + \frac{X}{2}\right) - \frac{1}{2} \ln(1 + X)\right]. \tag{3.23}$$

Table 3.4. Two approximations of the nonlinearity of a common-emitter amplifier due to the exponential characteristic of the base-emitter diode junction compared to the more exact analysis given in Table 3.1 (page 40) for several values of the variable X.

X	Percent distortion calculated from Table 3.1	Percent distortion approximated by Equation (3.21)	Percent distortion approximated from Table 3.2
0.9	-26.9	-26.0	-20.5
0.8	-19.4	-19.1	-16.7
0.7	-14.8	-14.6	-13.5
0.56	-10.2	-10.2	-9.72
0.32	-4.74	-4.74	-4.76
0.18	-2.45	-2.45	-2.47
0.10	-1.32	-1.32	-1.32
0.056	-0.732	-0.732	-0.720
0.032	-0.402	-0.402	-0.407
0.0	0.0	0.0	0.0
-0.032	0.389	0.389	0.394
-0.056	0.684	0.684	0.681
-0.10	1.19	1.19	1.19
-0.18	2.05	2.05	2.06
-0.32	3.43	3.43	3.45
-0.56	5.56	5.55	5.47
-1.0	8.61	8.58	8.33
-1.8	12.6	12.5	11.8
-3.2	17.3	17.1	15.4
-5.6	22.5	22.0	18.4
-10.0	27.9	26.8	20.8

The second approximation is obtained by comparing the expressions for integral nonlinearity of the common-emitter and emitter-follower amplifiers given in Table 3.1 (page 40). This approximation is

$$NL_{ef} \cong \frac{(\frac{kT}{q}) \ln(1 + X)}{V_m + (\frac{kT}{q}) \ln(1 + X)} \left[\frac{1}{2} - \frac{\sqrt{1 + X}}{X} + \frac{1}{X}\right]. \tag{3.24}$$

Note that the expression for the nonlinearity of the common-emitter amplifier is contained in the expression for the nonlinearity of the emitter-follower amplifier.

In Table 3.5, the two approximations given in Equations (3.23) and (3.24) above and the two-term polynomial approximation are compared for several values of the variable X with the nonlinearity prediction given in Table 3.1 (page 40). The value of the peak output voltage is arbitrarily chosen to be one volt for this comparison. The approximation given by Equation (3.21) is within 4% of the nonlinearity predicted by the more exact analysis for values of X from -0.9 to 10.0, and the approximation given by Equation (3.23) is within 16 percent of the nonlinearity predicted by the more exact analysis over the same range of X. The approximation obtained from the two-term polynomial is not nearly as accurate as the first two approximations; the magnitude of its fractional error is approximately equal to the value of the variable X.

The midpoint approximation greatly simplifies the expressions for the nonlinearity of the common-emitter, and emitter-follower amplifiers with a serious loss of accuracy.

Table 3.5. Three approximations of the nonlinearity of an emitter-follower amplifier due to the exponential characteristic of the base-emitter diode junction compared to the more exact analysis given in Table 3.1 (page 40) for several values of the variable X, and for V_m = 1 volt.

X	Percent distortion Table 3.1	Percent distortion approximation Equation (3.24)	Percent distortion approximation Equation (3.23)	Percent distortion approximation from Table 3.2
-0.9	1.71	1.65	1.44	2.73×10^{-1}
-0.8	8.49×10^{-1}	834×10^{-3}	7.64×10^{-1}	2.14×10^{-1}
-0.7	4.77×10^{-1}	472×10^{-3}	4.45×10^{-1}	1.63×10^{-1}
-0.56	2.22×10^{-1}	221×10^{-3}	2.13×10^{-1}	1.04×10^{-1}
-0.32	4.87×10^{-2}	48.7×10^{-3}	4.80×10^{-2}	3.36×10^{-2}
-0.18	1.29×10^{-2}	12.9×10^{-3}	1.28×10^{-2}	1.06×10^{-2}
-0.10	3.62×10^{-3}	3.62×10^{-3}	3.61×10^{-3}	3.26×10^{-3}
-0.056	1.08×10^{-3}	1.08×10^{-3}	1.08×10^{-3}	1.02×10^{-3}
-0.032	3.44×10^{-4}	344×10^{-6}	3.44×10^{-4}	3.33×10^{-4}
0.0	0.0	0.0	0.0	0.0
0.032	3.22×10^{-4}	3.22×10^{-4}	3.22×10^{-4}	3.33×10^{-4}
0.056	9.64×10^{-4}	9.64×10^{-4}	9.65×10^{-4}	1.02×10^{-3}
0.10	2.95×10^{-3}	2.95×10^{-3}	2.95×10^{-3}	3.24×10^{-3}
0.18	8.86×10^{-3}	8.86×10^{-3}	8.89×10^{-3}	1.05×10^{-2}
0.32	2.48×10^{-2}	2.48×10^{-2}	2.50×10^{-2}	3.31×10^{-2}
0.56	6.34×10^{-2}	6.33×10^{-2}	6.37×10^{-2}	1.01×10^{-1}
1.0	1.52×10^{-1}	1.52×10^{-1}	1.53×10^{-1}	3.21×10^{-1}
1.8	3.31×10^{-1}	3.28×10^{-1}	3.30×10^{-1}	1.05
3.2	6.27×10^{-1}	6.19×10^{-1}	6.19×10^{-1}	3.50
5.6	1.05	1.03	1.02	13.8
10.0	1.63	1.58	1.54	-813

The low-frequency transfer functions of some amplifier stages, such as the bipolar transistor differential and complementary amplifiers, have a zero coefficient of the second-order term (see Tables 3.2 and 3.3, pages 43 and 45). For these amplifiers, the peak deviation of the output occurs nearer to 57.7% of full scale (i.e. $1/\sqrt{3}$ of full scale). Therefore, the "midpoint approximation" will be more accurate for these amplifiers if the deviation is calculated at 57.7% of the maximum value of input or output voltage rather than at half of this maximum value.

IV. NONLINEARITY OF A COMMON-EMITTER AMPLIFIER DUE TO VARIATION OF D.C. CURRENT GAIN WITH COLLECTOR CURRENT

When a common-emitter amplifier is driven by a current source, the output current is independent of the exponential characteristics of the base-emitter diode junction, and is instead a function of the base-to-collector current gain of the transistor. Since this current gain is a function of the current level, nonlinearity is introduced. A three-term polynomial is developed in this section which gives the input current as a function of the output current. This polynomial may be used to approximate the nonlinearity of the transistor using the formulas developed in CHAPTER II for two-term polynomials.

The D.C. current gain of the bipolar transistor is related to the collector current by the empirical formula [8]

$$\beta = \frac{\beta_{mx}}{1 + A \cdot \ln^2(I_c/I_{mx})}, \qquad (3.25)$$

where A is a constant, I_c is the collector current, β_{mx} is the maximum current gain, and this current gain occurs at a value of collector current I_{mx}. The base current of the transistor may then be represented as a function of the collector current by

$$I_b(I_c) = \frac{I_c}{\beta} = \frac{I_c\left[1 + A \cdot \ln^2(I_c/I_{mx})\right]}{\beta_{mx}} \tag{3.26}$$

Expanding this function in a Taylor series about the initial value of the collector current, I_o, gives

$$I_b(I_c) = I_{bo} + I_b{}'(I_o) \cdot (I_c - I_o) + \frac{1}{2} I_b{}''(I_o) \cdot (I_c - I_o)^2 +$$

$$\cdots + \frac{1}{n!} I_b{}^n(I_o) \cdot (I_c - I_o)^n + \cdots \tag{3.27}$$

where I_{bo} is the initial value of the base current, and where the primes denote differentiation with respect to I_c. Since the input signal current, I_{in}, is equal to the value of the base current minus the initial base current, and since the output signal current, I_{out}, is equal to the value of the collector current minus the initial collector current, Equation (3.27) may be rewritten with the input current given as a function of the output current,

$$I_{in}(I_{out}) = I_b{}'(I_o) \cdot I_{out} + \frac{1}{2} I_b{}''(I_o) \cdot I_{out}{}^2 +$$

$$\frac{1}{6} I_b{}'''(I_o) \cdot I_{out}{}^3 + \cdots. \tag{3.28}$$

This equation may be rewritten as

$$I_{in}(I_{out}) \tilde{=} \left[\frac{1 + A\ \ln^2(I_o/I_{mx}) + 2A\ \ln(I_o/I_{mx})}{\beta_{mx}}\right] I_{out}$$
$$+ \frac{A\left[1 + \ln(I_o/I_{mx})\right]}{\beta_{mx} I_o} I_{out}^{\ 2} + \left[\frac{-A\ \ln(I_o/I_{mx})}{3\beta_{mx} I_o^{\ 2}}\right] I_{out}^{\ 3} \qquad (3.29)$$

after taking the required differentiations of Equation (3.26) to determine the coefficients. Terms of higher than third-order have been dropped.

The coefficient of the second term in the above polynomial is zero when the value of (I_o/I_{mx}) is approximately 0.368, and the coefficient of the third term in the above polynomial is zero when the value of (I_o/I_{mx}) is unity. Therefore, neither the second-order two-term polynomial approximation nor the third order two-term polynomial approximation are adequate for evaluating the nonlinearity of the above polynomial for all bias conditions. Therefore, the midpoint approximation for a multiple-term polynomial described by Equation (2.34) (page 27) is recommended for evaluating the nonlinearity of the three-term polynomial given above.

V. TESTING ACCURACY OF NONLINEARITY EXPRESSIONS WITH LABORATORY MEASUREMENTS

The nonlinearity of several bipolar transistor amplifiers was measured to test the accuracy of some of the expressions developed in this chapter. The nonlinearity of a common-emitter, a common-base, an emitter-follower, and a complementary amplifier was measured using the current-sum technique outlined in the IEEE

Nuclear Science Transactions [29]. These measured values of nonlinearity are compared to values calculated from the expressions given in Table 3.1 (page 40). Measured and predicted values of nonlinearity agree within 10%.

IEEE Test Procedure

The IEEE current-sum procedure for measuring integral nonlinearity is outlined in this section. The basic test arrangement is shown in Figure 3.3. The peak output of the voltage pulser is set at minus the full-scale output of the amplifier. The magnitude of the input voltage to the amplifier under test is adjusted by an attenuator until the peak output voltage is at full scale. If the voltage at the output of the amplifier has a linear portion, $A \cdot V_{in}$, and a nonlinear portion, -Del, the voltage appearing at the node where the two resistors intersect is equal to minus Del/2. The voltage level from the pulser is then varied until the maximum value of the deviation, Del, is determined.

Measurement and Calculation of Nonlinearity of a Common-Emitter Amplifier

The test arrangement shown in Figure 3.4 was used to measure the nonlinearity of a common-emitter amplifier. This test arrangement is slightly different from the basic arrangement shown in Figure 3.3. A unity-gain buffer follows the resistive attenuator to give a low impedance source to the input of the common-emitter amplifier, and another unity-gain buffer isolates the collector circuit from the current-sum network. The 47 ohm impedance of the buffer amplifier in the collector must be included with the resistance of the current-

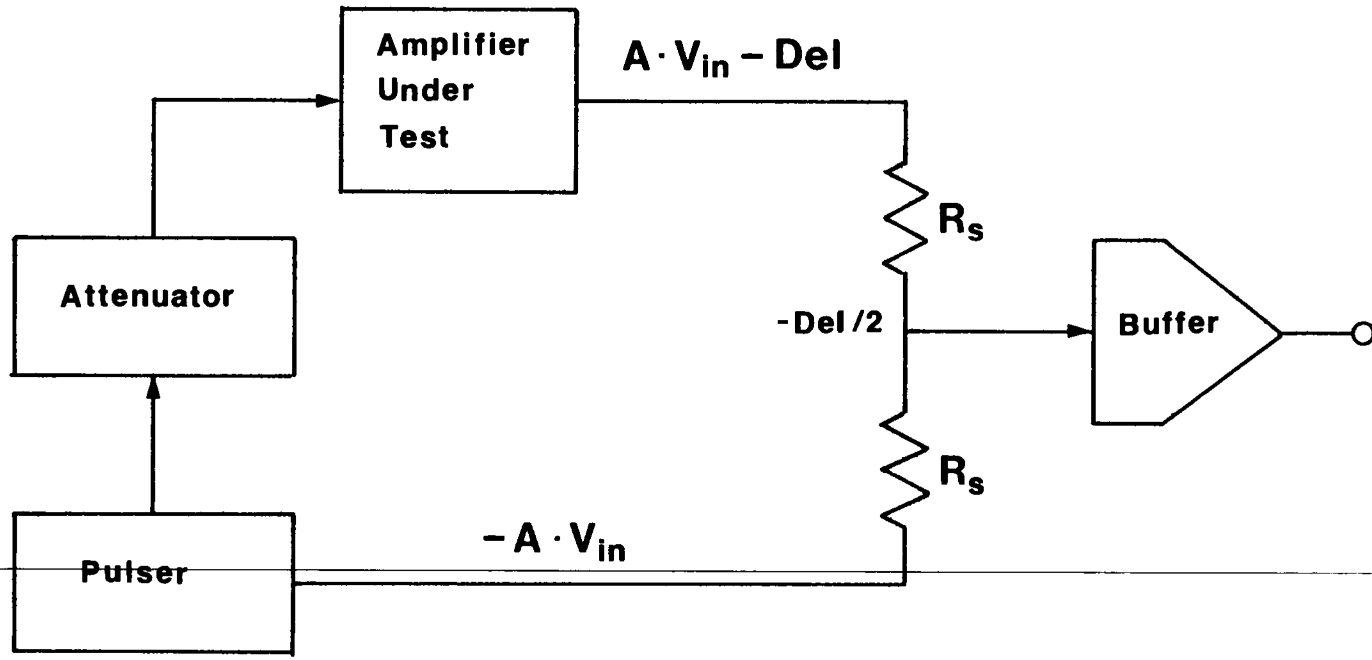

Figure 3.3. Test arrangement to measure the integral nonlinearity of an inverting amplifier using the basic IEEE current-summing procedure. The variable A is the integral gain of the amplifier under test and Del is its nonlinear deviation.

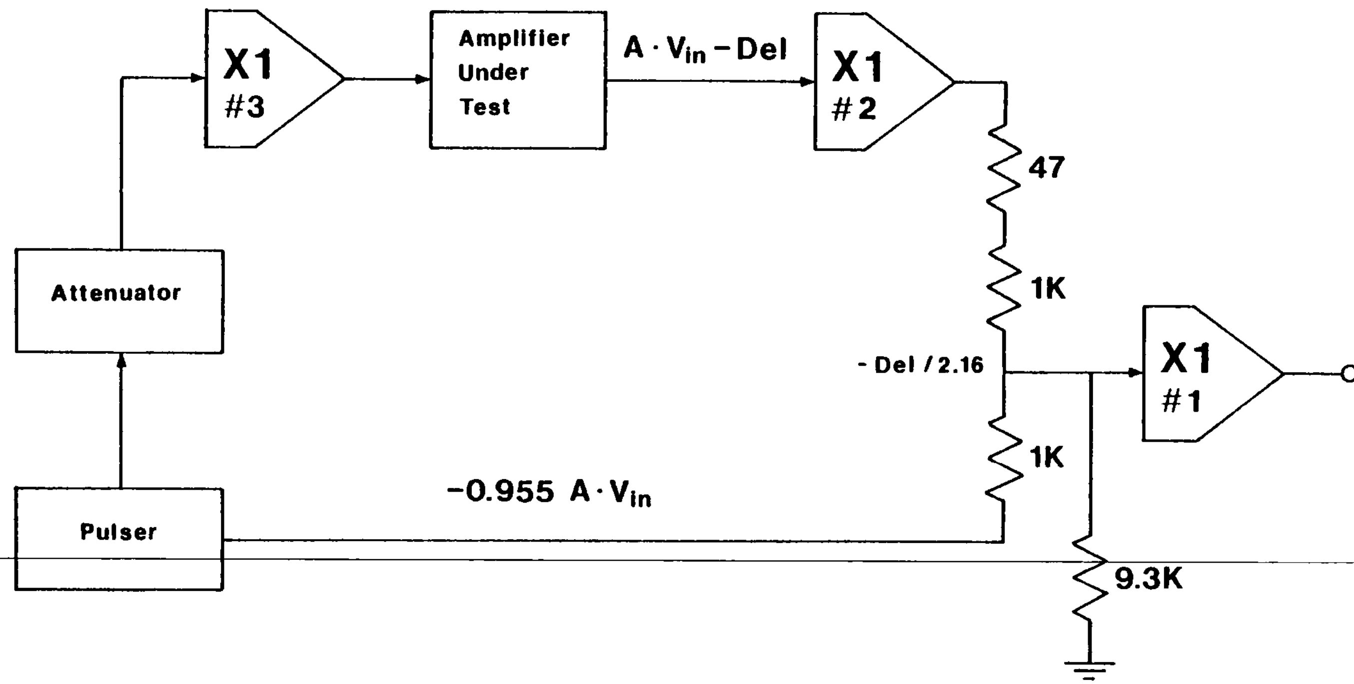

Figure 3.4. Test arrangement used to measure the integral nonlinearity of a common-emitter amplifier. The variable A is the integral gain of the common-emitter amplifier, and Del is its non-linear deviation.

sum network. Therefore, the magnitude of the output voltage from the pulser must be $-0.955\ A \cdot V_{in}$ to cancel the linear portion of the output voltage at the current-summing node. Including the effect of the 47 ohm output resistance of the collector circuit buffer amplifier, the magnitude of the voltage at the current-summing node is -Del/2.16 in this test arrangement.

The circuit diagrams of the individual buffer amplifiers are given in Appendix II.

The nonlinearity of the common-emitter amplifier shown in Figure 3.5 was measured for peak output voltages of plus two and minus two volts. For an output of plus two volts, the maximum deviation measured at the summing node was 73 millivolts. The maximum deviation at the output of the amplifier was 2.16 times greater, or 158 millivolts. The normalized nonlinearity of the amplifier is therefore -7.88% for this output level.

With an output of minus two volts, the maximum deviation measured at the summing node was 40 millivolts. Therefore, the maximum deviation at the output of the amplifier was 86.4 millivolts, and the normalized nonlinearity of the amplifier is 4.32% for this output level.

The nonlinearity of the amplifier shown in Figure 3.5 was calculated using the expression for nonlinearity given in Table 3.1 (page 40) for the common-emitter amplifier. The value of the variable X, which is the ratio of the peak signal current to the initial bias current, is 0.524 when V_{out} is plus two volts, and is -0.524 when V_{out} is minus two volts. The calculated nonlinearities

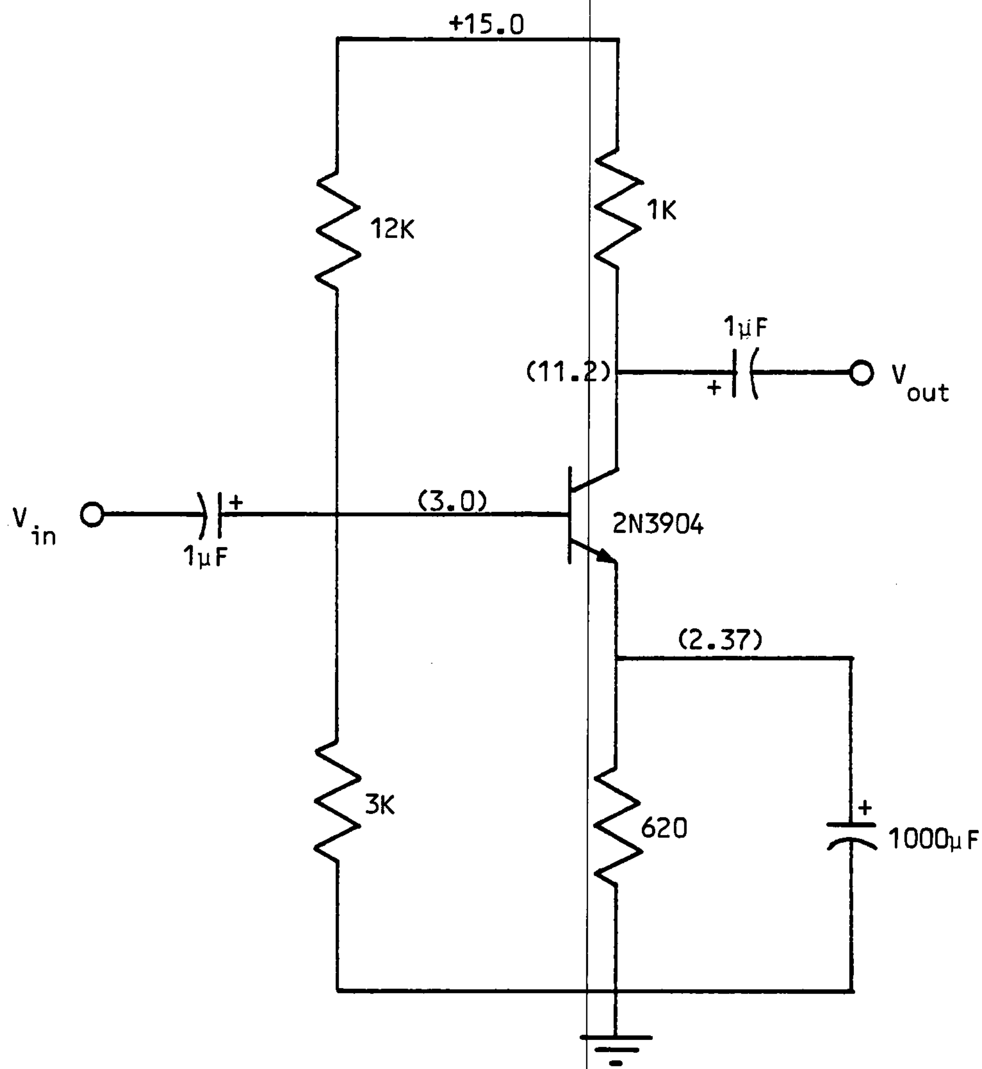

Figure 3.5. Schematic diagram of the common-emitter amplifier which was tested for integral nonlinearity. Measured bias voltages are given in parenthesis.

are −9.16% for the plus two-volt output and 5.23% for the minus two-volt output. These calculated values are somewhat higher than the measured values because the calculations do not include the effect of the base-spreading resistance of the transistor.

The effect of the base-spreading resistance was accounted for by an equivalent unbypassed emitter resistance (see "Effect of Generator and Base-Spreading Resistance," page 41). The magnitude of this equivalent unbypassed emitter resistance was determined from an integral gain measurement. The expression for the integral gain of a common-emitter amplifier with an unbypassed emitter resistor, given in Table 3.1 (page 40), may be rearranged to

$$R_E = \alpha R_L \left[\frac{kT}{qV_m} \ln(1 - X) - \frac{1}{A}\right], \tag{3.30}$$

where A is the integral gain of the amplifier, and V_m is the maximum value of the output voltage. When the output of the common-emitter amplifier was set at minus two volts, the measured value of the input voltage was 13.5 millivolts. Therefore, the integral gain was −148.7. Inserting the appropriate values into Equation (3.30),

$$R_E = (0.995)(1800\Omega)\left[\frac{0.026V}{-2.0V} \ln(1.524) - \frac{1}{(-148.7)}\right], \tag{3.31}$$

the calculated value of the equivalent unbypassed emitter resistance is 1.24 ohms.

Using this value of equivalent unbypassed emitter resistance, the nonlinearity of the amplifier was recalculated using the nonlinearity expression given in Table 3.1 (page 40) for the common-emitter amplifier with an unbypassed emitter resistor. The nonlinearity for plus two volts is -8.12% and the nonlinearity for minus two volts is 4.26%. These calculated values of nonlinearity are within 5% of the measured values.

Measurement and Calculation of the Nonlinearity of a Common-Base Amplifier

The test arrangement shown in Figure 3.6 was used to measure the nonlinearity of a common-base amplifier. Since the common-base amplifier is noninverting, an inverting unity-gain amplifier was used to buffer the input of the common-base amplifier from the resistive attenuator. The output impedance of this amplifier must be much less than 1.24 ohms because the nonlinearity of the common-base amplifier configuration is extremely sensitive to impedance in the emitter circuit. The inverting amplifier used in the test arrangement has a measured output impedance of less than 0.14 ohms, which was the limit of the resolution of the impedance measurement. This output impedance was determined from the percent attenuation of a small 10-microsecond pulse when a 10-ohm load was attached to the output of this buffer. A non-inverting, unity-gain amplifier isolates the collector circuit of the common-base amplifier from the input of the current summing circuit. The voltage appearing at the summing node is equal to the magnitude of the nonlinear portion, Del, of the output signal of the common-base amplifier divided by -2.11.

Circuit diagrams of the individual buffer amplifiers are given in Appendix II.

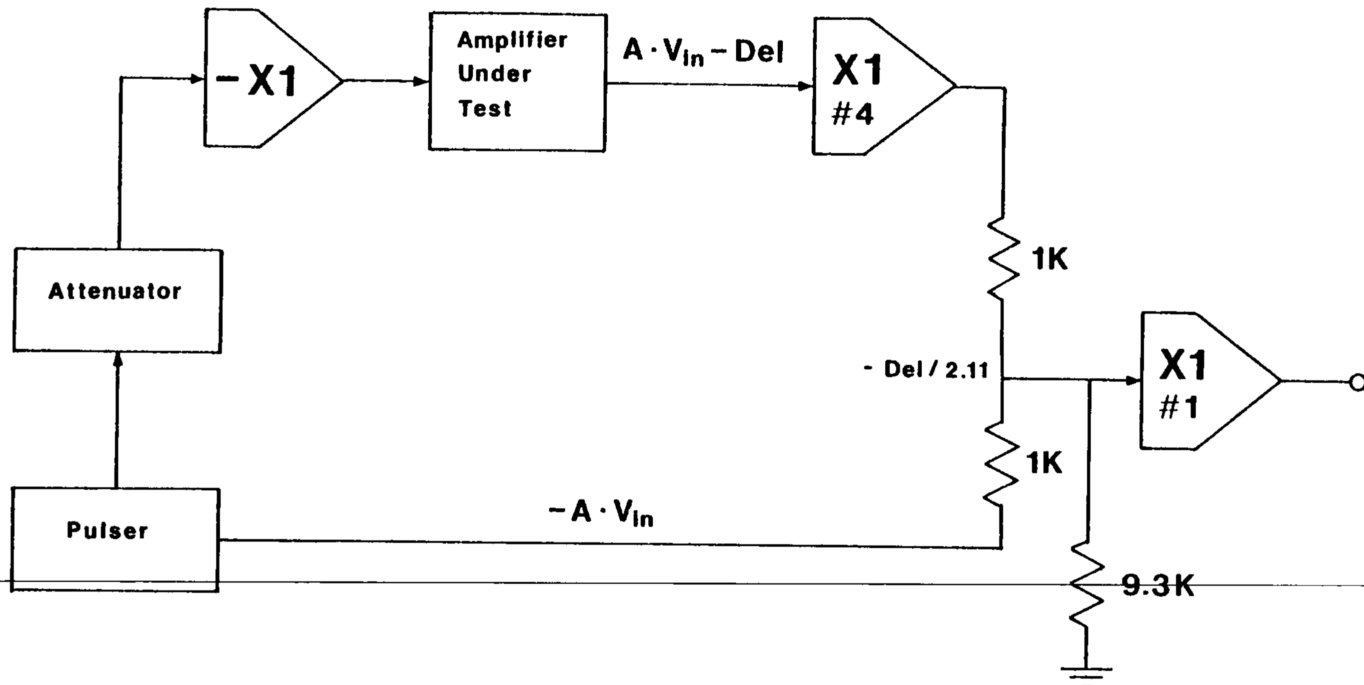

Figure 3.6. Test arrangement used to measure the integral nonlinearity of a common-base amplifier. The variable A is the integral gain of the common-base amplifier, and Del is the nonlinear deviation.

The nonlinearity of the common-base amplifier shown in Figure 3.7 was measured for plus two-volt and minus two-volt signals. The deviation measured from the summing node was 78 millivolts for the plus two-volt pulse, and the deviation at the output of the common-base amplifier was -2.11 times greater, or -164.6 millivolts. The normalized nonlinearity is therefore -8.23% for this output level.

The maximum deviation at the summing node was 43 millivolts for the minus two-volt signal, which corresponds to a 90.7 millivolt deviation at the output of the amplifier. The measured normalized nonlinearity is therefore 4.54% for the second output level.

The nonlinearity of the common-base amplifier was calculated using the expression given in Table 3.1 (page 40) for a common-emitter amplifier with an unbypassed emitter resistor. The value of the unbypassed emitter resistor, 1.24 ohms, was determined in the preceeding section. The value of the variable X is 0.493 when the output is plus two volts and is -0.493 when the output is minus two volts. The calculated nonlinearities are -7.88% for plus two volts and 4.45% for minus two volts. These calculated values of nonlinearity are within 5% of the magnitude of the two measured values.

Measurement and Calculation of Nonlinearity of an Emitter-Follower Amplifier

The test arrangement shown in Figure 3.8 was used to measure the nonlinearity of both an emitter-follower and a bipolar complementary amplifier. A noninverting unity-gain buffer provides a low impedance source to the input of the amplifier under test. The 100 ohm input impedance of the inverting gain-of-twenty amplifier

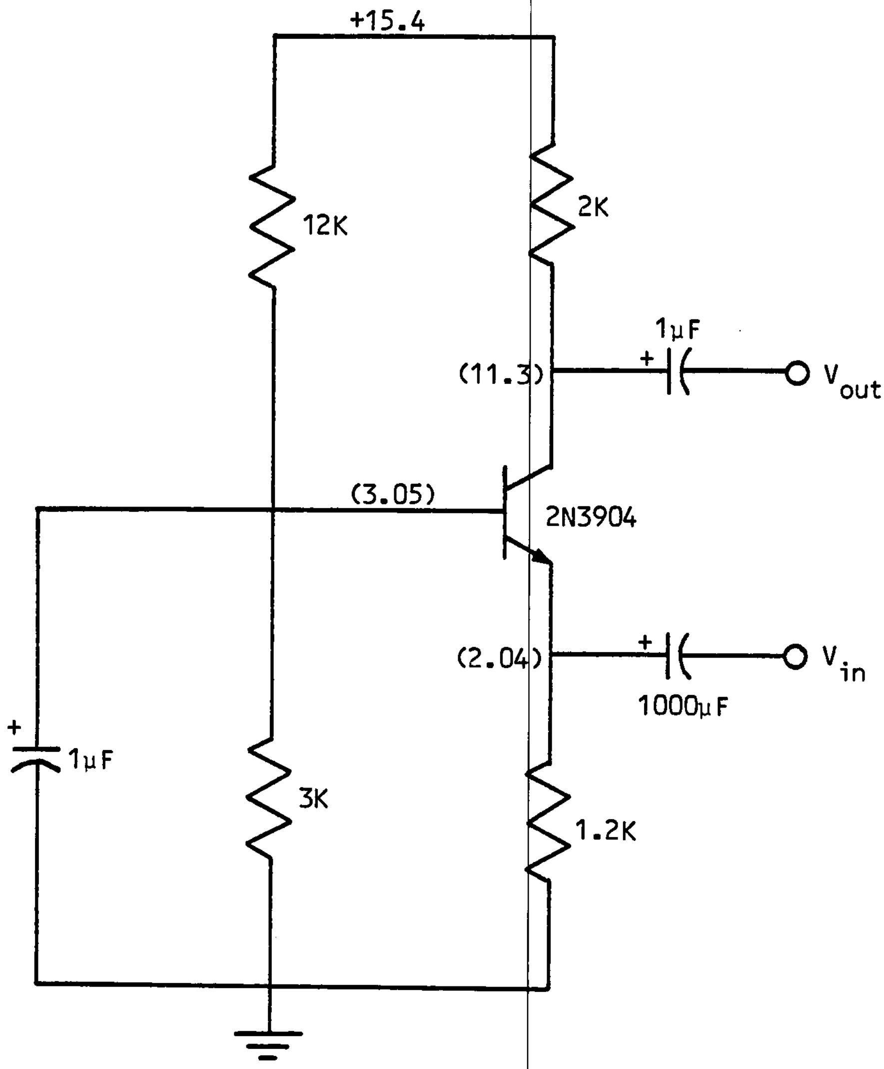

Figure 3.7. Schematic diagram of the common-base amplifier whose integral nonlinearity was measured. Measured bias voltages are given in parenthesis.

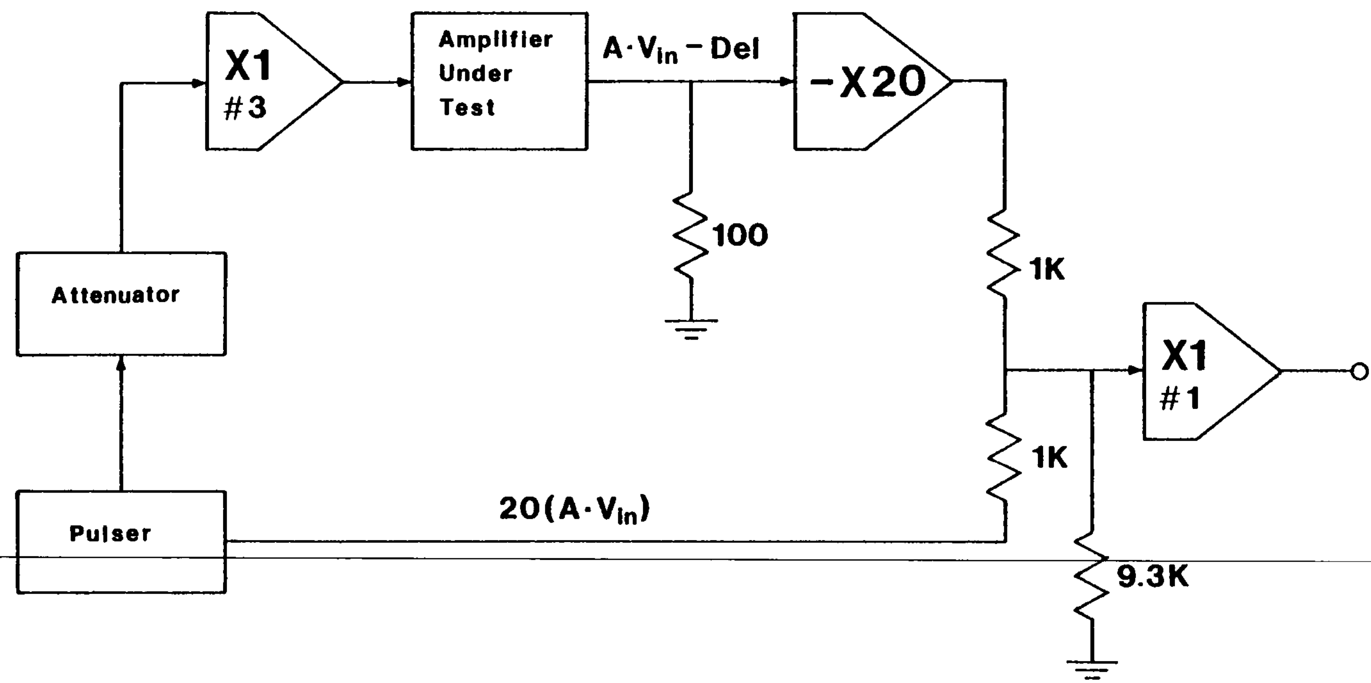

Figure 3.8. Test arrangement used to measure the integral nonlinearity of both an emitter-follower and a bipolar complementary amplifier.

acts as a load for the amplifier under test. The voltage appearing at the summing junction is 9.48 times the nonlinear portion, Del, of the output signal.

The nonlinearity of the emitter-follower amplifier shown in Figure 3.9 was measured for plus 100 millivolts and for minus 100 millivolts across a 100 ohm load. With the plus 100 millivolt output, the maximum deviation at the current summing node was 7.5 millivolts. The maximum deviation at the output of the emitter-follower is 9.48 times smaller, 0.791 millivolts. The nonlinearity of the amplifier is 0.791% for this output level.

With the minus 100 millivolt output, the maximum deviation at the current summing node was 31 millivolts, and the corresponding maximum deviation at the output of the emitter-follower amplifier is 3.27 millivolts. The nonlinearity is therefore -3.27% for this output level.

The nonlinearity of this amplifier was calculated from the expression for the nonlinearity of an emitter-follower amplifier given in Table 3.1 (page 40). The value of the variable X is 0.667 when the output signal is plus 100 millivolts and the value of the variable X is -0.667 when the output voltage is minus 100 millivolts. The calculated nonlinearities are 0.746% for the positive output and -3.01% for the negative output. These calculated values of nonlinearity are within 10% of the values measured.

Measurement and Calculation of the Nonlinearity of a Bipolar Complementary Amplifier

The test arrangement shown in Figure 3.8 was used to measure the nonlinearity of the complementary amplifier shown in Figure 3.10.

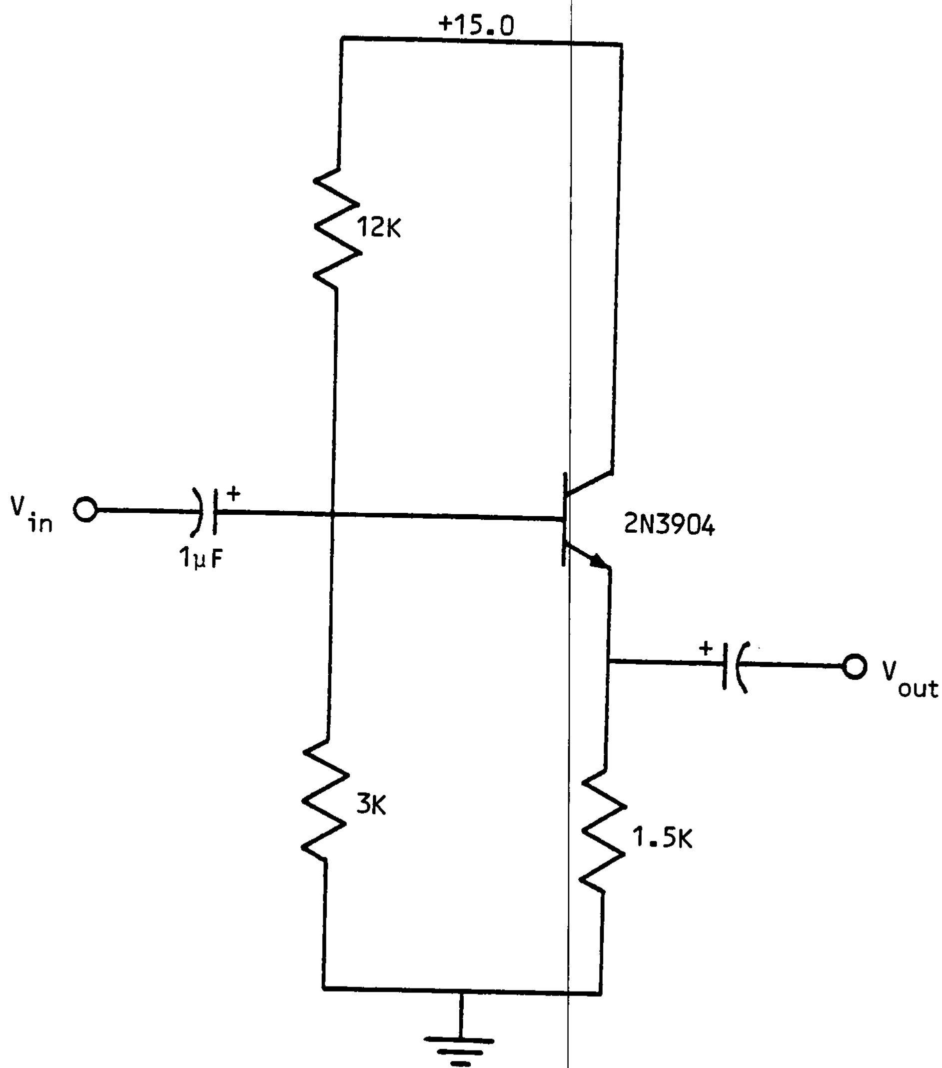

Figure 3.9. Schematic diagram of the emitter-follower amplifier whose integral nonlinearity was measured. Measured bias voltages are in parenthesis.

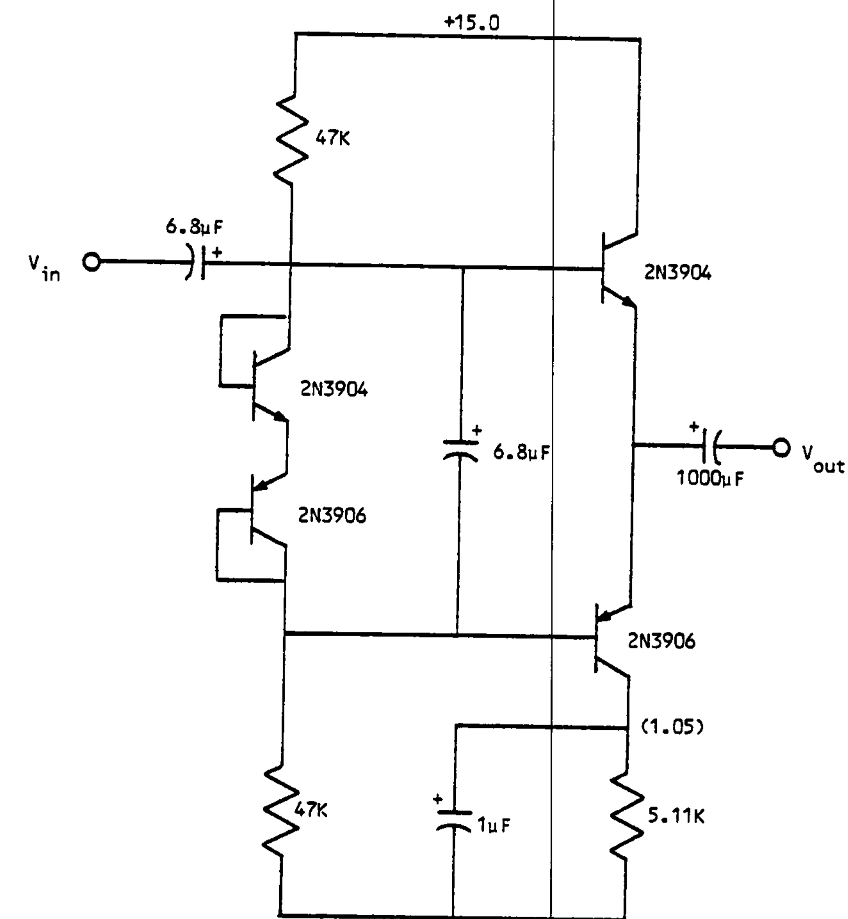

Figure 3.10. Schematic diagram of the bipolar complementary amplifier whose integral nonlinearity was measured. The 5.11 killohm resistor in the collector circuit of the complementary amplifier. The measured bias voltage is given in parenthesis.

The nonlinearity was measured for outputs of plus and minus 100 millivolts across a 100 ohm load resistance. For the plus 100 millivolt output, the maximum deviation at the summing node was 38 millivolts. The maximum deviation at the output of the complementary amplifier is 9.48 times less, or 4.01 millivolts. The nonlinearity of the amplifier is therefore 4.01%.

For the minus 100 millivolt output, the maximum deviation at the summing node was -39.5 millivolts. The maximum deviation at the output of the complementary amplifier is therefore -4.17 millivolts, and the corresponding normalized nonlinearity is 4.17%.

The nonlinearity of this amplifier was calculated from the expression for the nonlinearity of a bipolar complementary amplifier given in Table 3.1 (page 40). The value of the variable X is 4.87 when the output signal is plus 100 millivolts and the value of the variable X is -4.87 with the output signal is minus 100 millivolts. The calculated nonlinearities are 3.97% for both values of X. These calculated values of nonlinearity are within 5% of the values measured.

Summary of Test Results

A summary of the eight nonlinearity tests are given in Table 3.6.

Table 3.6. Summary of nonlinearity test results for several bipolar transistor amplifiers where the measured and calculated values of nonlinearity are compared. The variable X is the ratio of the peak signal current to the initial bias current.

Amplifier Configuration	V_{out}	X	NL measured	NL calculated	% error
Common-emitter amplifier	2.0	0.524	-7.88%	-8.12%	3.0%
	-2.0	-0.524	4.32%	4.26%	1.4%
Common-base amplifier	2.0	0.493	-8.23%	-7.88%	4.3%
	-2.0	-0.493	4.54%	4.45%	2.0%
Emitter-follower amplifier	0.1	0.677	0.791%	0.746%	5.7%
	-0.1	-0.677	-3.27%	-3.01%	8.0%
Bipolar complementary amplifier	0.1	4.87	4.01%	3.97%	1.0%
	-0.1	-4.87	4.17%	3.97%	4.8%

CHAPTER IV

NONLINEARITY OF SEVERAL SINGLE-STAGE JFET AMPLIFIERS

I. INTRODUCTION

The low-frequency nonlinearity of several single-stage JFET amplifiers is investigated in this chapter in detail. The square-law characteristic of the JFET is the source of nonlinearity that is investigated. The input voltage is found as a transcendental function of the output voltage for the common-source, common-gate, source-follower, and JFET differential amplifier configurations. The nonlinearity of these amplifier configurations is then calculated from these equations using a procedure outlined in CHAPTER II (page 14), and the results are tabulated. The nonlinear parameters of these four amplifier configurations are approximated from a two-term polynomial approximation of the transfer function.

Experimental results are included to illustrate the accuracy of the nonlinearity expressions derived in this chapter. The laboratory arrangements are carefully documented. All nonlinearity measurements except one were within 10% of the calculated values.

II. NONLINEARITY DUE TO SQUARE-LAW CHARACTERISTIC OF JFET

The nonlinearity of several single-stage JFET amplifier configurations due to the square-law characteristic of the device is calculated in this section. The nonlinearity expressions are given as transcendental functions of the output voltage and are accurate over large dynamic ranges.

Square-Law Model

The square-law characteristic of the JFET is an empirical relationship [15] between the gate-to-source voltage, V_{gs}, and the drain current, I_d, given by

$$I_d = I_{dss}\left(1 - \frac{V_{gs}}{V_p}\right)^2 \tag{4.1}$$

where I_{dss} is the saturation current (for $V_{gs} = 0$), and V_p is the pinch-off voltage of the device. This approximation is reasonably accurate, and has found wider acceptance than other more complex approximations [17, 18, 32].

Input Voltage Represented as a Function of the Output Voltage for Several Amplifier Configurations

The input voltage must be given as a function of the output voltage to use the procedure outlined in CHAPTER II (page 14) for determining the nonlinearity of the amplifier configurations. These functions are derived in this section for the common-source, common-gate, source-follower, and JFET differential amplifier configurations.

i) Common-Source and Common-Gate Configurations. The change in the drain voltage of a common-source amplifier, V_{out}, can be represented as a function of the change in gate-to-source voltage, V_{in}, by

$$V_{out} = -\frac{I_{dss}R_L}{V_p^{\,2}}\left(V_{in}^{\,2} - 2V_{in}V_p\sqrt{\frac{I_o}{I_{dss}}}\right) \tag{4.2}$$

where I_o is the initial bias current entering the drain of the JFET. The input voltage as a function of the output voltage is obtained from the above equation after completing the square and is

$$V_{in}(V_{out}) = V_p\sqrt{\frac{I_o}{I_{dss}}}\left(1 - \sqrt{1 - \frac{V_{out}}{I_oR_L}}\right). \tag{4.3}$$

For a common-gate amplifier, the polarity of the right-hand side of Equation (4.3) is reversed.

ii) Source-Follower Configuration. For a given change in source voltage, the gate-to-source voltage of a source-follower amplifier must change by an amount Del_{vgs}, where

$$Del_{vgs} = V_p\sqrt{\frac{I_o}{I_{dss}}}\left(1 - \sqrt{1 + \frac{V_{out}}{I_oR_L}}\right) \tag{4.4}$$

and V_{out} is the change in the source voltage. The corresponding input voltage, V_{in}, for that output is then

$$V_{in}(V_{out}) = V_{out} + V_p\left(\frac{I_o}{I_{dss}}\right)\left(1 - \sqrt{1 + \frac{V_{out}}{I_oR_L}}\right). \tag{4.5}$$

iii) JFET Differential Configuration. The model used to find the transfer function of the balanced JFET differential amplifier is shown in Figure 4.1. The bias current, I_o, of the amplifier is the sum of the two source currents. The voltage at the gate of Q_2

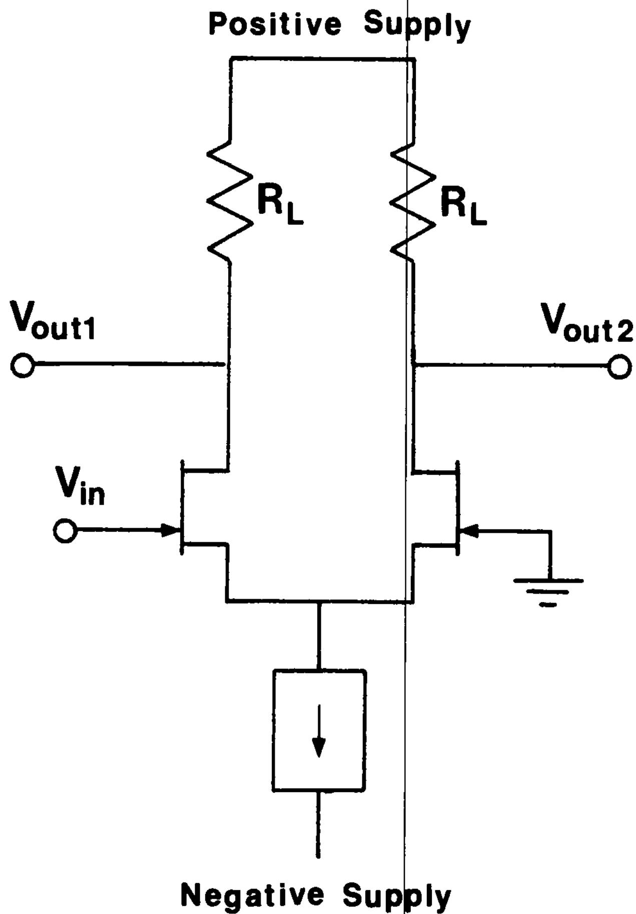

Figure 4.1. Model used to develop the low-frequency transfer function of the JFET differential amplifier.

is arbitrarily chosen to be zero volts, and the differential input voltage is V_{in}. In Appendix III, the output voltage at the drain of transistor Q_1 is shown to be

$$V_{out1} = -V_{in}\left(\frac{I_{dss}R_L}{V_p}\right)\sqrt{\frac{I_o}{2I_{dss}} - \left(\frac{V_{in}}{2V_p}\right)^2}, \tag{4.6}$$

and the output voltage at the drain of transistor Q_2 is shown to be

$$V_{out2} = V_{in}\left(\frac{I_{dss}R_L}{V_p}\right)\sqrt{\frac{I_o}{2I_{dss}} - \left(\frac{V_{in}}{2V_p}\right)^2}. \tag{4.7}$$

With the output voltage at the drain of transistor Q_2 as the independent variable, the input voltage is given by

$$V_{in}(V_{out2}) = V_p\sqrt{\frac{I_o}{I_{dss}}}\sqrt{1 - \sqrt{1 - \left(\frac{2V_{out2}}{I_oR_L}\right)^2}}. \tag{4.8}$$

Evaluation of the Square-Law Nonlinearity of the JFET and Tabulation of Results

The integral nonlinearity due to the square-law characteristics of the JFET was calculated for the common-source, common-gate, and source-follower amplifiers using the procedure outlined in CHAPTER II (page 14) and using Equations (4.3) and (4.5). The salient points of the analysis are given in Table 4.1, and include the integral gain, the output voltage at which the maximum deviation occurs, and the integral nonlinearity. The variable X, which is defined as the ratio of the peak signal current to the initial bias current, has been introduced to simplify the equations given in Table 4.1.

Table 4.1. Salient points of the integral nonlinearity analysis of four single-stage JFET amplifier configurations. The variable $X = (V_m/I_oR_L)$ is introduced to simplify the expressions.

Amplifier configuration	Integral gain	Output at which the maximum deviation occurs	Normalized integral nonlinearity
Common-source	$\dfrac{V_m}{V_p\sqrt{\dfrac{I_o}{I_{ds}}}\,(1 - \sqrt{1 - X})}$	$V_m\left[\dfrac{1}{X} - \dfrac{X}{4(1 - \sqrt{1 - X})^2}\right]$	$\dfrac{1}{2}\left(-\dfrac{1}{X} + \dfrac{\sqrt{1 - X}}{X} + \dfrac{1}{2}\right)$
Common-gate	$\dfrac{V_m}{V_p\sqrt{\dfrac{I_o}{I_{ds}}}\,(\sqrt{1 + X} - 1)}$	$V_m\left[\dfrac{1}{X} - \dfrac{X}{4(1 - \sqrt{1 - X})^2}\right]$	$\dfrac{1}{2}\left(-\dfrac{1}{X} + \dfrac{\sqrt{1 - X}}{X} + \dfrac{1}{2}\right)$
Source-follower	$\dfrac{V_m}{V_m - V_p\sqrt{\dfrac{I_o}{I_{ds}}}\,(\sqrt{1 + X} - 1)}$	$V_m\left[\dfrac{X}{4(\sqrt{1 + X} - 1)^2} - \dfrac{1}{X}\right]$	$\dfrac{-V_p\sqrt{\dfrac{I_o}{I_{ds}}}(\sqrt{1 + X} - 1)}{V_m - V_p\sqrt{\dfrac{I_o}{I_{ds}}}(\sqrt{1 + X} - 1)} \cdot \dfrac{1}{2}\left(-\dfrac{1}{X} + \dfrac{\sqrt{1 - X}}{X} + \dfrac{1}{2}\right)$
Common-source with an un-bypassed source resistor	$\dfrac{V_m}{V_m\left(\dfrac{R_s}{R_L}\right) + V_p\sqrt{\dfrac{I_o}{I_{ds}}}\,(\sqrt{1 - X} - 1)}$	$V_m\left[\dfrac{1}{X} - \dfrac{X}{4(1 - \sqrt{1 - X})^2}\right]$	$\dfrac{V_p\sqrt{\dfrac{I_o}{I_{ds}}}\,(\sqrt{1 - X} - 1)}{V_m\left(\dfrac{R_s}{R_L}\right) + V_p\sqrt{\dfrac{I_o}{I_{ds}}}\,(\sqrt{1 - X} - 1)}$ $\dfrac{1}{2}\left(\dfrac{1}{X} - \dfrac{\sqrt{1 + X}}{X} + \dfrac{1}{2}\right)$

The expressions for the nonlinearity of the JFET differential amplifier configuration could not be simplified by the author, and these expressions became prohibitively complex. Therefore, the midpoint approximation was used to give an expression for the nonlinearity of this amplifier configuration. Since the Taylor series expansion of the static characteristics of this amplifier does not have a second-order term, but does have a third-order term, the midpoint is approximated by $V_m\sqrt{3}$. The nonlinearity parameters of this approximation are given in Table 4.2.

Effect of Unbypassed Source Resistance

The nonlinearity of a common-source amplifier with an unbypassed source resistance may be determined in the same manner that the nonlinearity expression of the common-emitter amplifier with an unbypassed emitter resistor was determined. Since the current gain from the source to the drain of a JFET is a very nearly constant, the nonlinearity of the signals at the source and drain are nearly equal. The nonlinearity expressions given in Table 4.1 for the common-source amplifier with an unbypassed source resistor are determined by representing the source voltage term in the nonlinearity expressions of a source-follower amplifier by a function of the drain voltage.

Table 4.2. Nonlinearity parameters of the JFET differential amplifier configuration from the midpoint approximation. The variable $X = (V_m/I_oR_L)$ is used to simplify the expressions.

Integral gain	Output of max. dev.	Approximate normalized integral nonlinearity
$\dfrac{V_m}{V_p\sqrt{\dfrac{I_o}{I_{dss}}}\sqrt{1-\sqrt{1-4X^2}}}$	$\dfrac{V_m}{\sqrt{3}}$	$\sqrt{\dfrac{1-\sqrt{1-\frac{4}{3}X^2}}{1-\sqrt{1-4X^2}}}-\dfrac{1}{\sqrt{3}}$

III. TWO-TERM POLYNOMIAL APPROXIMATIONS OF THE TRANSFER FUNCTIONS AND NONLINEARITY DUE TO THE SQUARE-LAW CHARACTERISTIC OF SEVERAL SINGLE-STAGE JFET AMPLIFIERS

Two-term polynomials approximating the low-frequency transfer functions of several single-stage JFET amplifiers are given in this section. The integral gain and integral nonlinearity of these amplifier configurations are estimated from the equations derived in CHAPTER II for two-term polynomial functions (Tables 2.1 and 2.2 on pages 23-24). These expressions are simpler to use but are less accurate than the expressions given in Table 4.1. Some of these simplified expressions are used in a later chapter to compare the nonlinearity of certain amplifier configurations.

The input voltages are given as two-term polynomial functions of the output voltages in Table 4.3 for four amplifier configurations. These polynomials are the first two nonzero terms of the Maclaurin series expansions of the expressions which describe the input voltages as functions of the output voltages for these amplifier configurations.

In Table 4.4, the output voltages of the four amplifier configurations are given as two-term polynomial functions of their input voltages. The polynomials for the common-source, common-gate, and balanced JFET differential amplifiers were developed from the expressions describing the output voltages as functions of the input voltages. The polynomial for the source-follower amplifier was developed from the expression describing the input voltage as a function of the output voltage using the procedure described by Equations (3.18), (3.19), and (3.20)(page 44).

Table 4.3. The input voltage represented as a two-term polynomial function of the output voltage for several single-stage JFET amplifiers, plus the integral gain and integral nonlinearity calculated from the polynomials. The variable $X = (V_m/I_oR_L)$ is introduced to simplify the expressions. The term g_m refers to the individual transconductance of each transistor in the differential amplifier case.

Amplifier	Two-term polynomial	Integral gain	Integral nonlinearity
Common-sense	$V_{in} = \left(\frac{-1}{g_mR_L}\right) V_{out} + \left(\frac{-1}{4g_mI_oR_L^2}\right) V_{out}^2$	$\frac{-g_mR_L}{1 + \frac{X}{4}}$	$\frac{-(\frac{X}{16})}{1 + \frac{X}{4}}$
Common-gate	$V_{in} = \left(\frac{1}{g_mR_L}\right) V_{out} + \left(\frac{1}{4g_mI_oR_L^2}\right) V_{out}^2$	$\frac{g_mR_L}{1 + \frac{X}{4}}$	$\frac{-(\frac{X}{16})}{1 + \frac{X}{4}}$
Source-follower	$V_{in} = \left(\frac{g_mR_L + 1}{g_mR_L}\right) V_{out} - \left(\frac{1}{2g_mI_oR_L^2}\right) V_{out}^2$	$\frac{g_mR_L}{g_mR_L + 1 - \frac{X}{2}}$	$\frac{\frac{X}{8}}{g_mR_L + 1 - \frac{X}{2}}$
Balanced JFET differential	$V_{in} = \left(\frac{2}{g_mR_L}\right) V_{out} + \left(\frac{1}{g_mR_L}\right)\left(\frac{1}{I_oR_L}\right)^2 V_{out}^3$	$\frac{g_mR_L}{2 + X^2}$	$-\left(\frac{\sqrt{3}}{9}\right)\frac{X^2}{\left(1 + \frac{X^2}{2}\right)}$

Table 4.4. The output voltage represented as a two-term polynomial function of the input voltage for several single-stage transistor amplifiers, plus the integral gain and integral nonlinearity calculated from the polynomials. The term gm refers to the individual transconductance of each transistor in the differential amplifier case.

Amplifier	Two-term polynomial	Integral gain	Integral nonlinearity
Common-source	$V_{out} = \left(-g_m R_L\right) V_{in} + \left(\frac{I_{dss} R_L}{V_p^2}\right) V_{in}^2$	$-g_m R_L - \left(\frac{I_{dss} R_L}{V_p^2}\right) V_{nm}$	$\dfrac{\left(\frac{V_{nm}}{8}\right)}{\sqrt{\frac{I_o}{I_{dss}}}\, V_p + \left(\frac{V_{nm}}{2}\right)}$
Common-gate	$V_{out} = \left(g_m R_L\right) V_{in} + \left(\frac{I_{dss} R_L}{V_p^2}\right) V_{in}^2$	$g_m R_L + \left(\frac{I_{dss} R_L}{V_p^2}\right) V_{nm}$	$\dfrac{\left(-\frac{V_{nm}}{8}\right)}{\sqrt{\frac{I_o}{I_{dss}}}\, V_p - \left(\frac{V_{nm}}{2}\right)}$
Source-follower	$V_{out} = \left(\frac{g_m R_L}{g_m R_L + 1}\right) V_{in} + \left[\frac{g_m^2 R_L}{4 I_o (g_m R_L + 1)^3}\right] V_{in}^2$	$\left(\frac{g_m R_L + 1}{g_m R_L}\right) + \dfrac{g_m^2 R_L V_{nm}}{4 I_o (g_m R_L + 1)^3}$	$\dfrac{\left(\frac{g_m}{4 I_o}\right) V_{nm}}{4(g_m R_L + 1)^2 + \left(\frac{g_m}{I_o}\right) V_{nm}}$
Balanced JFET differential	$V_{out} = \left(\frac{g_m R_L}{2}\right) V_{in} - \frac{g_m R_L}{16} \left(\frac{g_m}{I_o}\right)^2 V_{in}^3$	$\frac{g_m R_L}{2} - \frac{g_m R_L}{16} \left(\frac{g_m V_{nm}}{I_o}\right)^2$	$\frac{1}{12\sqrt{3}} \left[\dfrac{-\left(\frac{g_m V_{nm}}{I_o}\right)^2}{1 - \frac{1}{8}\left(\frac{g_m V_{nm}}{I_o}\right)^2}\right]$

IV. DETERMINING THE ACCURACY OF THE NONLINEARITY EXPRESSIONS WITH LABORATORY MEASUREMENTS

The nonlinearity of several JFET amplifiers was measured to test the accuracy of the expressions developed in this chapter. The nonlinearity of a common-source, a common-gate, and a source-follower amplifiers was measured using a current-summing technique described in CHAPTER III (page 54). These measured values of nonlinearity are compared to values of nonlinearity calculated from expressions given in Table 4.1 (page 75).

Measurement and Calculation of Nonlinearity of a Common-Source Amplifier

The test arrangement used to measure the nonlinearity of a common-source amplifier is the same arrangement used to measure the nonlinearity of a common-emitter amplifier and is shown in Figure 3.4 (page 56). A description of this test arrangement is given on page 54.

The circuit diagram of the common-source amplifier is shown in Figure 4.2. This amplifier has been cascoded into a common-base amplifier to maintain a relatively constant drain-to-source voltage. The magnitude of the drain current of a JFET depends on the drain-to-source voltage to some extent, and this variation has not been accounted for in the modeling of the device. The added nonlinearity of the common-base stage is accounted for in the linearity calculations.

The nonlinearity of this amplifier was measured for outputs of plus two and minus two volts. For an output of plus two volts,

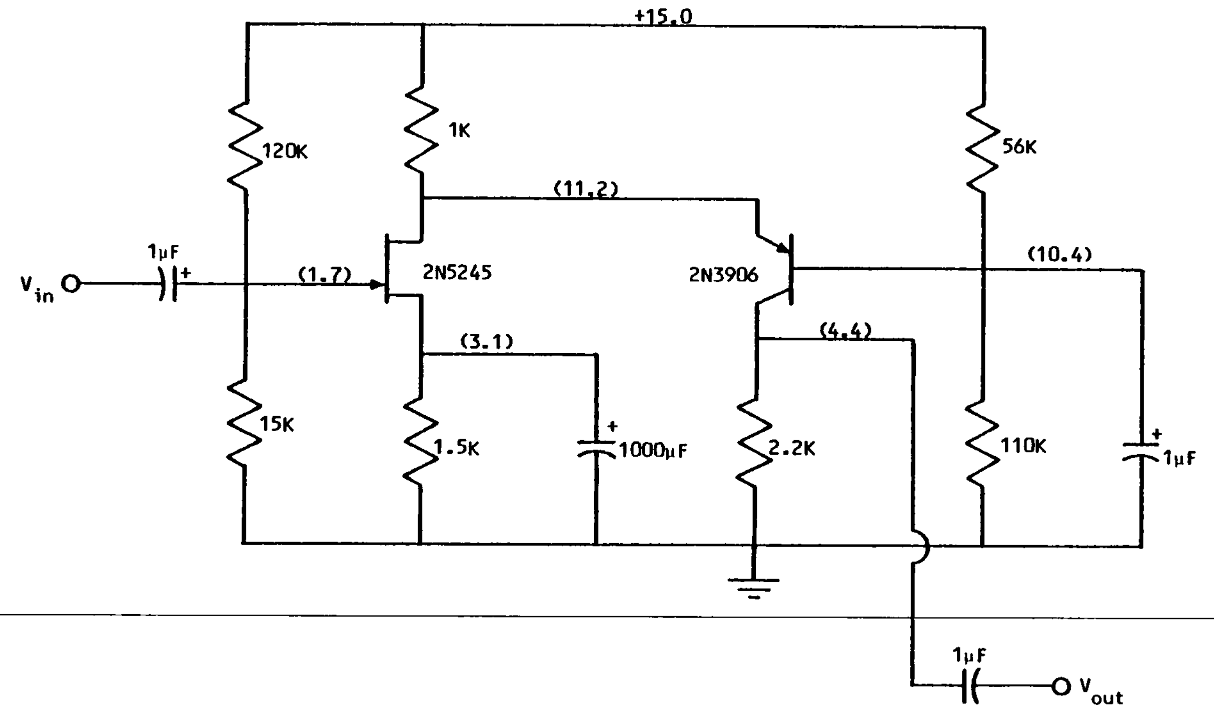

Figure 4.2. Common-source amplifier used to test the accuracy of the expression for integral nonlinearity given in Table 4.1 (page 75). The common-source amplifier is cascoded into a common-base amplifier to maintain a constant drain-to-source voltage. Measured bias values are given in parenthesis.

the maximum deviation measured at the summing node of the test arrangement was 27.5 millivolts. The maximum deviation at the output of the amplifier was 2.16 times greater, or 59.4 millivolts. The normalized nonlinearity of the amplifier is therefore -2.97% for this output level.

With an output of minus two volts, the maximum deviation measured at the summing node was 16 millivolts. The maximum deviation at the output of the amplifier was 2.16 times greater, or 34.56 millivolts, and the normalized nonlinearity of the amplifier is 1.73% for this output level.

The characteristics of the JFET with five volts from drain to source are

$$I_{dss} = 13.3 \text{ mA} \qquad \text{(a)}$$

$$V_p = -2.453 \text{ V} \qquad \text{(b)}$$

$$R_s = 71 \text{ ohms,} \qquad \text{(c)} \qquad (4.9)$$

where I_{dss} is the projected zero-bias drain current of the JFET, V_p is the pinch-off voltage of the device, and R_s is the value of the unbypassed source resistance intrinsic to the individual device. A description of the measurement of these parameters is given in Appendix III.

The nonlinearity of the common-source amplifier stage shown in Figure 4.2 was calculated using the expression for nonlinearity given in Table 4.1 (page 75) for the common-source amplifier with an unbypassed source resistor. The value of the variable X, which is the ratio of the peak signal current to the initial bias current, for the common-source stage is 0.446 when the output is plus two volts, and is -0.446 when the peak value of the output is minus two volts. The calculated value of nonlinearity of the common-source amplifier stage is -0.290%, and the calculated value of nonlinearity of the common-base amplifier stage is +0.05% for the plus two-volt output signal. The total nonlinearity for the amplifier is the sum, or -2.85%. For the minus two-volt output signal, the calculated values of nonlinearity of the common-source and common-base amplifiers are +1.72% and -0.13% respectively or 1.59% total. The calculated values of nonlinearity are within 10% of the measured values of nonlinearity.

Measurement and Calculation of Nonlinearity of a Common-Gate Amplifier

The test arrangement used to measure the nonlinearity of a common-gate amplifier is the same arrangement used to measure the nonlinearity of a common-base amplifier and is shown in Figure 3.6 (page 61). A description of this test arrangement is given on page 60.

The nonlinearity of the common-gate amplifier shown in Figure 4.3 was measured for plus two-volt and minus two-volt output signals. This circuit is the same as the common-source amplifier except that the gate is A.C. coupled to ground and the input signal is applied to the source terminal. The deviation at the summing node of the test arrangement was 28.5 millivolts for the plus two-volt output signal, and the deviation at the output of the cascode amplifier was -2.11 times greater, or -60.1 millivolts. The

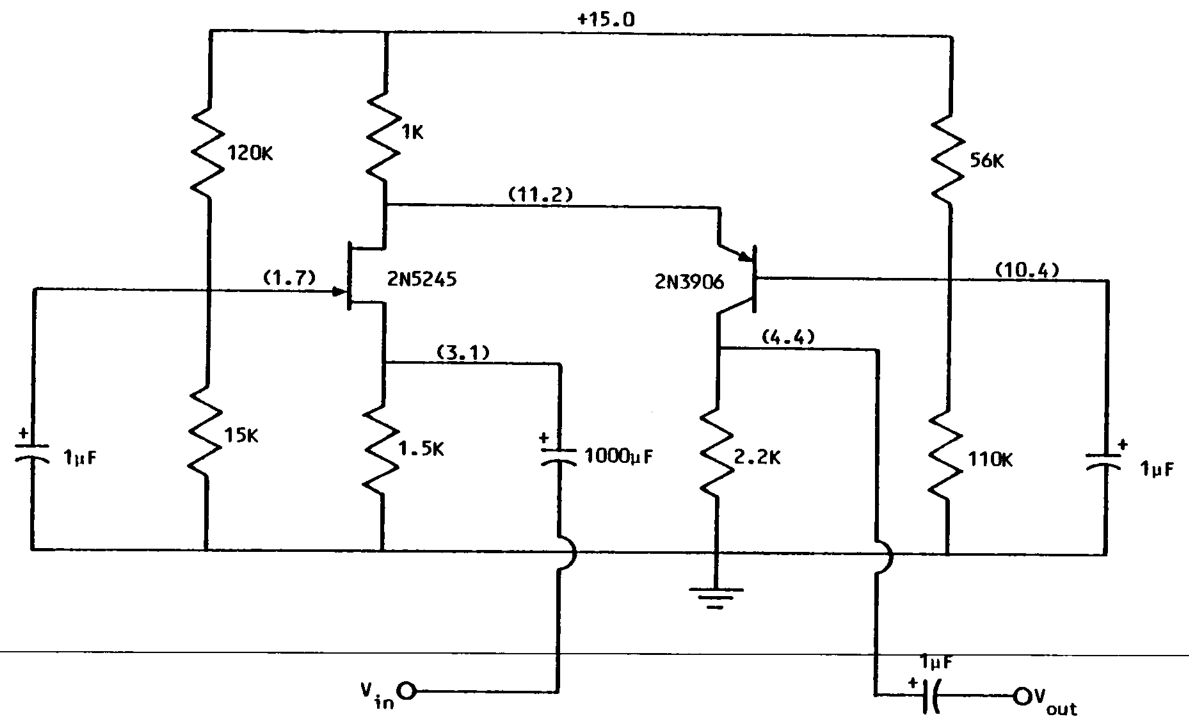

Figure 4.3. Common-gate amplifier used to test the accuracy of the expressions for integral nonlinearity given in Table 4.1 (page 75). The common-gate amplifier is cascoded into a common-base amplifier to maintain a constant drain-to-source voltage. Measured bias values are given in parenthesis.

measured normalized nonlinearity is therefore -3.01% for this output level.

The maximum deviation at the summing node was 16.25 millivolts for the minus two-volt signal, which corresponds to a -34.4 millivolt deviation at the output of the amplifier. The normalized value of nonlinearity at this output level is 1.71%.

The calculated values of nonlinearity for the common-gate amplifier are the same as those for the common-source amplifier. The calculated values of nonlinearity are -2.85% for the plus two-volt output level and 1.59% for the minus two-volt output level. These values of calculated and measured nonlinearities agree within 10%.

Measurement and Calculation of Nonlinearity of a Source-Follower Amplifier

The test arrangement used to measure the nonlinearity of a source-follower amplifier is the same arrangement used to measure the nonlinearity of an emitter-follower amplifier and is shown in Figure 3.8 (page 64). A description of this test arrangement is given on page 62.

The nonlinearity of the source-follower amplifier shown in Figure 4.4 was measured for plus 100 millivolts and minus 100 millivolts output signals across a 100 ohm load. With the plus 100 millivolt output, the maximum deviation at the current summing node was 12.0 millivolts. The maximum deviation at the output of the source-follower amplifier is 9.48 times smaller, or 1.27 millivolts. The normalized nonlinearity of the source-follower amplifier is, therefore, 1.27% for this output level.

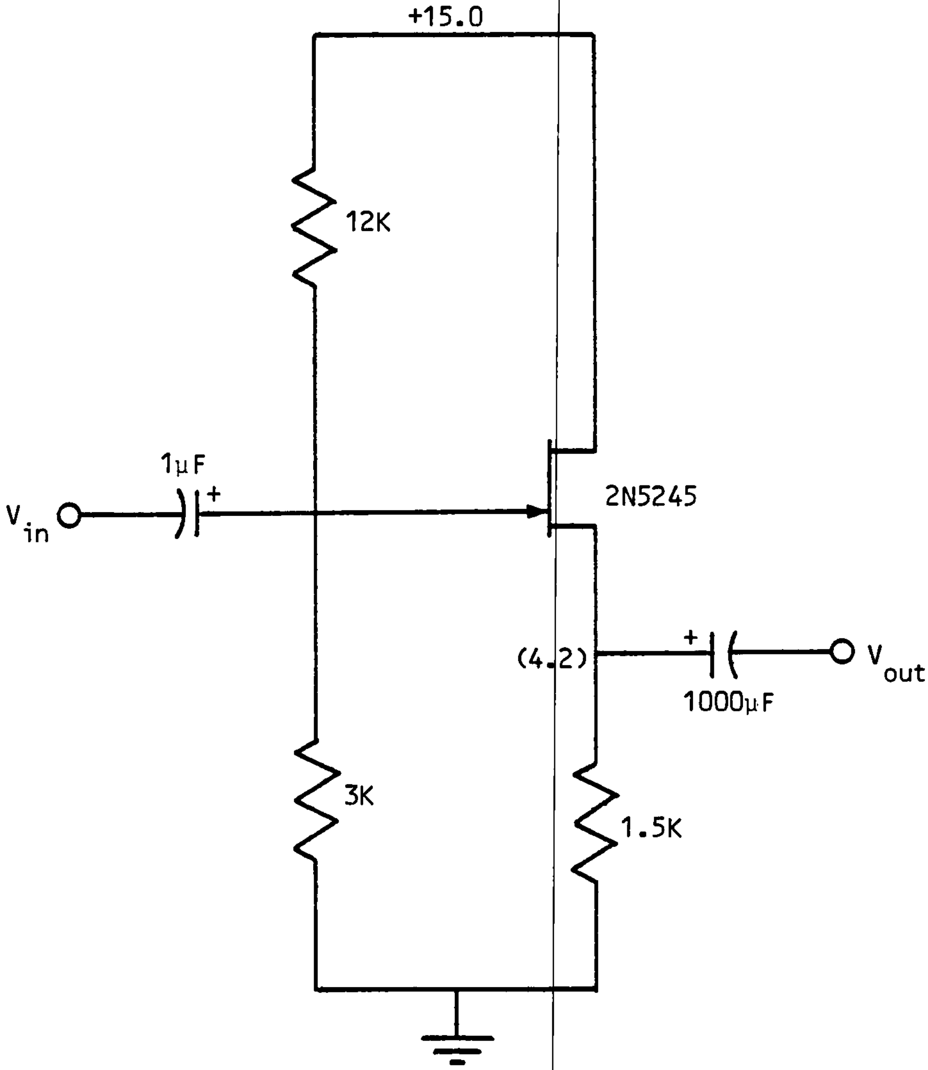

Figure 4.4. Schematic diagram of the source-follower amplifier used to test the accuracy of the expression for integral nonlinearity given in Table 4.1 (page 75). A measured bias value is given in parenthesis.

With the minus 100 millivolt output, the maximum deviation at the current-summing node was 16.5 millivolts, and the corresponding maximum deviation at the output of the source-follower amplifier is 1.68 millivolts. The normalized nonlinearity of the source-follower amplifier is therefore -1.68% at this output level.

The measured characteristics of the individual JFET used in the source-follower amplifier are described in Equation 4.9 (page 83) The 1.5 killohm source resistor in parallel with the 100 ohm input impedance of the inverting amplifier in the test arrangement is an equivalent load resistance of 93.8 ohms. This load is in series with the unbypassed source resistance of 71 ohms which is intrinsic to the individual device used in the amplifier. The maximum value of the signal at the metalurgial junction is then

$$V_m = \pm 100 \text{ mV}\left(\frac{93.8 + 71}{93.8}\right) = \pm 176 \text{ mV}. \tag{4.10}$$

The calculated values of nonlinearity from the expression given in Table 4.1 (page 75) for a source-follower amplifier are 1.06% for plus 100 millivolts and -1.73% for minus 100 millivolts. The calculated value of nonlinearity is 16% less than the measured value for the plus 100 millivolt output. The source of this unusually large error is not known. The calculated and measured values of nonlinearity agree within 5% for the minus 100 millivolt output.

Summary of Test Results

A summary of the six nonlinearity tests are given in Table 4.5.

Table 4.5 Summary of nonlinearity test results for several JFET amplifiers where measured and calculated values of nonlinearity are compared. The variable X is the ratio of peak signal current to the initial bias current.

Amplifier configuration	V_{out}	X	NL measured	NL calculated	% error
Common-source amplifier	2.0	0.446	-2.97%	-2.85%	4.2%
	-2.0	-0.446	1.73%	1.59%	8.8%
Common-gate amplifier	2.0	0.446	-3.01%	-2.85%	5.3%
	-2.0	-0.446	1.71%	1.59%	7.0%
Source-follower amplifier	0.1	0.381	1.27%	1.06%	16.5%
	-0.1	-0.381	-1.68%	-1.73%	3.0%

CHAPTER V

COMPARISON OF NONLINEARITY OF SIMILAR TYPE AMPLIFIER CONFIGURATIONS

I. INTRODUCTION

The nonlinearities produced by similar type amplifiers are compared in this section. These nonlinearities are compared for equal values of output voltage and for equal values of the variable X, the ratio of the peak signal current to the initial bias current. This comparison is particularly useful for the unity-gain type amplifiers which are typically used for output stages of multistage amplifiers. In this category, the nonlinearity of the bipolar complementary amplifier is shown to be less than the nonlinearity of the emitter-follower amplifier. Also, the nonlinearity of the emitter-follower amplifier is shown to be less than the nonlinearity of the source-follower amplifier for most practical situations.

For the given criteria, the nonlinearity of the common-source amplifier configuration is shown to be approximately half of the nonlinearity of the common-emitter amplifier configuration. However, the criteria used for the comparison may not be valid for certain situations. If the value of the transconductance of the device is important in the amplifier design, then a different criteria for comparing the nonlinearity of these amplifier configurations should be used.

II. COMPARISON OF COMMON-SOURCE TO COMMON-EMITTER AMPLIFIER CONFIGURATIONS

A simplification in the nonlinearity analysis for the common-emitter amplifier gives a nonlinearity expression that is very similar to the nonlinearity expression of a common-source amplifier. The maximum deviation from a linear response occurs near midscale for most amplifiers. By calculating the deviation at one-half of the maximum output signal, the nonlinearity expression for a common-emitter amplifier can be simplified to

$$NL_{ce} \cong \frac{1}{2} + \frac{\sqrt{1 - X}}{X} - \frac{1}{X}. \tag{5.1}$$

This approximation is within 4% of the nonlinearity predicted by a more exact analysis for values of X from -0.9 to 10.0. This approximation for the nonlinearity of a common-emitter amplifier is easily compared with the nonlinearity expression for a common-source amplifier,

$$NL_{cs} = \frac{1}{4} + \frac{\sqrt{1 - X}}{2X} - \frac{1}{2X}. \tag{5.2}$$

Within the accuracy of the approximation, a common-source amplifier has one-half the integral nonlinearity of a comparable common-emitter amplifier.

III. COMPARISON OF SOURCE-FOLLOWER TO EMITTER-FOLLOWER AMPLIFIER CONFIGURATIONS

Using the similarity between the nonlinearity equation for a common-emitter amplifier and the nonlinearity equation for an emitter-follower amplifier, and by further assuming that

$$V_m >> \frac{kT}{q} \ln(1 + X) \tag{5.3}$$

the integral nonlinearity of an emitter-follower amplifier can be approximated by

$$NL_{ef} \cong \frac{\frac{kT}{q} \ln(1 + X)}{V_m} \left(\frac{1}{2} - \frac{\sqrt{1 + X}}{X} + \frac{1}{X}\right). \tag{5.4}$$

By assuming that

$$V_m >> V_p \sqrt{\frac{I_o}{I_{dss}}} \left(\sqrt{1 + X} - 1\right), \tag{5.5}$$

the nonlinearity of a source-follower amplifier can be approximated by

$$NL_{sf} \cong \frac{V_p \sqrt{\frac{I_o}{I_{dss}}} \left(\sqrt{1 + X} - 1\right)}{2V_m} \left(\frac{1}{2} - \frac{\sqrt{1 + X}}{X} + \frac{1}{X}\right). \tag{5.6}$$

Using the approximations given in Equations (5.4) and (5.6) above, the ratio of the integral nonlinearity of a source-follower amplifier to the integral nonlinearity of an emitter-follower amplifier is approximately

$$\frac{NL_{sf}}{NL_{ef}} \cong \frac{V_p \sqrt{\frac{I_o}{I_{dss}}}}{\frac{2kT}{q}} \cdot \left[\frac{\sqrt{1 + X} - 1}{\ln(1 + X)}\right]. \tag{5.7}$$

The term in brackets in this equation is a slowly varing function of X and is initially 0.5. Therefore, Equation (5.7) indicates that an emitter-follower amplifier will be more linear than a source-follower amplifier unless the term $(V_p\sqrt{I_o/I_{dss}}$ is less than approximately 0.1 volts, a condition that would require the JFET to be biased at less than one percent of its saturation current, I_{dss}.

For output voltages less than 0.026 volts, the approximations made above the emitter-follower amplifier given by Equation (5.4) and for the source-follower amplifier given by Equation (5.6) are not valid. The nonlinearity of an emitter-follower amplifier can be twice as large as the nonlinearity of a comparable source-follower amplifier when the output voltage is nearly zero. The nonlinearities of the two amplifier configurations are nearly equal when

$$V_{out} \cong 26 \text{ mV} \left(X - \frac{1}{2}X^2\right) \tag{5.8}$$

and X is less than unity.

IV. COMPARISON OF EMITTER-FOLLOWER TO BIPOLAR COMPLEMENTARY AMPLIFIER CONFIGURATIONS

The integral nonlinearity of an emitter-follower amplifier can be compared to the nonlinearity of a bipolar complementary amplifier for values of X less than unity. When the value of X is less than unity, the integral nonlinearity expression for the emitter-follower amplifier can be approximated by

$$NL_{ef} \cong \frac{\frac{kT}{q}}{V_m + \frac{kT}{q}\ln(X+1)} \cdot \frac{X^2}{8} \tag{5.9}$$

and the integral nonlinearity equation for the bipolar complementary amplifier can be approximated by

$$NL_{cp} \cong \frac{\frac{kT}{q}}{V_m + \frac{kT}{q}\sinh^{-1}\left(\frac{X}{2}\right)} \cdot \frac{X^3}{36\sqrt{12}} \tag{5.10}$$

where the higher order terms of a power expansion of the equations have been eliminated as small. Whenever the peak signal voltage, V_m, is much greater than 26 mV, the ratio of the two approximations is

$$\frac{NL_{ef}}{NL_{cp}} = \frac{9\sqrt{3}}{X}. \tag{5.11}$$

This ratio indicates that a complementary amplifier is much more linear than a comparable emitter-follower whenever the value of X is less than unity. For values of X greater than unity, several comparisons of calculated nonlinearities indicates that the linearity of an emitter-follower amplifier slowly approaches that of a comparable complementary amplifier.

The bipolar complementary amplifier configuration is the most linear of the three unity-gain type amplifiers investigated.

CHAPTER VI

SPECTRAL DEPENDENCE OF INTEGRAL NONLINEARITY

I. INTRODUCTION

The integral nonlinearity of a waveform changes when the waveform goes through a frequency-dependent transfer function. A process for estimating this nonlinearity change is outlined in this section for second-order and third-order two-term polynomial nonlinearities. The process is applied to three example waveforms and the results of this analysis are compared to computer simulations.

The results of this analysis for the two-term polynomial nonlinearities are generalized such that these results can be extended to more complex nonlinearities with little additional analysis. The accuracy of this generalization is then tested by computer simulations for three sample functions from three different single-stage amplifiers.

II. SPECTRAL DEPENDENCE OF SECOND-ORDER AND THIRD-ORDER TWO-TERM POLYNOMIAL NONLINEARITIES

A procedure is given in this section for calculating the change in nonlinearity of a pulse that passes through a frequency-dependent transfer function.

The nonlinearity of a waveform is calculated at the peak value of that waveform. Since the waveshape can change drastically with a frequency-dependent transfer function, the input waveform and the output waveform can peak at significantly different times.

Therefore, the nonlinearity of the input is calculated at the time the input signal peaks, and the nonlinearity of the output is calculated at the time the output signal peaks.

Consider a linear waveform, $V\ f(t)$, where $f(t)$ is a normalized wave-form whose peak value of unity occurs at the t_{peak1}. A second-order nonlinearity then produces the nonlinear waveform

$$P(t) = V\ f(t) + N \cdot V^2 f^2(t) \tag{6.1}$$

where $f^2(t)$ has a peak value of unity at t_{peak1}. The nonlinearity of this waveform is

$$NL_n = \frac{N \cdot V}{4(1 + N \cdot V)} \cdot \tag{6.2}$$

The magnitude of this nonlinearity will change when the wave-form passes through a frequency-dependent function. Let the Laplace transform of P(t) be represented by

$$P(s) = V\ F_a(S) + N \cdot V^2 F_b(S), \tag{6.3}$$

where

$$F_a(S) = L[f(t)] \tag{6.4}$$

and

$$F_b(S) = L[f^2(t)]. \tag{6.5}$$

The Laplace transform of the output signal is

$$O(S) = V[F_a(S)\ H(S)] + N \cdot V^2\ [F_b(S)\ H(S)] \tag{6.6}$$

where H(S) is the frequency dependent transfer function. The nonlinear output waveform as a function of time is

$$O(t) = V\ G_a(t) + N \cdot V^2\ G_b(t), \tag{6.7}$$

where

$$G_a(t) = L^{-1}[F_a(S)\ H(S)] \tag{6.8}$$

and

$$G_b(t) = L^{-1}[F_b(S)\ H(S)]. \tag{6.9}$$

If the output waveform peaks at a time t_{peak2}, then the nonlinearity of the output waveform is

$$NL_o = \frac{A \cdot N \cdot V}{4(1 + A \cdot N \cdot V)} \tag{6.10}$$

where the variable A is defined by

$$A \equiv \frac{G_b(t_{peak2})}{G_a(t_{peak2})}\ . \tag{6.11}$$

After solving Equation (6.2) for NV as a function of NL_n and substituting into Equation (6.10), the magnitude of the output nonlinearity can be written as a function of the magnitude of the input nonlinearity by

$$NL_o = \frac{NL_n}{1 - 4\ NL_n(1 - A)}\ . \tag{6.12}$$

The procedure for determining the change in the nonlinearity of a third-order nonlinear waveform is the same as that used for a second-order nonlinear waveform. Given the third-order nonlinear input waveform

$$Q(t) = V\ f(t) + N \cdot V^3\ f^3(t), \tag{6.13}$$

the magnitude of the nonlinearity of this waveform is

$$NL_n = \frac{N \cdot V^2}{\frac{3\sqrt{3}}{2}(1 + N \cdot V^2)}. \tag{6.14}$$

If the Laplace transform of $f^3(t)$ is represented by

$$F_c(S) = L[f^3(t)], \tag{6.15}$$

and the inverse transform of the nonlinear portion of the output signal by

$$G_c(t) = L^{-1}[F_c(S)\ H(S)], \tag{6.16}$$

then the nonlinearity of the output waveform is

$$NL_o = \frac{B \cdot N \cdot V^2}{\frac{3\sqrt{3}}{2}(1 + B \cdot N \cdot V^2)}, \tag{6.17}$$

where the term B is defined by

$$B \equiv \frac{G_c(t_{peak2})}{G_a(t_{peak2})}. \tag{6.18}$$

The nonlinearity of the output waveform as a function of the nonlinearity of the input waveform is

$$NL_o = \frac{NL_n}{1 - \frac{3\sqrt{3}}{2} NL_n (1 - B)} . \tag{6.19}$$

III. THE CHANGE IN NONLINEARITY OF A SAMPLE WAVEFORM

The procedure given in the previous section to determine the change of nonlinearity of a pulse is illustrated here with an example waveform and example frequency-dependent function. The example nonlinear input waveform is

$$P(t) = V\left[\left(1 - \frac{t}{\tau}\right)e^{-\frac{t}{\tau}}\right] + N \cdot V^2\left[\left(1 - \frac{t}{\tau}\right)^2 e^{-\frac{2t}{\tau}}\right]. \tag{6.20}$$

The example frequency-dependent function is an ideal integrator whose Laplace transform is

$$H(S) = \frac{1}{SC} . \tag{6.21}$$

The Laplace transform of the nonlinear output waveform is then

$$O(S) = \frac{V}{C}\left[\frac{1}{\left(S + \frac{1}{\tau}\right)^2}\right] + \frac{N \cdot V^2}{C}\left[\frac{S^2 + \left(\frac{2}{\tau}\right)S + \left(\frac{2}{\tau}\right)^2}{S\left(S + \frac{2}{\tau}\right)^3}\right], \tag{6.22}$$

and the nonlinear output waveform as a function of time is

$$O(t) = \frac{V\tau}{C}\left[\frac{t}{\tau}\, e^{-\frac{t}{\tau}}\right] + \frac{N \cdot V^2 \cdot \tau}{C}\Bigg\{\frac{1}{4} +$$

$$\left[-\frac{1}{2}\left(\frac{t}{\tau}\right)^2 + \frac{1}{2}\left(\frac{t}{\tau}\right) - \frac{1}{4}\right]e^{-\frac{2t}{\tau}}\Bigg\}. \tag{6.23}$$

A sketch of the linear and nonlinear portions of the input waveform are shown in Figure 6.1. The input waveform peaks at zero seconds, and the normalized nonlinearity of the waveform at this time is

$$NL_n = \frac{N \cdot V}{4(1 + N \cdot V)}. \tag{6.24}$$

A sketch of the linear and nonlinear portions of the output waveform are shown in Figure 6.2. This output waveform peaks at approximately τ seconds. At this time, the magnitude of the linear portion of the output is

$$G_a(\tau) \cong \frac{V \cdot \tau}{C}\,(0.3679). \tag{6.25}$$

The magnitude of the nonlinear portion of the output waveform at this time is

$$G_b(\tau) \cong \frac{N \cdot V^2 \cdot \tau}{C}(0.2162). \tag{6.26}$$

The normalized nonlinearity of the output waveform is therefore

$$NL_o \cong \frac{N \cdot V\ (0.2162)}{4(0.3679)\left[1 + \dfrac{N \cdot V\ (0.2162)}{(0.3679)}\right]}. \tag{6.27}$$

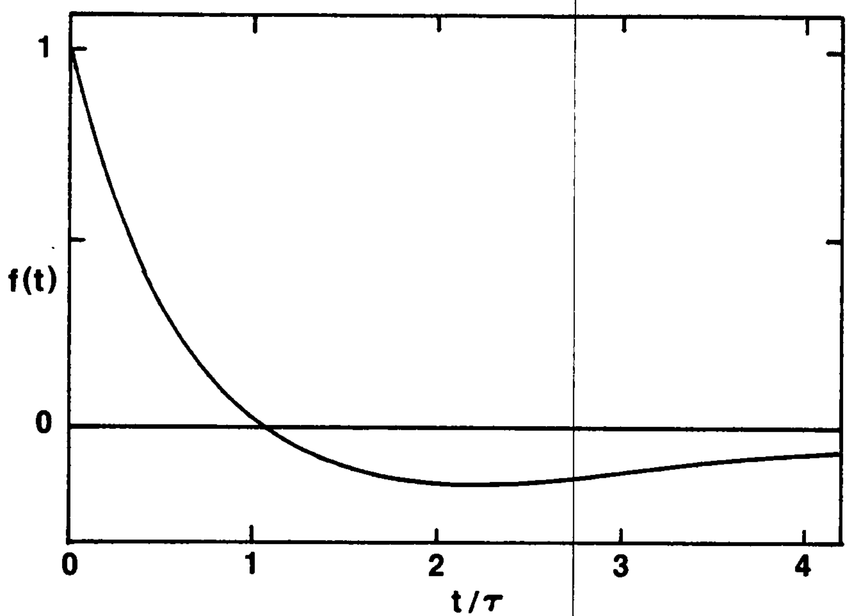

a) Linear portion of input waveform

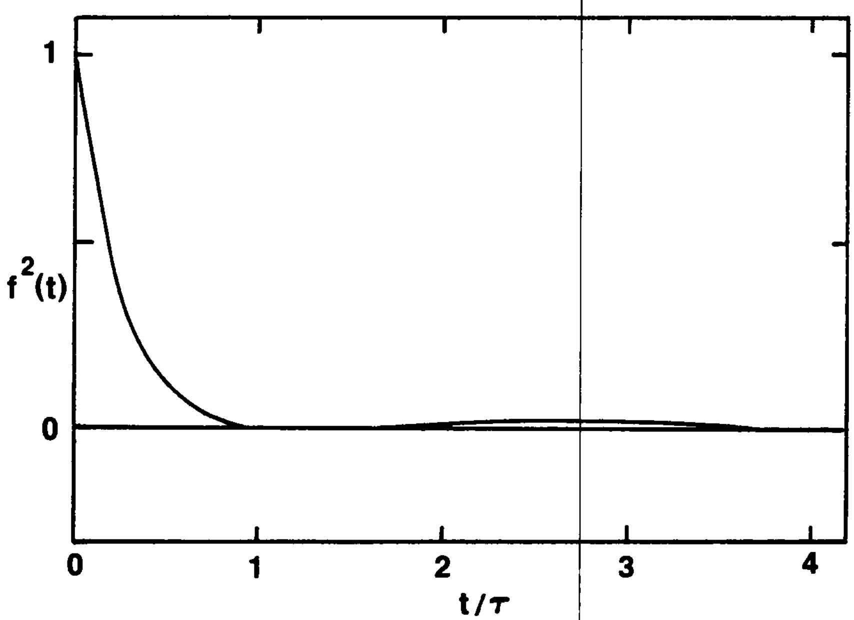

b) Nonlinear portion of input waveform

Figure 6.1. Linear and nonlinear components of input waveform that is used for illustration.

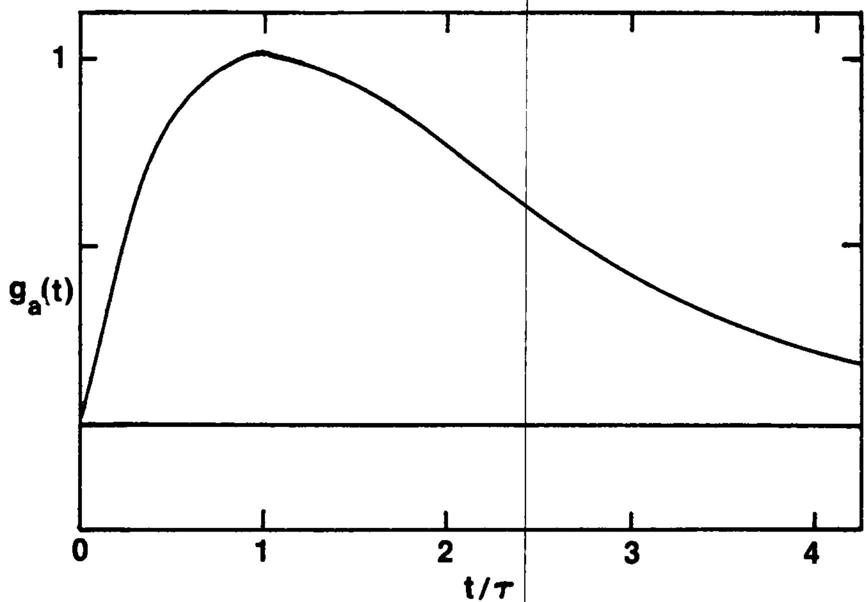

a) Linear portion of output waveform

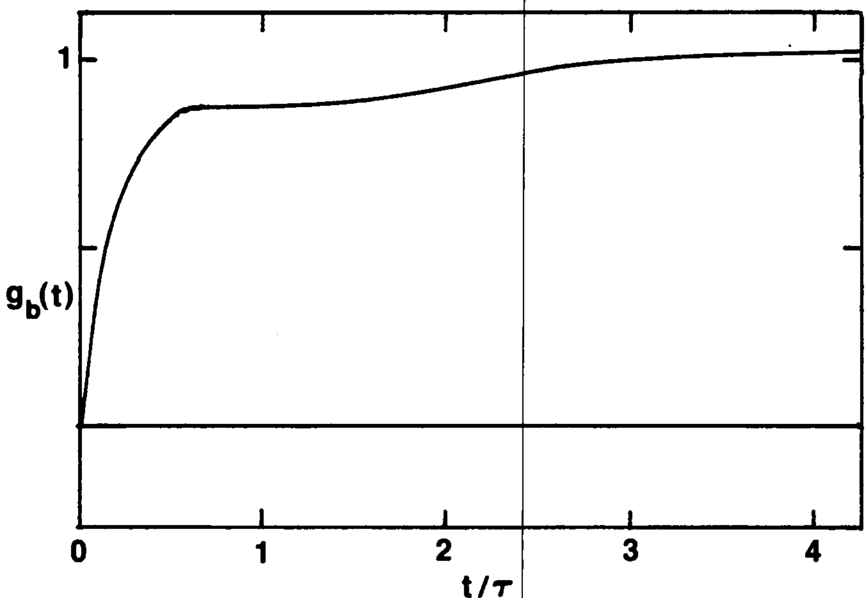

b) Nonlinear portion of output waveform

Figure 6.2. Linear and nonlinear components of the output waveform that is used for illustration.

The ratio of the output nonlinearity to the input nonlinearity is

$$\frac{NL_o}{NL_n} = \frac{0.5877(1 + N \cdot V)}{(1 + 0.5877\ N \cdot V)} . \tag{6.28}$$

The salient points of this analysis are summarized in Table 6.1 for the example waveform given in the text. Also included in this table are salient points from the procedure applied to two additional waveforms. These three waveforms are the first three of a class of common pulse shapes found in nuclear spectroscopy.

The procedure is reapplied for the same three example waveforms with the second-order nonlinearities replaced by third-order nonlinearities. The results of these analyses are summarized in Table 6.2.

IV. COMPUTER SIMULATION PROCEDURE

In this section, a two-step procedure is described for finding the nonlinearity of a system by computer simulations.

The block diagram for the first step of the procedure is shown in Figure 6.3. A linear input signal, PULSE, passes through a nonlinear function which provides a nonlinear signal, XY1, at the input to a frequency-dependent transfer function. The frequency-dependent transfer function is identified by its Laplace transform, H(S), in Figure 6.3. The nonlinear output signal is Y1. In step one, the magnitude of the linear input signal, PULSE, is determined for which the maximum deviation of the nonlinear input signal, XY1, occurs. Also in step one, the magnitude of the linear input signal, PULSE, is determined for which the maximum deviation of the nonlinear output signal, Y1, occurs.

Table 6.1. Summary of the analysis used to find the change in nonlinearity of three different waveforms for second-order nonlinearities.

Linear portion of input	Nonlinear portion input waveform	Linear portion of output waveform	Nonlinear portion of output waveform	G_a(tpeak2)/ G_b(tpeak2)
$V(1 - \frac{t}{\tau})\, e^{-\frac{t}{\tau}}$	$NV^2\,(1 - \frac{t}{\tau})^2\, e^{-\frac{2t}{\tau}}$	$\frac{V\tau}{C}\,(\frac{t}{\tau})\, e^{-\frac{t}{\tau}}$	$\frac{NV^2\tau}{4C} \cdot \left\{1 - \left[2(\frac{t}{\tau})^2 - 2\frac{t}{\tau} + 1\right] e^{-\frac{2t}{\tau}}\right\}$	0.5876
$Ve^{-\frac{t}{\tau}}(2.168) \cdot \left[2(\frac{t}{\tau}) - (\frac{t}{\tau})^2\right]$	$NV^2\, e^{-\frac{2t}{\tau}} \cdot \left[2(\frac{t}{\tau}) - (\frac{t}{\tau})^2\right]^2$	$\frac{V\tau}{C}\,(\frac{t}{\tau})^2\, e^{-\frac{t}{\tau}}$	$\frac{NV^2\tau}{4C} \cdot \left\{1 - \left[2(\frac{t}{\tau})^4 - 4(\frac{t}{\tau})^3 + 2(\frac{t}{\tau})^2 - 2(\frac{t}{\tau}) + 1\right] e^{-\frac{2t}{\tau}}\right\}$	0.7630
$Ve^{-\frac{t}{\tau}}\,(1.276)\,\left[3(\frac{t}{\tau})^2 - (\frac{t}{\tau})^3\right]$	$NV^2\, e^{-\frac{2t}{\tau}} \cdot \left[3(\frac{t}{\tau})^2 - (\frac{t}{\tau})^3\right]^2$	$\frac{V\tau}{C}\,(\frac{t}{\tau})^3\, e^{-\frac{t}{\tau}}$	$\frac{9NV^2\tau}{8C} \cdot \left\{1 - \left[\frac{4}{9}(\frac{t}{\tau})^6 - \frac{4}{3}(\frac{t}{\tau})^5 + \frac{2}{3}(\frac{t}{\tau})^4 + \frac{4}{3}(\frac{t}{\tau})^3 + 2(\frac{t}{\tau})^2 + 2(\frac{t}{\tau}) + 1\right] e^{-\frac{2t}{\tau}}\right\}$	0.7636

Table 6.2. Summary of the analysis used to find the change in nonlinearity of three different waveforms for simple third-order nonlinearities.

Linear portion of input waveform	Nonlinear portion of input waveform	Linear portion of output waveform	Nonlinear portion of output waveform	G_a(tpeak2)/ G_b(tpeak2)
$V \cdot e^{-\frac{t}{\tau}} \cdot \left[1 - (\frac{t}{\tau})\right]$	$NV^3 \cdot e^{-\frac{3t}{\tau}} \cdot \left[1 - (\frac{t}{\tau})\right]^3$	$\frac{V\tau}{C}(\frac{t}{\tau})\ e^{-\frac{t}{\tau}}$	$\frac{4NV^3\tau}{27C} \cdot \left\{1 + \left[\frac{9}{4}(\frac{t}{\tau})^3 - \frac{9}{2}(\frac{t}{\tau})^2 + \frac{15}{4}(\frac{t}{\tau}) - 1\right] e^{-\frac{3t}{\tau}}\right\}$	0.4127
$V \cdot e^{-\frac{t}{\tau}} \cdot \left[2(\frac{t}{\tau}) - (\frac{t}{\tau})^2\right]$	$NV^3 \cdot e^{-\frac{3t}{\tau}} \cdot \left[2(\frac{t}{\tau}) - (\frac{t}{\tau})^2\right]^3$	$\frac{V\tau}{C}(\frac{t}{\tau})e^{-\frac{t}{\tau}}$	$\frac{243NV^3\tau}{16C} \cdot \left\{1 + \left[\frac{81}{16}(\frac{t}{\tau})^6 - \frac{81}{4}(\frac{t}{\tau})^5 + 27(\frac{t}{\tau})^4 - \frac{9}{2}(\frac{t}{\tau})^3 - \frac{9}{2}(\frac{t}{\tau})^2 - 3(\frac{t}{\tau}) - 1\right] e^{-\frac{3t}{\tau}}\right\}$	0.6386
$V \cdot e^{-\frac{t}{\tau}} \left[3(\frac{t}{\tau})^2 - (\frac{t}{\tau})^3\right]$	$NV^3 \cdot e^{-\frac{3t}{\tau}} \left[3(\frac{t}{\tau})^2 - (\frac{t}{\tau})^3\right]^3$	$\frac{V\tau}{C}(\frac{t}{\tau})^3\ e^{-\frac{t}{\tau}}$	$\frac{320NV^3}{729C} \cdot \left\{1 + \left[\frac{243}{320}(\frac{t}{\tau})^9 - \frac{729}{160}(\frac{t}{\tau})^8 + \frac{2673}{320}(\frac{t}{\tau})^7 - \frac{81}{80}(\frac{t}{\tau})^6 - \frac{81}{40}(\frac{t}{\tau})^5 - \frac{27}{8}(\frac{t}{\tau})^4 - \frac{9}{2}(\frac{t}{\tau})^3 - \frac{9}{2}(\frac{t}{\tau})^2 - 3(\frac{t}{\tau}) - 1\right] e^{-\frac{3t}{\tau}}\right\}$	0.6398

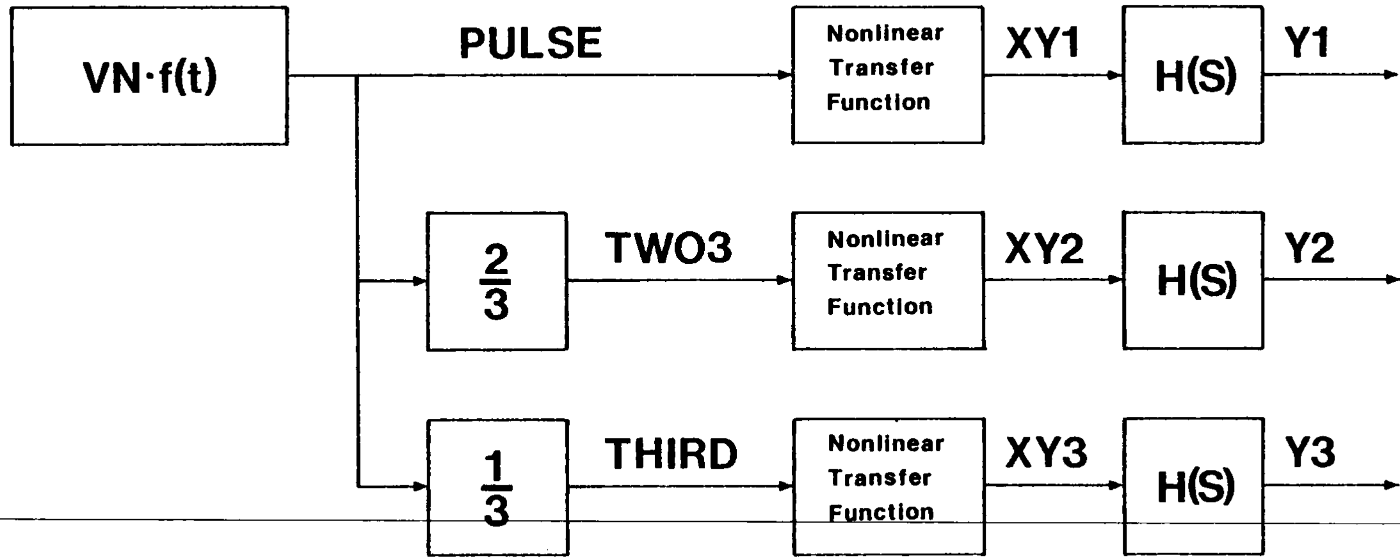

Figure 6.3. Block diagram illustrating the CSMP program used to find the magnitudes of the input pulse at which the nonlinear input signal, XY, and the nonlinear output signal, Y, have their largest deviation from the integral gain curve.

These two input signal magnitudes may be estimated by modeling the deviations of the nonlinear signals as third-order functions of the linear input.

$$\mathrm{Del}(V_n) = G \left(1 - \frac{V_n}{V_{nm}}\right)\left(\frac{V_n}{V_{nm}} - Q\right)\left(\frac{V_n}{V_{nm}}\right), \tag{6.29}$$

where V_n is the linear input signal, V_{nm} is the peak value of the input signal, and where G and Q are constants. The function $\mathrm{Del}(V_n)$ is restricted to have a single polarity between V_n equal to zero, and V_n equal to V_{nm}.

The magnitudes of the nonlinear input signal and nonlinear output signal are determined when the linear input, PULSE, is at two thirds and one third of its maximum value. These magnitudes are used to determine the two values of the input signal for which the maximum deviations of the nonlinear signals occur.

Given that the magnitude of the deviation, $\mathrm{Del}(V_n)$, is B when the input signal is two thirds of V_{nm}, and that the magnitude of the deviation is C when the input signal is one third of V_{nm}, then the linear input signal at which the maximum deviation occurs is approximately

$$X \cdot V_{nm} \cong \left\{\frac{1 + Q \pm \sqrt{Q^2 - Q + 1}}{3}\right\} \cdot V_{nm}, \tag{6.30}$$

where

$$Q = \frac{2C - B}{3(C - B)}\,. \tag{6.31}$$

The derivation of Equation (6.30) is given in Appendix IV. When the magnitude of the variable Q is undefined (i.e. infinite), the maximum deviation occurs at half of V_{nm}.

The block diagram shown in Figure 6.3 outlines the computer program used to find the magnitudes of the input voltage at which the two maximum deviations occur. The figure shown three identical but separate signal paths. The upper most path processes the signal at full amplitude; the integral gain of the system is established here. The center path processes the signal at two thirds of maximum amplitude, and the lower most path processes the signal at one third of maximum amplitude.

Let the peak values of the variables XY1, XY2, XY3, Y1, Y2, and Y3 shown in Figure 6.3 be represented by XYMAX1, XYMAX2, XYMAX3, YMAX1, YMAX2, and YMAX3 respectively. The deviations of the nonlinear signal at the input to the frequency-dependent function are

$$B_n = \frac{2}{3}\,\mathrm{XYMAX1} - \mathrm{XYMAX2} \tag{6.32}$$

when the linear input is at two thirds of maximum amplitude, and

$$C_n = \frac{1}{3}\,\mathrm{XYMAX1} - \mathrm{XYMAX3} \tag{6.33}$$

when the linear input is at one third of maximum amplitude. The deviations of the nonlinear signal at the output are

$$B_o = \frac{2}{3}\,\mathrm{YMAX1} - \mathrm{YMAX2} \tag{6.34}$$

when the linear input is at two thirds of maximum amplitude, and

$$C_o = \frac{1}{3}\,YMAX1 - YMAX3 \tag{6.35}$$

when the linear input is at one third of maximum amplitude. These values of the variables B and C can then be substituted into Equation (6.31) to determine values for the intermediate variable, Q, with which the input signal magnitude can be determined from Equation (6.30).

In the second step of this process, the magnitudes of the two maximum deviations are found. The block diagram of the computer program used to find these values is shown in Figure 6.4. The upper signal path determines the magnitude of the maximum deviation of the nonlinear signal at the input of the frequency-dependent function, and the lower signal path determines the magnitude of the maximum deviation of the nonlinear signal at the output.

The magnitudes of the multiplying factors X_n and X_o are between zero and unity, and they each represent the fraction of an input signal to full scale. Their values are determined in the previous simulation.

Let the peak values of the variables XYD, and YD shown in Figure 6.4 be represented by XYMAXD and YMAXD respectively. The normalized nonlinearity of the signal at the input to the frequency-dependent function is then

$$NL_n = \frac{X_n \cdot XYMAX1 - XYMAXD}{XYMAX1}, \tag{6.36}$$

and the normalized nonlinearity of the signal at the output of the frequency-dependent function is

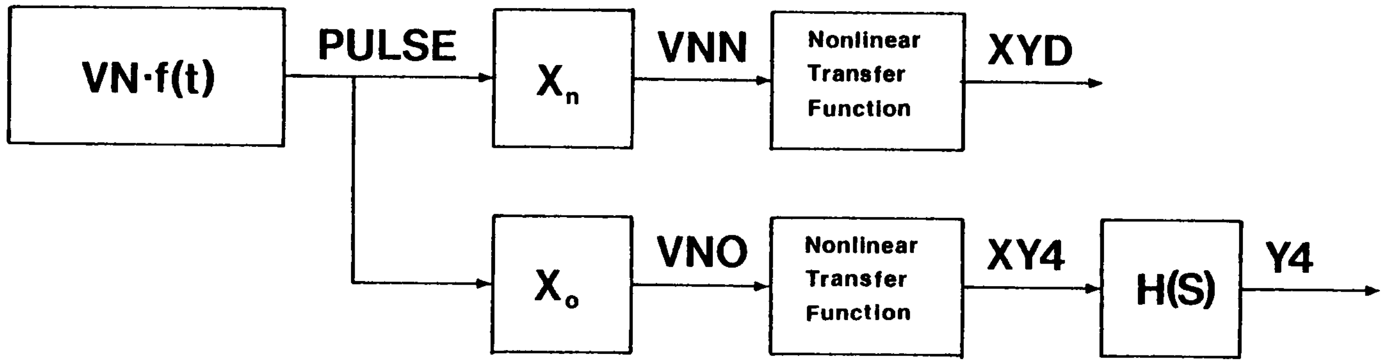

Figure 6.4. Block diagram illustrating the CSMP program used to find the maximum deviation of the nonlinear input signal, XYD, before the frequency-dependent element, and the maximum deviation of the nonlinear output signal, YD, after the frequency-dependent element.

$$NL_o = \frac{X_o \cdot \text{YMAX1} - \text{YMAXD}}{\text{YMAX1}} . \tag{6.37}$$

V. SIMULATION MEASUREMENTS OF NONLINEARITY FOR THREE EXAMPLE WAVEFORMS

In this section, the computer simulations used to determine the nonlinearity of three example waveforms before and after passing through a frequency-dependent function are given. The three sample waveforms are from a class of waveshapes common in nuclear spectroscopy, and the frequency-dependent function used in these simulations was integration. The type of nonlinearities are second-order and third-order two-term polynomials. The nonlinearity simulation results are compared to those obtained from hand analyses.

A block diagram illustrating one of these simulations is shown in Figure 6.5. The CSMP computer code for this simulation is given in Appendix V. The nonlinearity is second-order in this example; therefore, the maximum deviations of the nonlinear input and nonlinear output signals both occur when the linear input signal is at half of its maximum value.

The peak value of the nonlinear input waveform was 15.0000 when the linear input was at full magnitude, and the peak value of the nonlinear input waveform was 7.3500 when the linear input was at half of its maximum amplitude. From Equation (6.36)(page 109) the value of the normalized nonlinearity is

$$NL_n = \frac{(0.5)(15.0000) - (7.3500)}{15.0000} = 1.00\%. \tag{6.38}$$

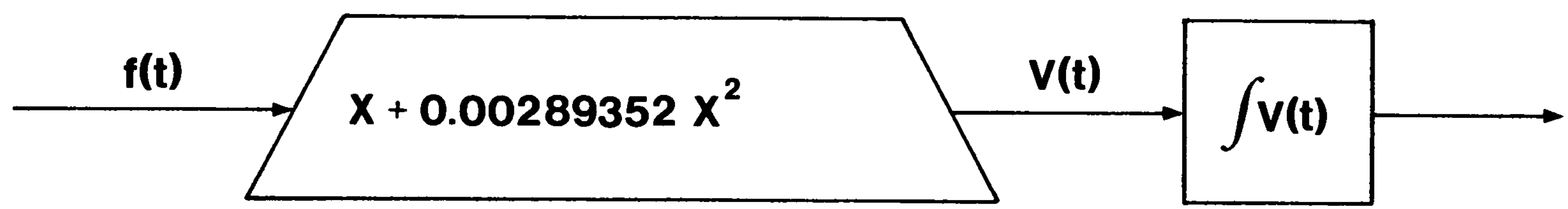

Figure 6.5. Block diagram of a system for which the integral nonlinearity is found by computer simulation.

The peak value of the nonlinear output waveform was 5.4271 when the linear input was at full scale, and the peak value of the nonlinear output was 2.6811 when the linear input waveform was at half of its maximum amplitude. From Equation (6.37)(page 111) the value of the normalized nonlinearity is

$$NL_o = \frac{(0.5)(5.4271) - (2.6811)}{5.4271} = 0.5979\%. \tag{6.39}$$

From Table 6.1 (page 104) and Equation (6.28)(page 103) the change in nonlinearity for this combination of waveshape and frequency-dependent function is 0.5975. The analysis and simulation agree well.

Simulation results for this and two other waveforms are compared in Table 6.3 to hand analyses for second-order nonlinearities. In all three cases, the simulation results and analyses agree well. The magnitude of the errors is generally within round-off error of the computer's output. Simulation results for the same three waveforms are compared in Table 6.4 to hand analyses for third-order nonlinearities. These simulations and analyses also agree well.

VI. SPECTRAL DEPENDENCE OF COMPLEX NONLINEARITIES

In this section, an analytical procedure is given for finding the change in nonlinearity of a pulse which passes through a frequency-dependent function for nonlinearities which are more complex than two-term polynomials. The change in nonlinearity of a complex nonlinear waveform which has a second-order term in its Taylor

Table 6.3. Comparison between analysis and computer simulations of the change in nonlinearity of three example waveforms after being integrated for second-order nonlinearities.

Input waveforms	NL_n analysis	NL_n, computer simulation	NL_o analysis	NL_o, computer simulation
$V \cdot e^{-\frac{t}{\tau}} \cdot \left[1 - (\frac{t}{\tau})\right]$	1.0000%	1.0000%	0.5975%	0.5979%
$V \cdot e^{-\frac{t}{\tau}} \cdot \left[2(\frac{t}{\tau}) - (\frac{t}{\tau})^2\right]$	1.0000%	1.0010%	0.7703%	0.7693%
$V \cdot e^{-\frac{t}{\tau}} \cdot \left[3(\frac{t}{\tau})^2 - (\frac{t}{\tau})^3\right]$	1.0000%	0.9994%	0.7709%	0.7695%

Table 6.4. Comparison between analysis and computer simulations of the change in nonlinearity of three example waveforms after being integrated for simple third-order nonlinearities.

Input waveforms	NL_n analysis	NL_n, computer simulation	NL_o analysis	NL_o, computer simulation
$V \cdot e^{-\frac{t}{\tau}} \cdot \left[1 - (\frac{t}{\tau})\right]$	1.0000%	0.9997%	0.4191%	0.4199%
$V \cdot e^{-\frac{t}{\tau}} \cdot \left[2(\frac{t}{\tau}) - (\frac{t}{\tau})^2\right]$	1.0000%	1.0008%	0.6446%	0.6456%
$V \cdot e^{-\frac{t}{\tau}} \cdot \left[3(\frac{t}{\tau})^2 - (\frac{t}{\tau})^3\right]$	1.0000%	0.9992%	0.6459%	0.6443%

series expansion is estimated to be equal to the change in nonlinearity of a second-order two-term polynomial nonlinear waveform as given by Equation (6.12)(page 97). The change in the nonlinearity of a complex nonlinear waveform which does not have a second-order term in its Taylor series expansion, but does have a third-order term, is estimated to be equal to the change in nonlinearity of a third-order two-term polynomial nonlinear waveform as given by Equation (6.19)(page 99). The accuracy of these approximations is tested by computer simulations for several values of nonlinearity and for three different nonlinear functions.

The three complex nonlinear functions evaluated are the voltage-dependent functions for the common-emitter, bipolar differential, and JFET differential amplifier stages. The three functions for these amplifiers are derived in CHAPTER III (pages 34-39) and in CHAPTER IV (pages 71-74), and these functions are:

a) common-emitter

$$V_{out} = -I_o R_L \left(e^{\frac{qV_n}{kT}} - 1 \right),$$

b) bipolar differential

$$V_{out} = \frac{1}{2} I_o R_L \tanh \left(\frac{qV_n}{2kT} \right),$$

c) JFET differential

$$V_{out} = \frac{I_{dss} V_n}{V_p} \sqrt{\frac{I_o}{2I_{dss}} - \left(\frac{V_n}{2V_p} \right)^2}.$$

The nonlinear function of the common-emitter amplifier has a second-order term in its Taylor series expansion. The nonlinear functions of the bipolar differential and JFET differential stages do not have second-order terms, but do have third-order terms in their Taylor series expansions.

The single waveshape used in this analysis is the representative waveform

$$V(t) = V\left(1 - \frac{t}{\tau}\right)e^{-\frac{t}{\tau}}, \tag{6.40}$$

and the frequency-dependent transfer function is an ideal integrator. The value of the variable A in Equation (6.12)(page 97) for this combination of waveshape and frequency-dependent transfer function is approximately 0.5876. The value of the variable B in Equation (6.19)(page 99) for this combination of waveshape and frequency-dependent transfer function is approximately 0.4127.

The nonlinearity of the waveform at the output of the system with the complex nonlinear function from the common-emitter amplifier was predicted from Equation (6.12)(page 97). The nonlinearity of the waveform at the output of the two systems with the complex nonlinear functions from the bipolar and JFET differential amplifiers was predicted from Equation (6.19)(page 99). The nonlinearities predicted from these hand analyses were compared to the values determined by the computer simulation procedures outlined in Section IV of this chapter (pages 103-111).

Table 6.5. Comparison of the output nonlinearity found by computer simulations to the nonlinearity predicted by analysis for three complex transfer functions. The example waveform is $V(t) = (1 - t/\tau)e^{-t/\tau}$ and the frequency dependent device an ideal integrator.

Input nonlinearity	Output nonlinearity					
	Common-emitter		Bipolar differential		JFET differential	
	Analysis	Simulation	Analysis	Simulation	Analysis	Simulation
1%	0.5975%	0.5892%	-0.4065%	-0.4130%	-0.4065%	-0.4039%
3.2%	1.9851%	1.9106%	-1.2592%	-1.3222%	-1.2592%	-1.2354%
10%	7.0368%	6.2018%	-3.5806	-4.1754%	-3.5806	-3.3783%

The comparison between analysis and computer simulation is shown in Table 6.5. The magnitude of the nonlinearity at the input to the integrator was set at 1.0%, 3.2%, and 10.0% for each function. The nonlinearity of the waveforms at the output of the integrator were predicted from Equations (6.12) and (6.19)(pages 97, 99). These predicted values agree reasonably well with the computer simulations. The accuracy of the predictions is worse for larger values of nonlinearity.

CHAPTER VII

CLOSED-LOOP NONLINEARITY OF NEGATIVE FEEDBACK AMPLIFIERS WITH MEMORY

I. INTRODUCTION

The closed-loop nonlinearity of a feedback system at midband is approximately equal to the open-loop nonlinearity of the amplifier divided by the loop transmission plus one. However, when energy storage devices distort the waveshape of a nonperiodic signal, the value of the loop transmission is not defined and the closed-loop nonlinearity is not known. Two computer simulation models are presented in this chapter to determine the closed-loop nonlinearity of feedback systems with memory to nonperiodic signals. Both models are shown to be accurate for sample simulations but one of the two models uses computer time more efficiently.

Computer simulations in this chapter are used to determine the closed-loop nonlinearity of feedback amplifiers with integrating stages in the forward plant. The results of these simulations indicate that the closed-loop nonlinearity of this type of feedback amplifier is inversely proportional to the gain-bandwidth product of the loop transmission squared, and that for best linearity performance the phase margin of the feedback amplifier should be greater than 45 degrees. The closed-loop nonlinearity of many practical amplifiers, particularly operational amplifiers, can be approximated using the results of this analysis.

II. COMPUTER SIMULATION MODELS

Nonlinearity is modeled in this chapter by a simple two-term polynomial,

$$f(V) = a_1 \cdot V + a_2 \cdot V^n, \tag{7.1}$$

where a_1 and a_2 are constant coefficients and n is a positive integer power of V greater than unity. In CHAPTER II of this dissertation (page 19), the peak deviation with this type non-linearity is shown to occur when the input voltage is

$$V_{nd} = V_{nm} n^{\left(\frac{1}{1-n}\right)}. \tag{7.2}$$

where V_{nm} is the peak value of the input voltage. The magnitude of the peak deviation is then

$$\text{Delmax} = a_2 V_{nm}{}^n \left(\frac{n-1}{n}\right) n^{\left(\frac{1}{1-n}\right)}. \tag{7.3}$$

Handling nonlinearities that are more complex than the two-term polynomial are discussed at the end of this section.

First Computer Model

Two models for simulating the nonlinearity of feedback systems are presented in this chapter. This first model is shown in Figure 7.1. The rectangular blocks G_1, G_2, and H are linear functions which may or may not have frequency dependent elements. The memoryless nonlinearity is contained in the nonrectangular block.

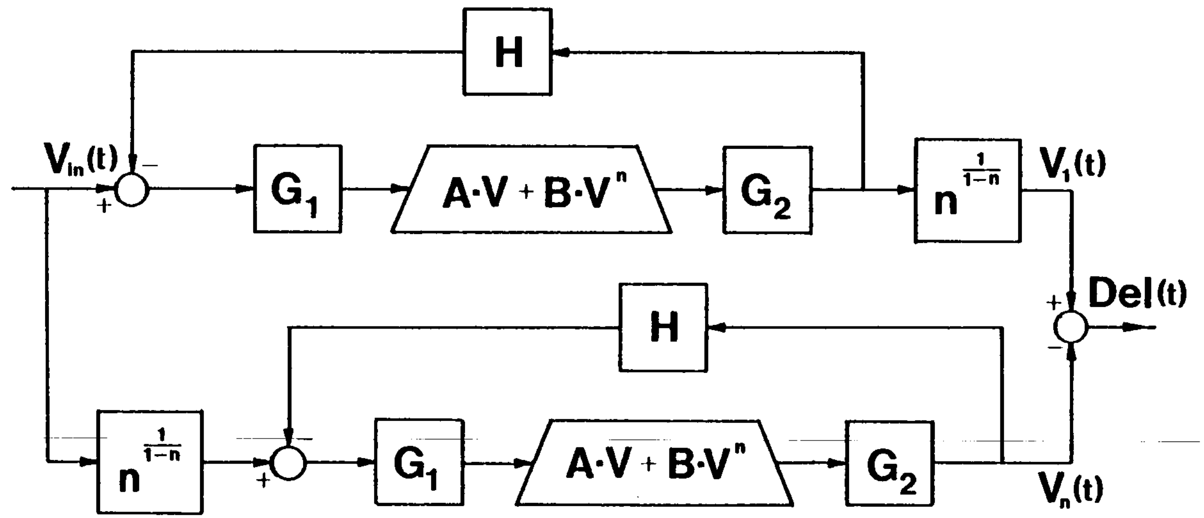

Figure 7.1. First procedure for simulating the integral nonlinearity of a system as a function of time.

Although the feedback generates higher-order nonlinear terms, the accuracy of this model relies on the deviation of the output being near its maximum value when the input voltage has a magnitude given by Equation (7.2). The ideal magnitude of the output, V_1, for this signal level is determined by the upper feedback loop in Figure 7.1, and the actual magnitude of the output, V_n, is determined by the lower feedback loop. The difference in these two signals,

$$Del(t) = V_1(t) - V_n(t), \tag{7.4}$$

gives an approximation of the maximum deviation of the output from the integral gain curve.

The magnitude of the closed-loop nonlinearity of a system is often in the order of parts per million. For this reason, the accuracy and resolution of a computer simulation using this first model often must be relatively high to simulate accurately the nonlinearity.

Second Computer Model

A block diagram of the second simulation procedure is shown in Figure 7.2. This procedure uses an approximation that has been used by Billan to predict the harmonic distortion of Sallen and Key type filters [34]. The upper feedback loop shown in Figure 7.2 simulates the linear portion of the signal, and the lower feedback loop simulates the first order portion of the nonlinear signal generated from the linear waveform. The maximum deviation is then approximated as the fraction given in Equation (7.3),

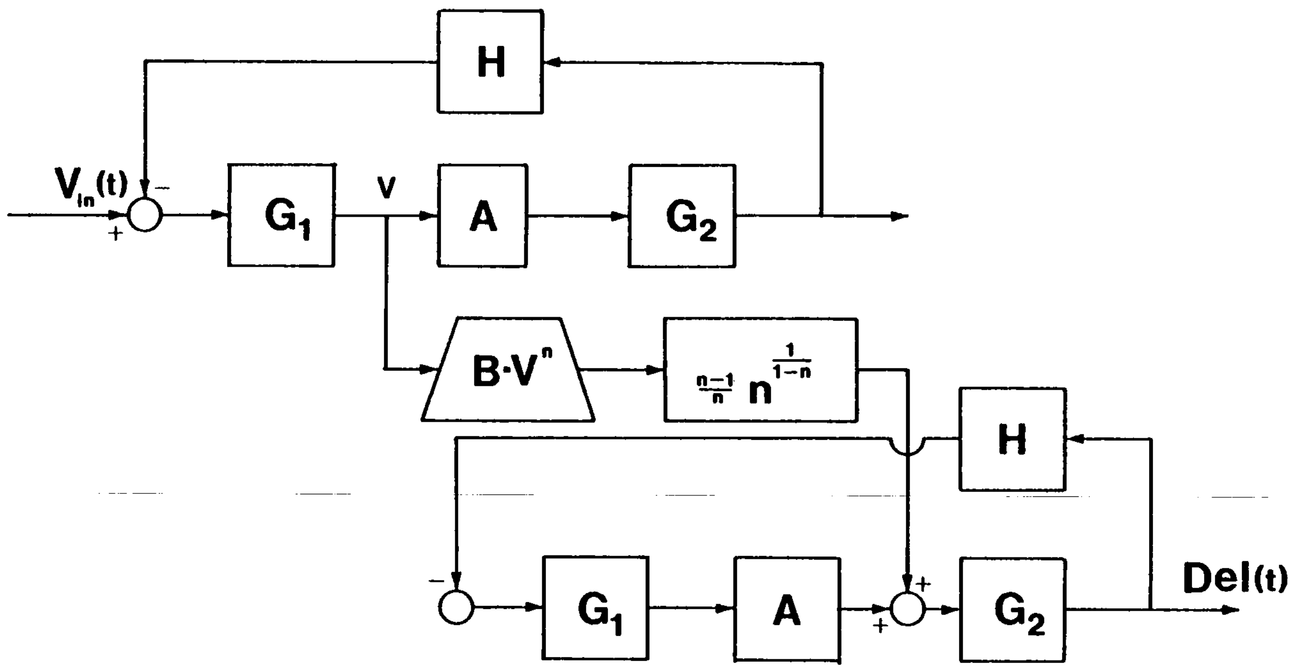

Figure 7.2. Second procedure for simulating the integral nonlinearity of a system as a function of time.

$$\text{Delmax} \cong \frac{n-1}{n} \cdot n^{\left(\frac{1}{1-n}\right)} \cdot B \cdot V_{nm}^{(n-1)} \tag{7.5}$$

of the nonlinear signal. With this approximation, the fundamental nonlinearity is fed back, but no cross distortion terms are considered. The accuracy of this approximation requires that the inequality

$$A \cdot V >> B \cdot V^n \tag{7.6}$$

holds true.

This second procedure uses computer time more efficiently than the first model. Since this approximation does not depend on small differences between two signals to determine the nonlinearity, the high resolution and accuracy of computation that the previous model requires are not needed.

In addition, when several nonlinear sources are included in a single feedback system, the individual contribution from each of the nonlinearities can be found with the second model by using a single feedback loop to simulate the linear portion of the signal, plus one feedback loop for each nonlinearity. Therefore, the contributions from N independent nonlinearities can be evaluated with only N+1 feedback loop simulations. The first model requires two feedback loop simulations per nonlinearity, regardless of the number of nonlinearities present in the system. Evaluating the individual contributions from N nonlinearities using the first model requires 2N feedback loop simulations.

The second procedure can, therefore, save computer time by requiring fewer simulations for a given nonlinear system, and by requiring less resolution per simulation.

Since the feedback systems shown in Figure 7.2 are linear, the output nonlinearity from this second model can be determined with Laplace transform techniques. The open-loop nonlinear operation is evaluated by taking the inverse transform of V before raising this voltage to the n^{th} power, and then taking the Laplace transform of the resulting nonlinear function of time. Unfortunately, the waveforms generated are usually complex, and the process becomes tedious.

Results from an Example Simulation

The results from several computer simulations indicate that the first procedure for finding the closed-loop nonlinearity of a feedback system is much more accurate than the second procedure. The results from a typical simulation are given here to illustrate this point.

The example nonlinear system is shown in Figure 7.3. Since the nonlinearity is second order, the peak deviation using the first procedure is estimated to occur when the input is at half of its maximum value. Since the nonlinearity is second order, the value of the maximum deviation calculated from Equation (7.5) is $0.25\ B \cdot V_{nm}^{2}$, and the magnitude of the peak deviation using the second procedure is estimated to be one quarter of the magnitude of the nonlinear waveform. The input waveform used in these example simulations is one that is common in nuclear spectroscopy and is described by

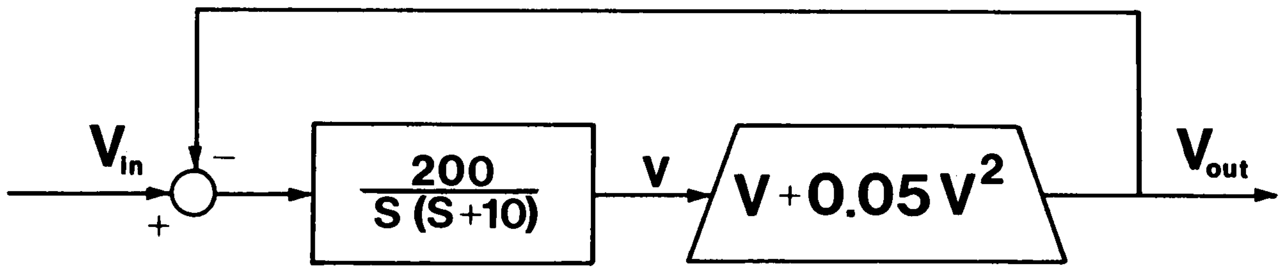

Figure 7.3. An example nonlinear system which is used to illustrate the two procedures for determining integral nonlinearity.

$$V_{in}(t) = 2.718\ te^{-t}. \tag{7.7}$$

The constant, 2.718, normalizes the pulse to a peak value of unity.

The nonlinearity outputs from the computer simulations using the two procedures are sketched as functions of time in Figure 7.4. The solid line is the output from the first-procedure simulation, and the dashed line is the output from the second-procedure simulation.

The first procedure has error when the maximum deviation occurs with an input whose value is other than the one predicted by Equation (7.2)(page 121). The magnitude of this error was found by comparing the true maximum deviation of the system to the deviations predicted by the first procedure. These true maximum deviations were found by finding the deviations of the system for different values of input using repeated simulations. The error at any instant of time was less than 1.0% of the peak value of the nonlinearity for this example run. The measurement of this error is complicated since the maximum deviations at different points of the waveform occur at different values of input voltage.

The error produced by the second model exceeded 14% of the peak magnitude of the nonlinearity. This number seems large considering that the peak value of the open-loop nonlinearity is only 1.19%.

The second model contains two major sources or error. First, the voltage waveform, V, in Figure 7.2 is altered by removing the nonlinear term from the feedback loop. Second, the frequency of

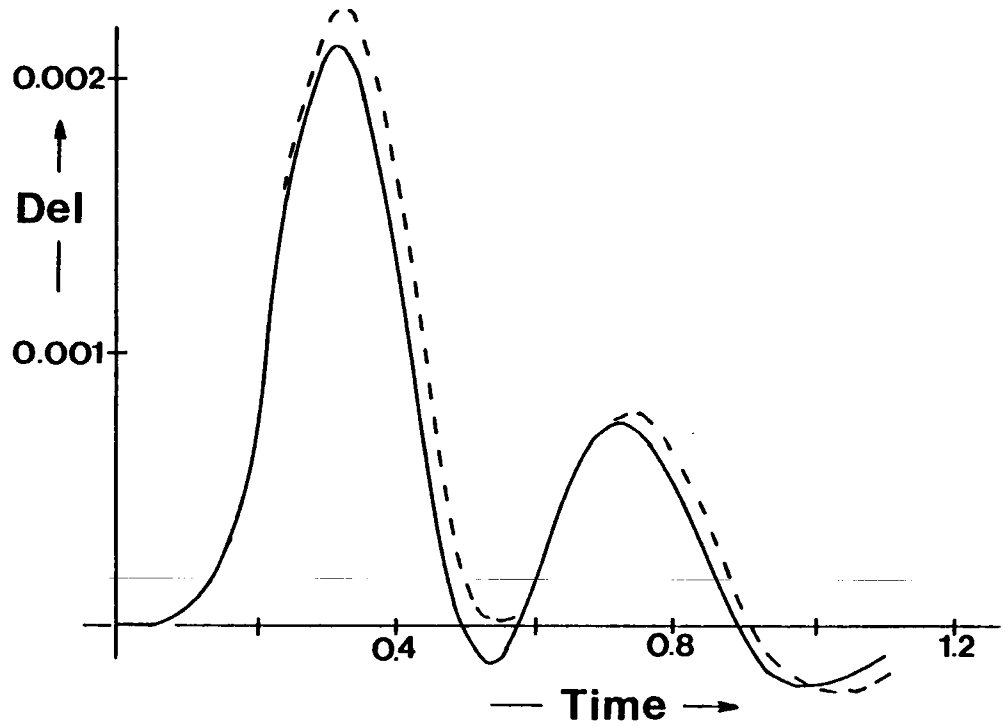

Figure 7.4. Nonlinearity as a function of time from simulations by the first procedure (solid line) and second procedure (dashed line) for a representative nonlinear system presented in the text.

oscillation in the nonlinearity is too low because the linear gain, A, is always less than the integral gain of this nonlinear system. Modifications to the second model are given in the next section to reduce the magnitude of these errors.

Modified Second Procedure

Two modifications of the second procedure are shown in the block diagram in Figure 7.5. The first modification is the inclusion of the nonlinear term in the upper feedback loop. This modification provides a more accurate simulation of the variable labeled V in the block diagram. The second modification is the calculation of the integral gain of the feedback system for the lower feedback loop. This gain must be calculated from variables in the upper feedback loop. Neither of these two modifications seriously reduces the efficiency of this computer simulation procedure.

This modified second procedure was used to determine the nonlinearity of the example nonlinear system given in the previous section. The predicted value of nonlinearity at any instant of time was within 1% of the actual value of nonlinearity of the system. This value of error is significantly less than the 14% error obtained with the unmodified second procedure. However, this modified second procedure was not quite as accurate as the first procedure. The magnitude of the error of the modified second procedure is typically 25% larger than the error from the first procedure.

Handling Nonlinearities that are More Complex than Two-Term Polynomials

More complex nonlinearities than two-term polynomials may be used with the first procedure given in this chapter. However,

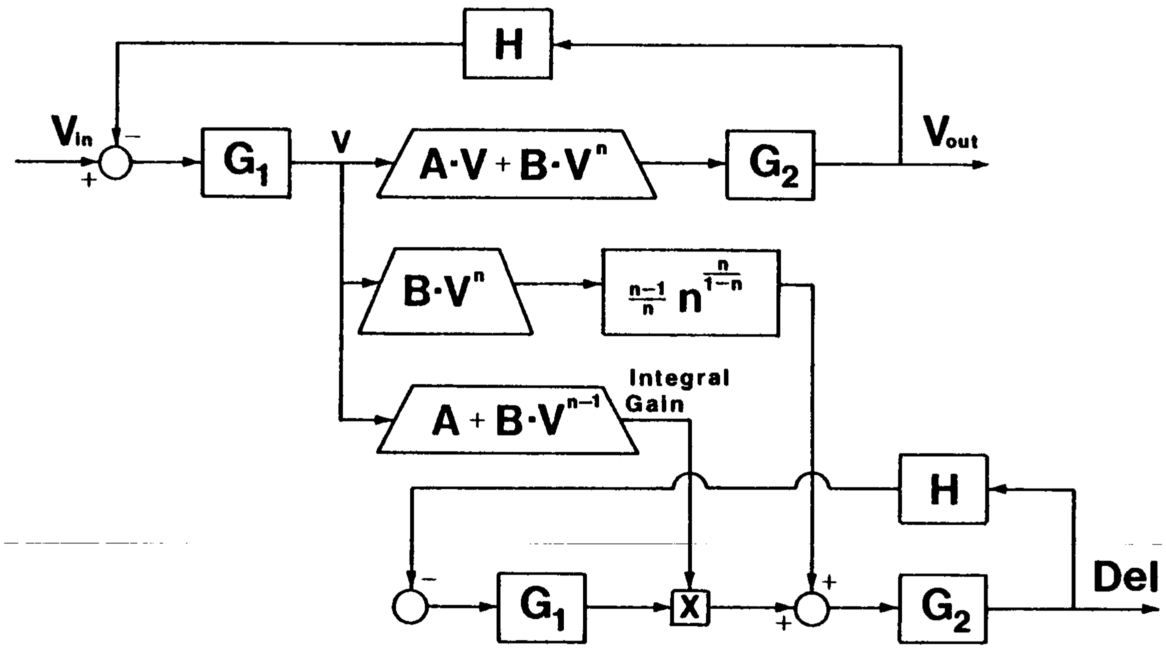

Figure 7.5. Modified second procedure with more accurate simulation of variable labeled V in upper feedback loop and calculation integral gain for lower feedback-loop simulation.

some criteria is needed to estimate the value of the input variable at which the maximum deviation occurs. As a simple example, consider the nonlinear function described by

$$f(V) = a_1 \cdot V + a_2 \cdot V^2 + a_3 \cdot V^3 + \cdot \cdot \cdot, \tag{7.8}$$

where the number of terms of the polynomial is large. The input for which the maximum deviation occurs can be estimated by using the first two terms of the polynomial. For example, if the coefficient a_2 is zero, then the magnitude of the input at which the maximum deviation occurs could be estimated to be that of a third-order two-term polynomial, which is 57.7% of the maximum input. In the absence of any other criteria, half of full scale is usually an adequate estimate for the input at which the maximum deviation occurs.

More complex nonlinearities may also be used with the second procedure given in this paper if the maximum deviation of the system can be estimated from the nonlinear components of the output. Generally, this estimation requires an estimate for the magnitude of the input variable for which the maximum deviation occurs. For example, given the polynomial described by Equation (7.8) above, the deviation at midscale could be assumed near the maximum value. At midscale, the deviation of the polynomial is given by

$$\mathrm{Del} = \frac{1}{4} a_2 \cdot V_{nm}^{\ 2} + \frac{3}{8} a_3 \cdot V_{nm}^{\ 3} + \frac{7}{16} a_4 \cdot V_{nm}^{\ 4} + \cdot \cdot \cdot \cdot . \tag{7.9}$$

A block diagram showing the modified second procedure using this nonlinearity is shown in Figure 7.6. The coefficients of the nonlinear terms inserted into the lower feedback loop are weighted to give the peak deviation at the output of that system.

III. SIMULATIONS OF CLOSED-LOOP NONLINEARITY WITH AN INTEGRATOR IN THE FORWARD PLANT

Nonlinearity Located before Integration

Simulation results are given in this section for a feedback system with a single frequency-dependent element, and integrating stage in the forward plant of the system. Many practical amplifiers, particularly operational amplifiers, can be approximated with this model. A common pulse shape was used in the simulations.

The model given in Figure 7.2 was used for the simulations. This model was chosen because it efficiently uses computer time, and because the magnitude of the nonlinearity varies linearly with signal amplitude. This means that the model in Figure 7.2 gives a first-order, or small-signal, analysis of the nonlinearity. To obtain small-signal results with the model given in Figure 7.1, the signal amplitude would have to be kept very small, and the resolution of the simulation very high.

Simulations were obtained first for nonlinear functions occurring before the integrating stage. For these simulations, the elements of the model in Figure 7.2 are described by

$$B = G_1 = H = 1, \qquad \text{(a)}$$

and $$G_2 = \frac{1}{S}. \qquad \text{(b)} \qquad (7.10)$$

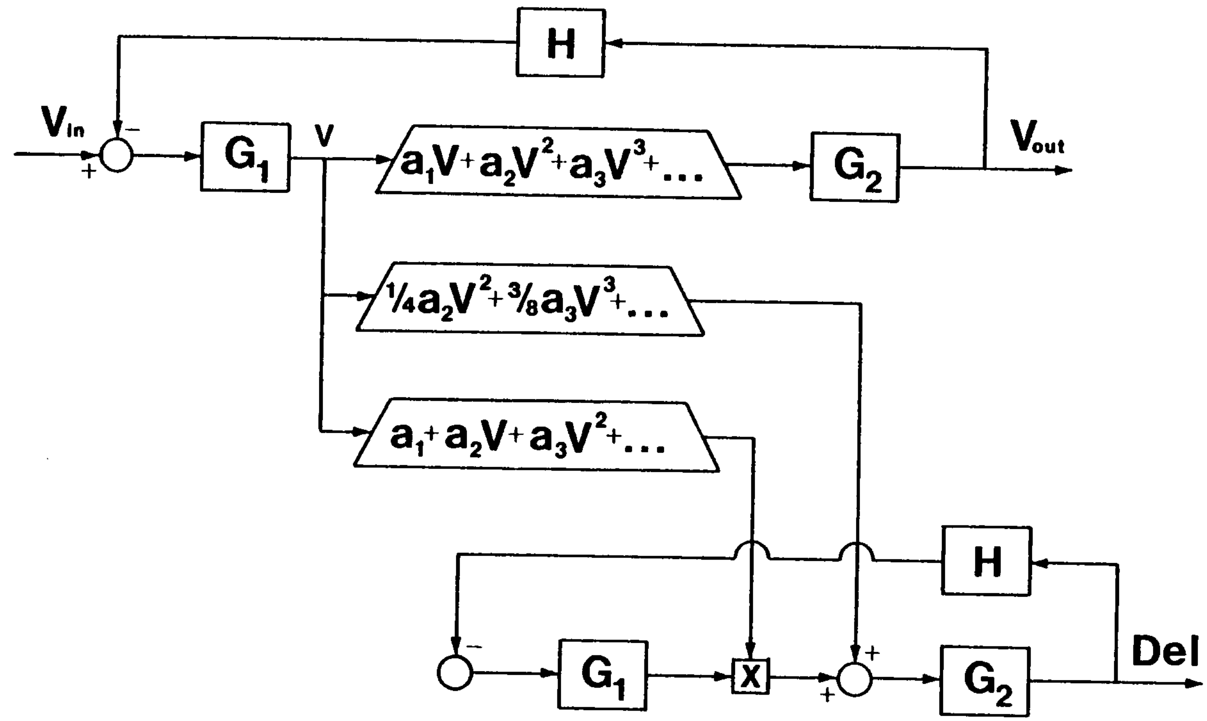

Figure 7.6. Block diagram illustrating the modified second procedure which has a polynomial nonlinear function with a large number of terms.

Second-order and third-order nonlinearities were simulated individually such that n had values of 2 and 3 for separate simulations. The value of the linear gain, A, was varied from 2 to 1,000 in nearly logarithmic steps. The input waveform was given by

$$V_{in}(t) = 2.718\ te^{-t}. \tag{7.11}$$

A sample output is shown in Figure 7.7. In this particular run, n has a value of 2, and A has a value of 20. The CSMP computer program for this simulation is listed in Appendix V. The output waveform, VL, has a peak value of 0.99855 at 1.05 seconds. At that instant of time, the nonlinear waveform, VN, has a value of 9.01×10^{-7}.

Results from this and the other runs are tabulated in Table 7.1. The closed-loop nonlinearity strongly depends on the magnitude of the linear gain, A, for both the second-order and third-order nonlinearities. The second-order nonlinearity is inversely proportional to the linear gain raised approximately to the fifth power, and the third-order nonlinearity is inversely proportional to the linear gain raised approximately to the seventh power. This reduction of nonlinearity is due to the reduced signal magnitude before the integrating stage, and due to the increased loop transmission of the amplifier.

Nonlinearity Located after the Integrator

The nonlinear system was next simulated with the nonlinear functions occurring after the integrating stage. The elements of

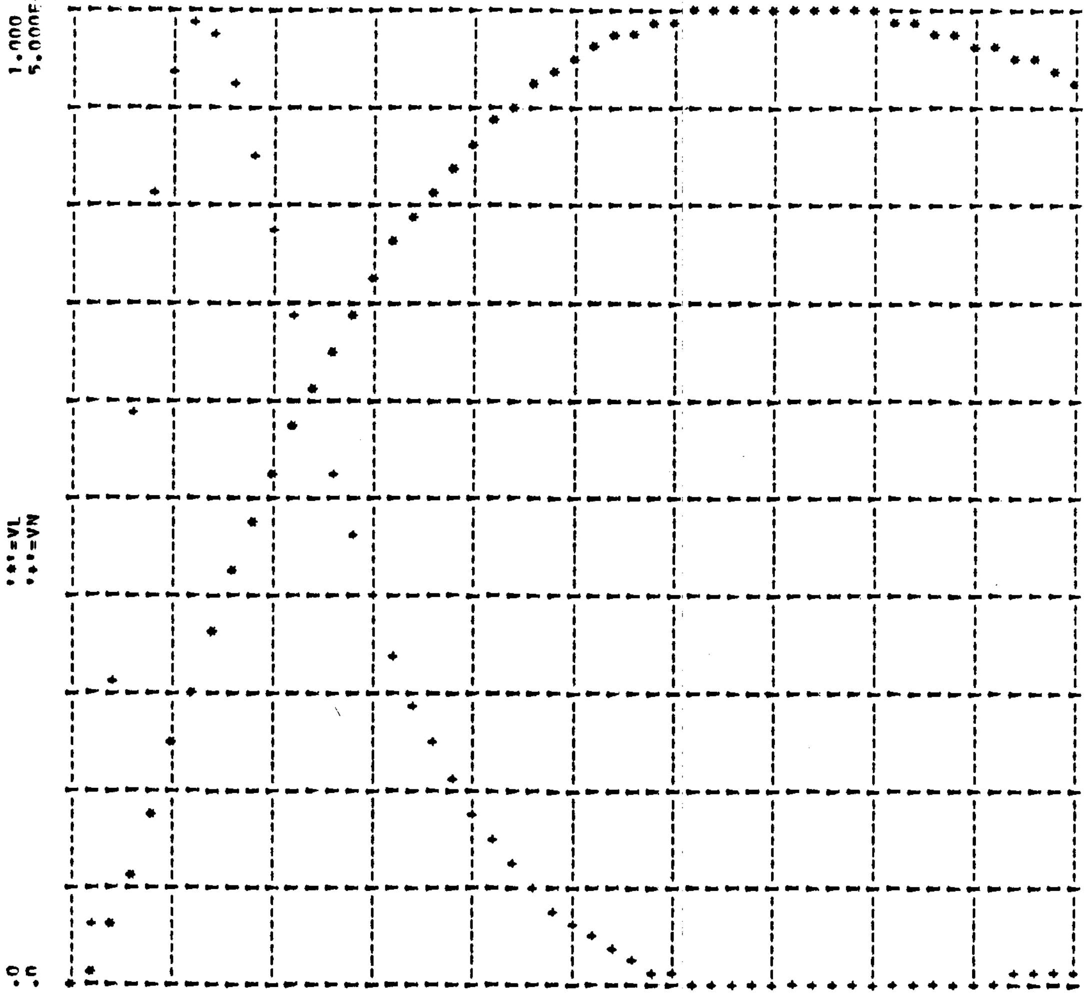

TIME	VN	VL
.0	.0	.0
3.0000E-02	3.5394E-05	1.9805E-02
6.0000E-02	1.5507E-04	6.5210E-02
9.0000E-02	2.9448E-04	.12260
.12000	4.0341E-04	.18461
.15000	4.6717E-04	.24727
.18000	4.9048E-04	.30849
.21000	4.8426E-04	.36721
.24000	4.5922E-04	.42293
.27000	4.2373E-04	.47543
.30000	3.8359E-04	.52467
.33000	3.4250E-04	.57072
.36000	3.0268E-04	.61365
.39000	2.6534E-04	.65358
.42000	2.3104E-04	.69063
.45000	2.0000E-04	.72493
.48000	1.7217E-04	.75661
.51000	1.4742E-04	.78579
.54000	1.2553E-04	.81258
.57000	1.0626E-04	.83710
.60000	8.9391E-05	.85947
.63000	7.4679E-05	.87978
.66000	6.1910E-05	.89914
.69000	5.0883E-05	.91465
.72000	4.1410E-05	.92939
.75000	3.3327E-05	.94247
.78000	2.6465E-05	.95396
.81000	2.0697E-05	.96395
.84000	1.5892E-05	.97251
.87000	1.1936E-05	.97973
.90000	8.7245E-06	.98567
.93000	6.1652E-06	.99041
.96000	4.1743E-06	.99400
.99000	2.6770E-06	.99652
1.0200	1.6059E-06	.99801
1.0500	9.0112E-07	.99955
1.0800	5.0896E-07	.99819
1.1100	3.8167E-07	.99698
1.1400	4.7679E-07	.99496
1.1700	7.5664E-07	.99220
1.2000	1.1879E-06	.98872
1.2300	1.7413E-06	.98459
1.2600	2.3908E-06	.97984
1.2900	3.1138E-06	.97451
1.3200	3.8905E-06	.96863
1.3500	4.7037E-06	.96226
1.3800	5.5385E-06	.95541
1.4100	6.3821E-06	.94813
1.4400	7.2236E-06	.94045
1.4700	8.0536E-06	.93239
1.5000	8.8643E-06	.92398

Figure 7.7. Sample output of a nonlinearity simulation run with the nonlinearity located before the integrating stage in a feedback amplifier.

Table 7.1. Comparison of nonlinearities of several systems with integrating stages in the forward plant for several values of linear gain. Nonlinear functions were located before the integrating stage and were second-order and third-order two-term polynomial nonlinearities.

Linear gain	Second-order nonlinearity	Third-order nonlinearity
2	2.43×10^{-2}	8.52×10^{-3}
5	1.23×10^{-3}	1.99×10^{-4}
10	3.76×10^{-5}	1.88×10^{-6}
20	9.01×10^{-7}	8.34×10^{-9}
50	7.11×10^{-9}	9.52×10^{-12}
100	2.15×10^{-10}	5.78×10^{-14}
200	5.89×10^{-12}	4.14×10^{-16}
500	7.29×10^{-14}	-2.19×10^{-18}
1000	2.19×10^{-15}	6.63×10^{-21}

the model in Figure 7.2 are described by

$$A = G_2 = H = 1, \qquad \text{(a)}$$

$$B = 0.05, \qquad \text{(b)}$$

and $$G_1 = \frac{K}{S}, \qquad \text{(c)} \qquad (7.12)$$

where the value of the variable K was varied from 2 to 1,000 in nearly logarithmic steps. As in the previous simulations, the variable n took on the values of 2 and 3 for separate simulations of second-order and third-order nonlinearities. With this arrangement, the magnitude of the voltage at the nonlinear function did not vary with the values of loop gain. The input waveform used for the simulation is described by Equation (7.11).

The results of these simulations are given in Table 7.2. The closed-loop nonlinearity varied inversely with the square of the loop transmission for both the third-order and the second-order nonlinearities.

IV. INTRODUCTION OF A SECOND FREQUENCY-DEPENDENT ELEMENT

Many electronic amplifiers have more than one significant frequency-dependent elements. To approximate this situation, a second high-frequency pole was added to the forward plant of the nonlinear feedback systems given in the preceding section. The nonlinearity as a function of the phase margin of the Bode plot of the system was found for several values of loop gain. The results from these simulations may be used to estimate the

Table 7.2. Comparison of nonlinearities of several systems with integrating stages in the forward plant for several values of linear gain. Nonlinear functions were located after the integrating stage and were second-order and third-order two-term polynomial nonlinearities.

Linear gain	Second-order nonlinearity	Third-order nonlinearity
2	8.84×10^{-3}	1.04×10^{-2}
5	3.49×10^{-3}	5.37×10^{-3}
10	9.22×10^{-4}	1.51×10^{-3}
20	1.60×10^{-4}	3.49×10^{-4}
50	4.15×10^{-5}	6.21×10^{-5}
100	1.03×10^{-5}	1.55×10^{-5}
200	2.30×10^{-6}	3.45×10^{-6}
500	4.06×10^{-7}	6.11×10^{-7}
1000	1.08×10^{-7}	1.56×10^{-7}

nonlinearity of feedback systems with more complex frequency-dependent elements, but with the same combination of loop gain and phase margin.

Only second-order nonlinearities were used in the models because of the large number of simulations that were required.

Nonlinearity Located before the Frequency-Dependent Elements

The results from several computer simulations of feedback systems with a nonlinear function before the frequency-dependent elements are given in this section. The system model is described by identifying the symbols in Figure 7.2 as

$$B = G_1 = H = 1, \qquad \text{(a)}$$

$$G_2 = \frac{1}{S} \cdot \frac{1}{PS + 1}, \qquad \text{(b)}$$

$$\text{and} \quad n = 2, \qquad \text{(c)} \qquad (7.13)$$

where the magnitude of the variable P was adjusted to obtain certain phase margins for each value of linear gain, A. The variable A was assigned several values between 10 and 1,000.

A sample computer output is shown in Figure 7.8. In this particular run, the variable A had a value of 20, and the variable P had a value of 0.2 which corresponds to a phase margin of 28 degrees. The CSMP computer program for this simulation is listed in Appendix V. This is the same system that was used for the previous sample output given in Figure 7.7 (page 136) except for the additional high-frequency pole. The linear waveform, VL, in

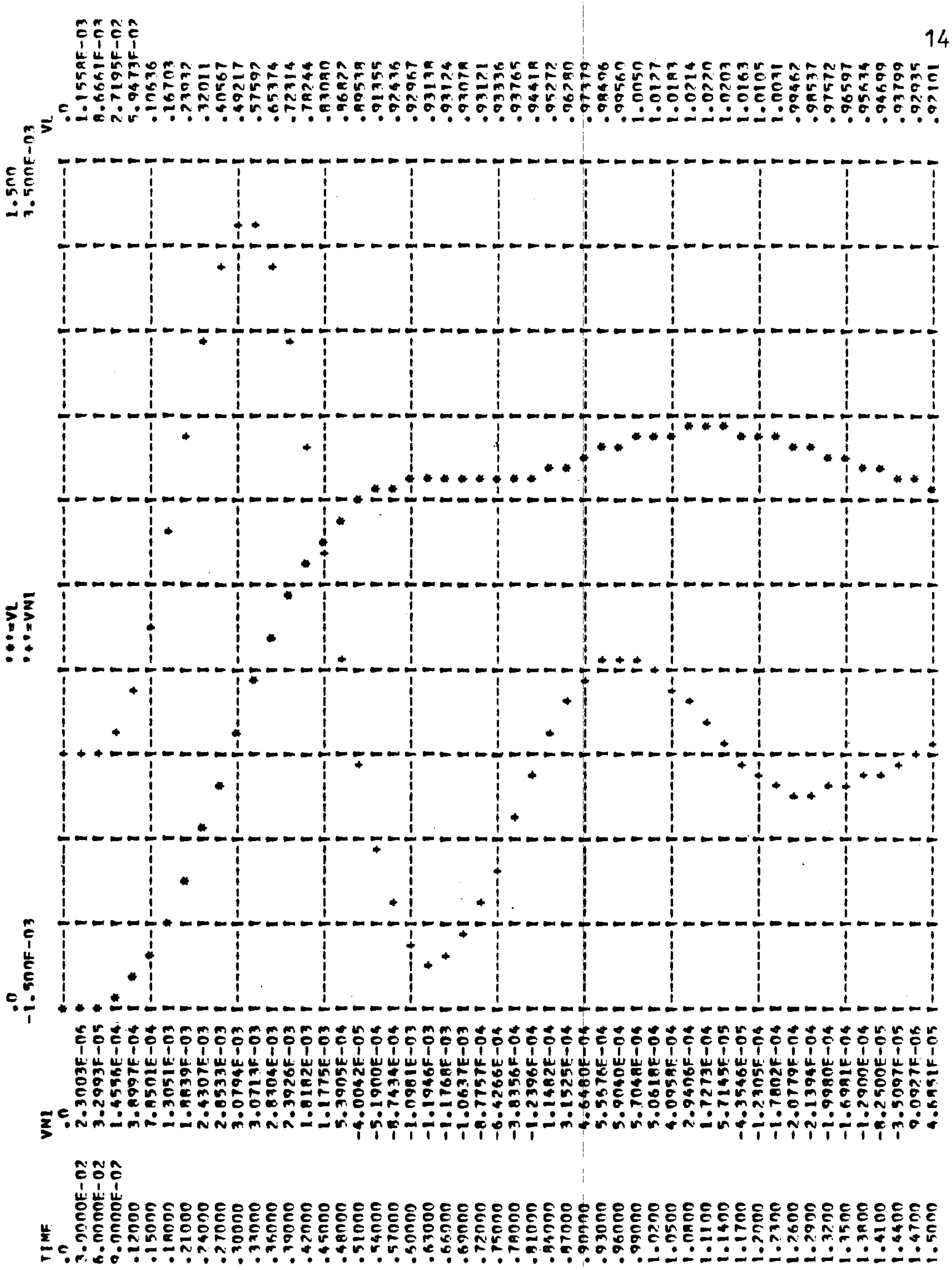

Figure 7.8. Sample output of a nonlinearity simulation run for a feedback amplifier which has a phase margin of only 28 degrees. This output shows considerable ringing compared to the sample output shown in Figure 7.7 (page 136).

Figure 7.8 has a peak value of 1.02 at 1.11 seconds. At that instant of time, the nonlinear waveform, VN1, has a value of 1.73×10^{-4}.

A comparison between Figures 7.7 (page 136) and 7.8 shows that the additional high-frequency pole causes the nonlinearity as a function of time to have considerable ringing. The magnitude of the nonlinearity is generally larger with the additional high-frequency pole. At the instants of time that the linear outputs peak, the nonlinearity in Figure 7.8 is approximately 200 times larger than the nonlinearity in Figure 7.7 (page 136).

Nonlinearities for many combinations of linear gain, A, and phase margin are given in Table 7.3. Since a phase margin of 90 degrees corresponds to a single integrating element in the forward plant, this is the initial value of phase margin given in the table. For every value of gain, A, the nonlinearity initially decreases slowly with decreasing phase margin. Below some critical phase margin, the magnitude of the nonlinearity increases rapidly.

This effect is illustrated in Figure 7.9 which is a graph of the nonlinearity as a function of phase margin for a linear gain, A, of 20. The initial value of the nonlinearity (at a phase margin of 90 degrees) is 9.01×10^{-7}. The magnitude of the nonlinearity remains below this value until the phase margin drops below its first critical value, PM1, of 48 degrees. As the phase margin decreases just 4 additional degrees, the magnitude of the nonlinearity rapidly increases a factor of five times the initial value of nonlinearity, and reaches a value of 5.14×10^{-6}. The nonlinearity reverses polarity past this point and drops to large negative values.

Table 7.3. Closed-loop nonlinearity of example nonlinear feedback systems with the nonlinearity preceding the frequency-dependent elements.

Phase margin (degrees)	Value of linear gain						
	10	20	50	100	200	500	1000
90.0	3.76×10^{-5}	9.01×10^{-7}	7.44×10^{-9}	2.15×10^{-10}	5.89×10^{-12}	7.29×10^{-14}	2.19×10^{-15}
78.9	2.04×10^{-5}	4.33×10^{-7}	5.68×10^{-9}	1.31×10^{-10}	4.04×10^{-12}	4.53×10^{-14}	*
69.5	4.89×10^{-6}	1.31×10^{-7}	3.05×10^{-9}	5.64×10^{-11}	1.80×10^{-12}	1.60×10^{-14}	1.10×10^{-15}
59.0	1.20×10^{-5}	-1.60×10^{-7}	-2.00×10^{-10}	-3.67×10^{-11}	-1.04×10^{-12}	-1.21×10^{-14}	-1.25×10^{-16}
56.3	3.86×10^{-5}	*	*	*	*	*	*
54.0	7.97×10^{-5}	*	*	*	*	*	*
51.8	1.30×10^{-4}	-3.95×10^{-7}	-2.58×10^{-9}	-1.08×10^{-10}	-3.24×10^{-12}	-3.34×10^{-14}	-7.24×10^{-16}
49.9	1.74×10^{-4}	-6.92×10^{-8}	-3.18×10^{-9}	-1.29×10^{-10}	*	*	*
48.2	1.94×10^{-4}	8.33×10^{-7}	-3.69×10^{-9}	-1.46×10^{-10}	*	*	*
46.6	1.74×10^{-4}	2.34×10^{-6}	-4.11×10^{-9}	-1.62×10^{-10}	*	*	*
45.2	1.03×10^{-4}	4.06×10^{-6}	-4.45×10^{-9}	-1.75×10^{-10}	-5.20×10^{-12}	-5.75×10^{-14}	-1.29×10^{-15}
43.9	-2.95×10^{-4}	5.14×10^{-6}	-4.71×10^{-9}	-1.86×10^{-10}	*	*	*
42.7	-1.83×10^{-3}	4.45×10^{-6}	-4.82×10^{-9}	-1.94×10^{-10}	*	*	*
41.6	-2.36×10^{-3}	9.15×10^{-7}	-4.59×10^{-9}	-2.00×10^{-10}	*	*	*
40.5	-2.48×10^{-3}	-6.19×10^{-6}	-3.95×10^{-9}	-2.03×10^{-10}	*	*	*
39.6	-2.42×10^{-3}	-1.70×10^{-5}	-6.85×10^{-9}	-2.04×10^{-10}	*	*	*
38.7	-2.37×10^{-3}	-3.79×10^{-5}	-8.49×10^{-9}	-2.02×10^{-10}	-6.09×10^{-12}	-6.86×10^{-14}	-1.63×10^{-15}
35.6	*	*	*	*	-5.36×10^{-12}	*	*
33.2	*	*	*	*	-3.50×10^{-12}	-4.12×10^{-14}	8.64×10^{-16}
28.0	1.58×10^{-3}	1.97×10^{-4}	-1.23×10^{-6}	5.84×10^{-10}	8.59×10^{-12}	7.66×10^{-14}	9.19×10^{-16}
23.8	*	*	*	*	*	2.17×10^{-12}	1.21×10^{-14}

* Not determined

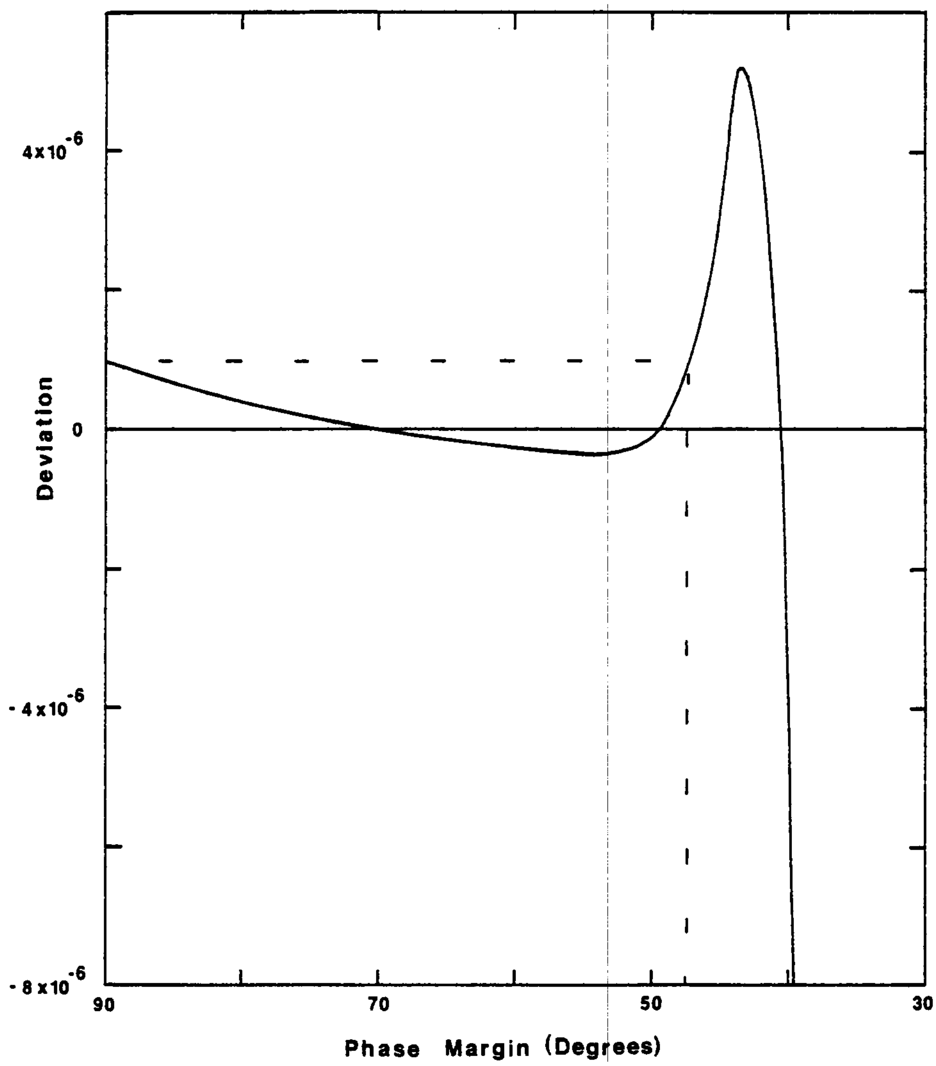

Figure 7.9. Closed-loop nonlinearity as a function of phase margin for example feedback systems with the nonlinear function located before the frequency-dependent elements.

A second critical phase margin, PM2, is identified at 41 degrees where the value of the nonlinearity drops below -5.14×10^{-6}.

Critical values of phase margin were found for every value of linear gain, A, given in Table 7.3. These critical phase margins are sketched as a function of the linear gain in Figure 7.10 (dashed line). From the limited data given in this figure, the critical phase margin appears to approach a constant value of 27 degrees as the magnitude of the linear gain gets large.

Nonlinearity Located after the Frequency-Dependent Elements

The results of simulations are given in this section for systems with nonlinear functions located after the frequency-dependent elements. For these simulations, the symbols in Figure 7.2 are described by

$$A = G_2 = H = 1, \qquad \text{(a)}$$

$$G_1 = \frac{1}{S} \cdot \frac{1}{PS + 1}, \qquad \text{(b)}$$

$$B = 0.05, \qquad \text{(c)}$$

$$\text{and} \quad n = 2, \qquad \text{(d)} \qquad (7.14)$$

where the linear gain, K, was given several values between 10 and 1,000. The value of the variable P was adjusted to vary the phase margin of the system at each value of K. The input waveform for all the simulations is described by Equation (7.11) again.

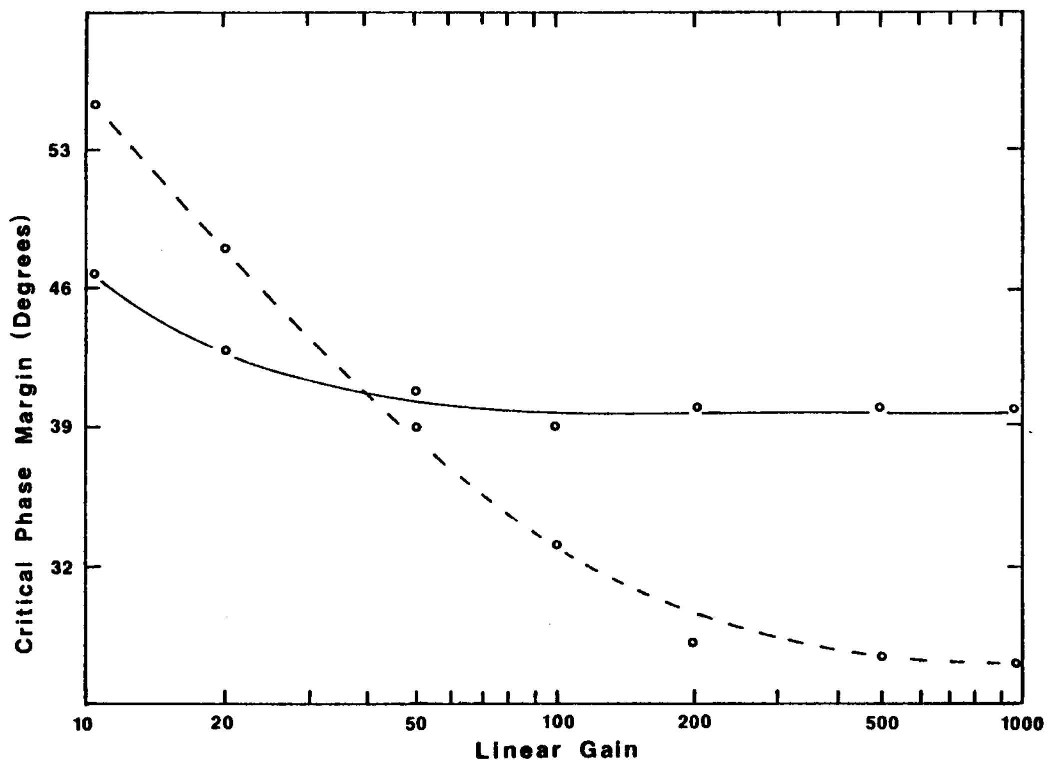

Figure 7.10. Critical phase margins of nonlinear feedback systems with the nonlinearity located before the frequency-dependent elements (dashed lines) and the nonlinearity located after the frequency-dependent elements (solid line).

Nonlinearities obtained for several combinations of gain, K, and phase margin are listed in Table 7.4. As with the previous set of simulation results, the magnitude of the nonlinearity initially decreases with decreasing phase margin, regardless of the value of the variable K. Below a certain value of phase margin, the magnitude of the nonlinearity increases rapidly. This point is illustrated in Figure 7.11 with the nonlinearity plotted as a function of the phase margin for the system with the linear gain set at 20. The critical value of phase margin for this particular system is approximately 42 degrees.

The critical phase margins, found from the data in Table 7.4, were plotted as a function of the linear gain in Figure 7.10 (solid line). The critical phase margin appears to approach a constant value of 40 degrees for increasing values of linear gain.

V. A PRACTICAL CONSIDERATION FOR MEASURING NONLINEARITY

Since the nonlinearity of pulse amplifiers is a function of time, there is a practical consideration to take into account when measuring or quantifing the magnitude of the nonlinearity of an amplifier. Depending on the type of peak detector, the magnitude of the pulse height might be determined slightly before or after the actual peak of pulse. This type of error can greatly affect the magnitude of the nonlinearity of an amplifier, and the nonlinearity of a specific pulse amplifier can vary significantly from one spectroscopy system to another. Therefore, nonlinearity of pulse amplifiers should be

Table 7.4. Closed-loop nonlinearity of example nonlinear feedback systems with the nonlinearity following the frequency-dependent elements.

Phase margin (degrees)	Value of linear gain						
	10	20	50	100	200	500	1000
90.0	9.22×10^{-4}	1.60×10^{-4}	3.63×10^{-5}	1.03×10^{-5}	2.30×10^{-6}	4.06×10^{-7}	1.08×10^{-7}
78.9	9.34×10^{-4}	1.91×10^{-4}	3.37×10^{-5}	8.20×10^{-6}	2.04×10^{-6}	3.46×10^{-7}	*
69.5	6.17×10^{-4}	1.26×10^{-4}	2.48×10^{-5}	6.07×10^{-6}	1.52×10^{-6}	2.03×10^{-7}	7.26×10^{-8}
59.0	3.25×10^{-4}	9.10×10^{-5}	1.14×10^{-5}	2.89×10^{-6}	7.45×10^{-7}	3.35×10^{-8}	2.42×10^{-8}
51.8	-2.83×10^{-6}	-7.18×10^{-6}	-2.14×10^{-6}	-2.94×10^{-7}	-1.86×10^{-8}	1.49×10^{-8}	2.24×10^{-8}
49.9	-1.69×10^{-4}	-3.41×10^{-5}	-6.60×10^{-6}	-7.19×10^{-7}	*	*	*
48.2	-5.07×10^{-4}	-5.36×10^{-5}	-1.11×10^{-5}	-1.78×10^{-6}	*	*	*
46.6	-1.08×10^{-3}	-6.68×10^{-5}	-1.56×10^{-5}	-2.85×10^{-6}	*	*	*
45.2	-1.92×10^{-3}	-8.14×10^{-5}	-2.01×10^{-5}	-3.89×10^{-6}	-1.04×10^{-6}	-1.64×10^{-7}	-1.49×10^{-7}
43.9	-3.80×10^{-3}	-1.12×10^{-4}	-2.45×10^{-5}	-4.96×10^{-6}	*	*	*
42.7	-6.00×10^{-3}	-1.74×10^{-4}	-2.91×10^{-5}	-6.09×10^{-6}	*	*	*
41.6	-4.26×10^{-3}	-2.83×10^{-4}	-3.35×10^{-5}	-7.22×10^{-6}	*	*	*
40.5	-3.47×10^{-3}	-4.47×10^{-4}	-3.80×10^{-5}	-8.33×10^{-6}	*	*	*
39.6	-2.01×10^{-3}	-6.63×10^{-4}	-4.25×10^{-5}	-9.36×10^{-6}	*	*	*
38.7	-1.34×10^{-3}	-9.40×10^{-4}	-4.70×10^{-5}	-1.04×10^{-5}	-2.59×10^{-6}	-4.14×10^{-7}	-1.14×10^{-7}
35.6	*	*	*	*	-3.61×10^{-6}	*	*
33.2	*	*	*	*	-4.65×10^{-6}	-7.34×10^{-7}	-1.97×10^{-7}
28.0	1.13×10^{-2}	4.69×10^{-3}	3.63×10^{-5}	-3.15×10^{-5}	-7.74×10^{-6}	-1.21×10^{-6}	-2.98×10^{-7}
23.8	*	*	*	*	*	-3.53×10^{-6}	-4.69×10^{-7}

* Not determined

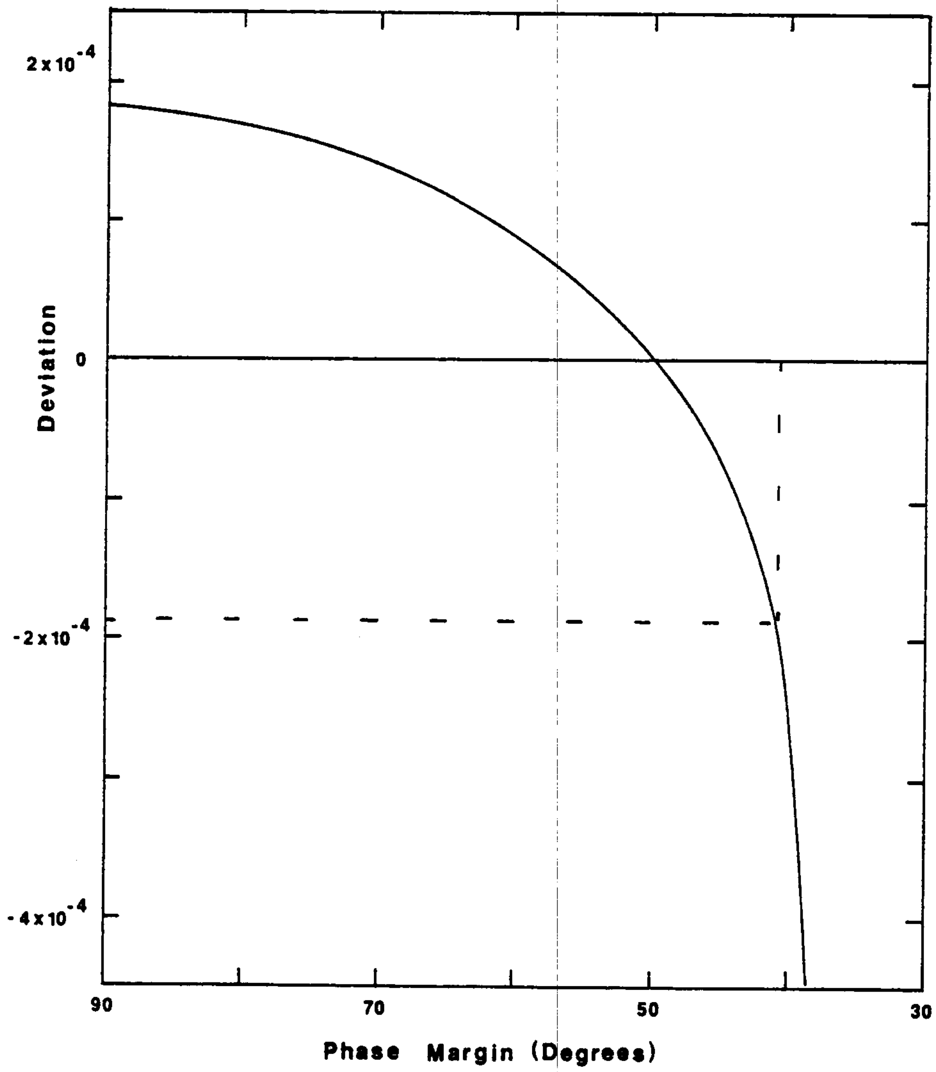

Figure 7.11. Closed-loop nonlinearity as a function of phase margin for example feedback systems with the nonlinear function located after the frequency-dependent elements.

specified as the maximum value within a specified neighborhood of the peak of the pulse.

CHAPTER VIII

SUMMARY

I. OVERALL RESULTS

Methods were developed in this study to help a designer determine the integral nonlinearity of a given instrument. Analytical techniques were investigated for determining the integral nonlinearity of frequency-independent nonlinear functions, and computer simulation techniques were developed for determining the integral nonlinearity of frequency-dependent nonlinear systems. Useful tables of formulas and some design guidelines are generated from the development of these methods.

II. SUBRESULTS

Direct-Procedure Calculations of Frequency-Independent Nonlinearities

A procedure for determining the integral nonlinearity of a function at low frequencies was developed. Using this procedure, the integral nonlinearities of six single-stage bipolar transistor amplifier configurations due to the exponential characteristic of the base-emitter junction of the bipolar transistor were determined. Since this source of nonlinearity is important in bipolar transistor amplifiers, the results of the analysis are listed in tables for ready reference. Also, the integral nonlinearity of four single-stage JFET amplifier configurations due to the square-law characteristic of the device in the saturated region were determined using the same procedure. Since this is an important source of nonlinearity in JFET amplifiers, these results were also listed in tables for ready reference.

Laboratory measurements given in this study indicate that the nonlinearity expressions in the two tables are accurate. Nonlinearity measurements for bipolar transistor amplifiers were typically within 5% of the predicted values, and nonlinearity measurements for JFET amplifiers were typically within 10% of the predicted values.

This procedure for evaluting the nonlinearity of a function proved to be cumbersome for all but the most simple functions. The nonlinearity expressions that were generated were usually complex and not easy to evaluate. For example, the expressions generated for the JFET differential amplifier configuration were so complex that the author deemed them useless. Therefore, for most nonlinear functions, this direct approach of evaluating integral nonlinearity is not recommended unless the utmost accuracy is needed, or unless the approximation techniques given in this study do not work.

Two-Term Polynomial Approximations of Nonlinearities

The nonlinearities of some polynomial functions were evaluated in this study. The two-term polynomials seem to provide the most insight into the evaluation of the nonlinearities. For example, the point of maximum deviation for the second-order two-term polynomial is at half of full scale. Therefore, functions which have a significant second-order term in their Taylor series expansions should have peak deviations at approximately half of full scale. Amplifier configurations which have nonlinear functions of this type are common-emitter, common-source, emitter-follower, and source-follower amplifiers. The third-order two-term polynomial has a peak deviation at 57.7% of full scale. Therefore, nonlinear functions which do not have significant second-order terms in their Taylor series expansions, but do have significant third-order terms, should have peak deviations at approximately 57.7% of full scale. Amplifier configurations which have nonlinear functions in this category are balanced differential and complementary output amplifiers. These two approximate locations of maximum deviation have been used in computer models for simulating the closed-loop nonlinearity of feedback systems, and are used in midpoint approximations of the nonlinearity of functions.

Expressions for the point of maximum deviation, integral gain, and integral nonlinearity are summarized in tables for the second-order and third-order two-term polynomials. The nonlinear functions of most single-stage amplifier configurations can be approximated by one of these two polynomials. The expressions are simple and can provide quick evaluation of the nonlinearity of a given amplifier configuration as long as the nonlinearity is less than approximately 1%. Also, these simple expressions allow comparison of the nonlinearities of similar type amplifiers.

Two-term polynomial expansions were derived for the eleven single-stage amplifier configurations that were evaluated in this study. The polynomials and nonlinearity parameters of the amplifier configurations are listed in tables for easy reference.

Midpoint Approximation of Nonlinearities

The midpoint approximation assumes that the maximum deviation of a function from its integral gain curve occurs near midscale. Using this approximation, nonlinearity expressions for two bipolar transistor amplifier configurations were derived from their nonlinear functions. For these two amplifier configurations, these nonlinearity expressions were much less complex than those developed from the exact analysis, but were more complex than the nonlinearity expressions developed from the two-term polynomial approximations. The expressions from the midpoint approximation could be evaluated quickly with a hand-held calculator. The midpoint approximation was accurate for values of nonlinearity as large 50% where the two-term polynomial approximation was accurate for values of nonlinearity only as large as 1%. The midpoint approximation appears to offer the best trade off between accuracy and ease of use for calculating integral nonlinearities.

Significance of Integral Gain in Feedback Systems

Analysis in CHAPTER II showed that loop transmission of a feedback amplifier should be calculated from the integral gain of that amplifier when evaluating the closed-loop nonlinearity at midband. In addition, some laboratory measurements have indicated that loop transmissions of feedback amplifiers calculated from the integral gain of the amplifier predict closed-loop rise times and closed-loop output impedances more accurately than loop transmissions calculated from small-signal gains. Therefore, the integral gain expressions given in the tables of nonlinearity parameters of the single-stage amplifiers may prove valuable for evaluating the performance of negative feedback amplifiers.

Comparison of Similar-Type Amplifier Configurations

Similar-type amplifier configurations were compared in CHAPTER V. The criteria for this comparison is most useful for comparing the nonlinearity of output stages of multistage amplifiers. For the most common output stage configurations, the bipolar complementary amplifier configuration is much more linear than either the emitter-follower or the source-follower amplifier configurations.

Spectral Dependence of Nonlinear Waveforms

The integral nonlinearity of a waveform changes when the waveform goes through a frequency-dependent transfer function. A hand analysis procedure for estimating this change in nonlinearity was developed in CHAPTER VI, and a computer simulation procedure for measuring the change in nonlinearity was given also. The computer simulation procedure is much easier to use than the hand analysis procedure. However, the hand analysis provides an empirical feel for the mechanism involved in the spectral dependence.

With the example combinations of waveforms and frequency-dependent transfer function, the change in nonlinearity of the example waveforms seemed moderate (about a factor of 2) for seemingly great distortions of waveshape (pure integration).

Integral Nonlinearity of Negative Feedback Systems with Memory

Three computer models were introduced in this study for determining the closed-loop nonlinearity of negative feedback systems with memory. These models give the nonlinearity of the feedback systems as a function of time. Using one of these computer models, a large number of computer simulations were run to determine the nonlinearity characteristics of certain types of feedback systems to a pulse shape that is common in nuclear spectroscopy. The results of these simulations indicate that the closed-loop nonlinearity of operational-type feedback amplifiers is inversely proportional to the square of the gain-bandwidth product of the loop transmission. Further simulations revealed that for best linearity performance that the phase margin of the closed-loop amplifier should be greater than approximately 45 degrees.

The minimum value of acceptable phase margin for good linearity performance of a given system can be particularly important. For phase margins down to a certain level, the closed-loop nonlinearity of the example systems remained at relatively low levels. Once the phase margin dropped below a critical value, the closed-loop nonlinearity of the amplifier increased rapidly. The significance of this result is that the linearity performance of a physical amplifier over a given temperature range may depend on the phase margin of the system remaining above the critical value.

The time dependence of the nonlinearity of feedback amplifiers has significance for physical systems. The nonlinearity of a waveform at the output of a feedback amplifier can vary greatly in the neighborhood of the peak. Some spectroscopy systems may determine the amplitude of a pulse slightly before or slightly after the actual peak, and the nonlinearity of a particular amplifier may differ from one spectroscopy system to another. Therefore, the linearity performance of pulse amplifiers should be specified for a given neighborhood of the pulse peak.

III. AREAS FOR FURTHER RESEARCH

Only a few sources of nonlinearity in solid-stage amplifiers were investigated in this dissertation. However, these sources of nonlinearity were investigated in great detail such that the methods involved could be carefully examined and compared. The next logical step in the investigation would be to evaluate many sources of nonlinearity in solid-state amplifiers in little detail, perhaps using the two-term polynomial approximations.

Another area for future investigation is the case where the derivative of the nonlinear function is neither monotonically increasing nor monotonically decreasing. In such a case, the deviation may have more than one local maximum/minimum. An example is given in Appendix IV of a deviation which can have more than one local maximum/minimum.

REFERENCES

REFERENCES

[1] B. Gilbert, "A Versatile Monolithic Voltage-to-Frequency Converter," IEEE Journal of Solid-State Circuits, Vol. SC-11 No. 6, pp. 852-864, Dec. 1976.

[2] K.P.P. Nambiar and A.R. Boothroyd, "Junction-Transistor Bootstrap Linear-Sweep Circuits," Proceedings of IEE (London), Vol. 104, pt. B, pp. 293-306, Jan. 1957.

[3] E.G. Shapiro, "Linear Seven-Decade Current/Voltage-to-Frequency Convert," IEEE Nuclear Science Transactions, Vol. NS-17, No. 1, pp. 335-344, Feb. 1970.

[4] D.R. Fewer, "Design Principles for Junction Transistor Audio Power Amplifiers," IRE Transactions on Audio, Vol. AU-3, No. 6, pp. 183-201, Nov.-Dec. 1955.

[5] J.R. MacDonald, "Nonlinear Distortion Reduction by Complementary Distortion," IRE Transactions on Audio, Vol. AU-7, No. 5, pp. 128-133, Sept.-Oct. 1959.

[6] J.R. MacDonald, "More on Nonlinear Distortion Correction," IRE Transactions on Audio, Vol. AU-9, No. 4, pp. 103-105, July-Aug. 1961.

[7] D.R. Fewer, "Transistor Nonlinearity--Dependence on Emitter Bias Current in PNP Alloy Junction Transistors," IRE Transactions on Audio, Vol. AU-6, No. 2, pp. 41-44, Mar.-Apr. 1958.

[8] G.M. Riva, P.J. Beneteau, E.D. Volta, "Amplitude Distortion in Transistor Amplifiers," Proceedings of IEE (London), Vol. 111, No. 3, pp. 481-490, Mar. 1964.

[9] Y.L. Kuo, "Distortion Analysis of Bipolar Transistor Circuits," IEEE Transactions on Circuit Theory, Vol. CT-20, No. 6, pp. 709-716, Nov. 1973.

[10] K. Gopal, M.S. Nakhla, K. Singhal, J. Vlach, "Distortion Analysis of Transistor Networks," IEEE Transactions on Circuits and Systems, Vol. CAS-25, No. 2, pp. 99-106, Feb. 1978.

[11] S. Narayanan, "Transistor Distortion Analysis Using Volterra Series Representation," The Bell System Technical Journal, Vol. 46, No. 5, pp. 991-1024, May 1967.

[12] R. Beaufoy, and J.J. Sparkes, "The Junction Transistor as a Charge-Controlled Device," Automated Telephone and Electric Co. Journal (London), Vol. 13, No. 4, pp. 310-327, Oct. 1957.

[13] D.J. Hamilton, F.A. Lindholm, and J.A. Narud, "Comparison of Large Signal Models for Junction Transistors," Proceedings of the IEEE, Vol. 52, No. 3, pp. 239-248, Mar. 1964.

[14] H.K. Gummel, and H.C. Poon, "An Integral Charge Control Model of Bipolar Transistors," The Bell System Techical Journal, Vol. 49, No. 5, pp. 827-852, May 1970.

[15] I. Richer, and R.D. Middlebrook, "Power-Law Nature of Field-Effect Transistor Experimental Characteristics," Proceedings of the IEEE, Vol. 51, No. 8, pp. 1145-1146, Aug. 1963.

[16] R.D. Middlebrook, "A Simple Derivation of Field-Effect Transistor Characteristics," Proceedings of the IEEE, Vol. 51, No. 8, pp. 1146-1147, Aug. 1963.

[17] W. Shockley, "A Unipole 'Field-Effect' Transistor," Proceedings of the IRE, Vol. 40, No. 11, pp. 1365-1376, Nov. 1952.

[18] G.C. Dacey, and I.M. Ross, "The Field Effect Transistor," The Bell System Technical Journal, Vol. 34, No. 11, pp. 1149-1189, Nov. 1955.

[19] A.B. Grebene, and S.K. Ghandhi, "General Theory for Pinched Operation of the Junction-Gate FET," Solid-State Electronics, Vol. 12, pp. 573-589, 1969.

[20] K. Lehovec, and R. Zuleeg, "Voltage-Current Characteristics of GaAs J-FET's in the Hot Electron Range," Solid-State Electronics, Vol. 13, pp. 1415-1426, 1970.

[21] T. Taki, "Approximation of Junction Field-Effect Transistor Characteristics by a Hyperbolic Function," IEEE Journal of Solid-State Circuits, Vol. SC-13, No. 5, pp. 724-726, Oct. 1978.

[22] D.P. Kennedy, and R.R. O'Brien, "Computer Aided Two-Dimensional Analysis of the Junction Field-Effect Transistor," IBM Journal of Research and Development, Vol. 14, No. 3, pp. 125-141, Mar. 1970.

[23] H.S. Black, "Stabilized Feedback Amplifiers," The Bell System Technical Journal, Vol. 13, pp. 1-18, Jan. 1934.

[24] C.A. Desoer, "Nonlinear Distortion in Feedback Amplifiers," IRE Transactions on Circuit Theory, Vol. CT-9, No. 3, pp. 2-6, Mar. 1962

[25] R.W. Ketchledge, "Distortion in Feedback Amplifiers," The Bell System Technical Journal, Vol. 34, No. 11, pp. 1265-1285, Nov. 1955.

[26] G. Zames, "Functional Analysis Applied to Nonlinear Feedback Systems," IEEE Transactions on Circuit Theory, Vol. CT-10, No. 9, pp. 392-404, Sept. 1963.

[27] L. Strauss, Wave Generation and Shaping, (McGraw-Hill, 1970), Chapter 6, pp. 273-275.

[28] J. Millman, and H. Taub, Pulse, Digital, and Switching Waveforms, (McGraw-Hill, 1965), Chapter 14, pp. 515-516.

[29] "USA Standard and IEEE Test Procedure for Amplifiers and Preamplifiers for Semiconductor Radiation Detectors," IEEE Transactions on Nuclear Science, NS-16 (6), pp. 283-301, Dec. 1969.

[30] E.L. Zuch, Data Acquisition and Conversion Handbook, (Datel-Intersil, 1979), Chapter 2, pp. 44-45.

[31] J.J. Ebers, and J.L. Moll, "Large-Signal Behavior of Junction Transistors," Proceeding of the IRE, Vol. 42 (12), pp. 1761-1772, Dec. 1954.

[32] D.M. Miller, "Nonlinearity and Cross Modulation in Field-Effect Trasistors," IEEE Journal of Solid-State Circuits, Vol. SC-6, No. 4, pp. 244-250, Aug. 1971.

[33] B.D. Wedlock, "Direct Determination of the Pinch-Off Voltage of a Depletion-Mode Field-Effect Transistor," Proceeding of the IEEE, Vol. 57 (1), pp. 75-77, Jan. 1969.

[34] P.J. Billam, "Harmonic Distortion in a Class of Linear Active Filter Network," Journal of the Audio Engineering Society, Vol. 26, No. 6, pp. 426-429, June 1978.

APPENDICES

APPENDIX I

DERIVATION OF THE LOW-FREQUENCY TRANSFER FUNCTIONS OF BIPOLAR COMPLEMENTARY AND DIFFERENTIAL AMPLIFIERS

The following two low-frequency derivations use the simplified Ebers-Moll model of the bipolar transistor described by Equations (3.3) and (3.4) (page 34). The model of the bipolar complementary amplifier is shown in Figure 3.1 (page 37). The initial bias current leaving the emitter of transistor Q_1 and entering the emitter of transistor Q_2 in Figure 2 is given by

$$I_{oe} \cong I_{s1}\, e^{\frac{qV_1}{kT}} = I_{s2}\, e^{\frac{qV_2}{kT}} \tag{A1.1}$$

where I_{s1} and I_{s2} are the pseudo-saturation currents of the two transistors, and V_1 and V_2 are the initial base-to-emitter voltages. The bias network of the complementary stage maintains the sum of the two base-to-emitter voltages at a constant $(V_1 + V_2)$. For a given output voltage, the output current is given by

$$I_{out} = \frac{V_{out}}{R_L} = I_{s1}\, e^{\frac{q(V_1 + \Delta V_{BE})}{kT}} - I_{s2}\, e^{\frac{q(V_2 - \Delta V_{BE})}{kT}} \tag{A1.2}$$

or

$$\frac{V_{out}}{R_L} = I_{oe}\left(e^{\frac{q\Delta V_{BE}}{kT}} - e^{-\frac{q\Delta V_{BE}}{kT}}\right). \tag{A1.3}$$

This equation can be simplified to the following form,

$$\frac{V_{out}}{R_L} = 2I_{oe} \sinh\left(\frac{q\Delta V_{BE}}{kT}\right). \tag{A1.4}$$

The variation in base-to-emitter voltage as a function of output voltage can be obtained from Equation (A1.4) and is

$$\Delta V_{BE} = \frac{kT}{q} \sinh^{-1}\left(\frac{V_{out}}{2I_{oe}R_L}\right). \tag{A1.5}$$

The model of the bipolar differential amplifier is shown in Figure 3.2 (page 43). The sum of the two emitter currents, I_1 and I_2, is equal to the bias current, I_o. The voltage at the emitters of the two transistors is V_x. The emitter current of the transistor Q_1 is

$$I_1 \cong I_s\, e^{\frac{q(V_n - V_x)}{kT}} = I_s e^{-\frac{qV_x}{kT}}\, e^{\frac{qV_n}{kT}} \tag{A1.6}$$

and the emitter current of the transistor Q_2 is

$$I_2 \cong I_s\, e^{\frac{-qV_x}{kT}}. \tag{A1.7}$$

The variable V_x may be eliminated by rewriting I_1 as a function of I_2, or

$$I_1 = I_2\, e^{\frac{-qV_n}{kT}}. \tag{A1.8}$$

Since the sum of the two emitter currents is equal to the bias current,

$$I_o = I_1 + I_2 \tilde{=} I_2\, e^{\frac{qV_n}{kT}} + I_2, \tag{A1.9}$$

the emitter current, I_2, can be given as a function of the variable input voltage, V_n, and constant bias current I_o by rearranging Equation (A1.9) to

$$I_2 = \frac{I_o}{\left(1 + e^{\frac{qV_n}{kT}}\right)} . \tag{A1.10}$$

The emitter current in transistor Q_1 is then

$$I_1 \tilde{=} I_o \frac{e^{\frac{qV_n}{kT}}}{\left(1 + e^{\frac{qV_n}{kT}}\right)} . \tag{A1.11}$$

The output current of the transistor Q_1 is the increase in the collector current over the quiescent level

$$I_{out1} = \frac{V_{out1}}{R_L} \tilde{=} \alpha_1 \left(I_1 - \frac{I_o}{2}\right) = \frac{\alpha_1 I_o}{2} \frac{\left(e^{\frac{qV_n}{kT}} - 1\right)}{\left(e^{\frac{qV_n}{kT}} + 1\right)} \tag{A1.12}$$

and the output current of the transistor Q_2 is

$$I_{out2} = \frac{V_{out2}}{R_L} \tilde{=} \frac{-\alpha_2 I_o}{2} \frac{\left(e^{\frac{qV_n}{kT}} - 1\right)}{\left(e^{\frac{qV_n}{kT}} + 1\right)} \tag{A1.13}$$

where α_1 and α_2 are the emitter-to-collector current gains of Q_1 and Q_2 respectively.

APPENDIX II

SCHEMATIC DIAGRAMS OF AMPLIFIERS USED IN NONLINEARITY-MEASUREMENT TEST ARRANGEMENTS

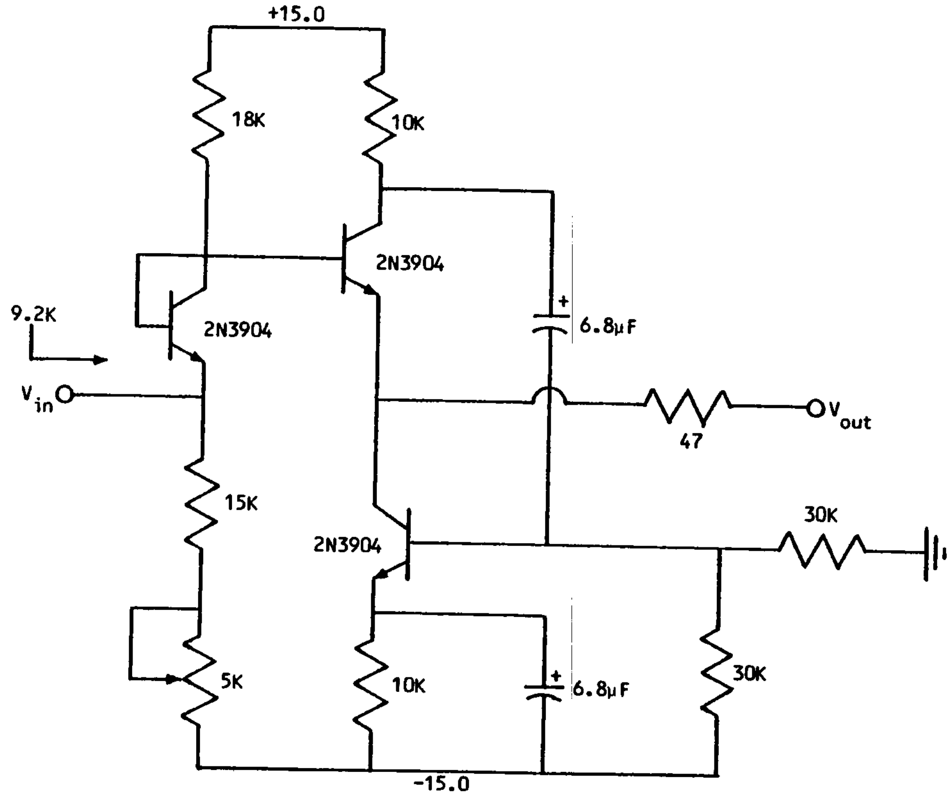

Figure A2.1. Schematic diagram of a noninverting, unity-gain amplifier, numbered one.

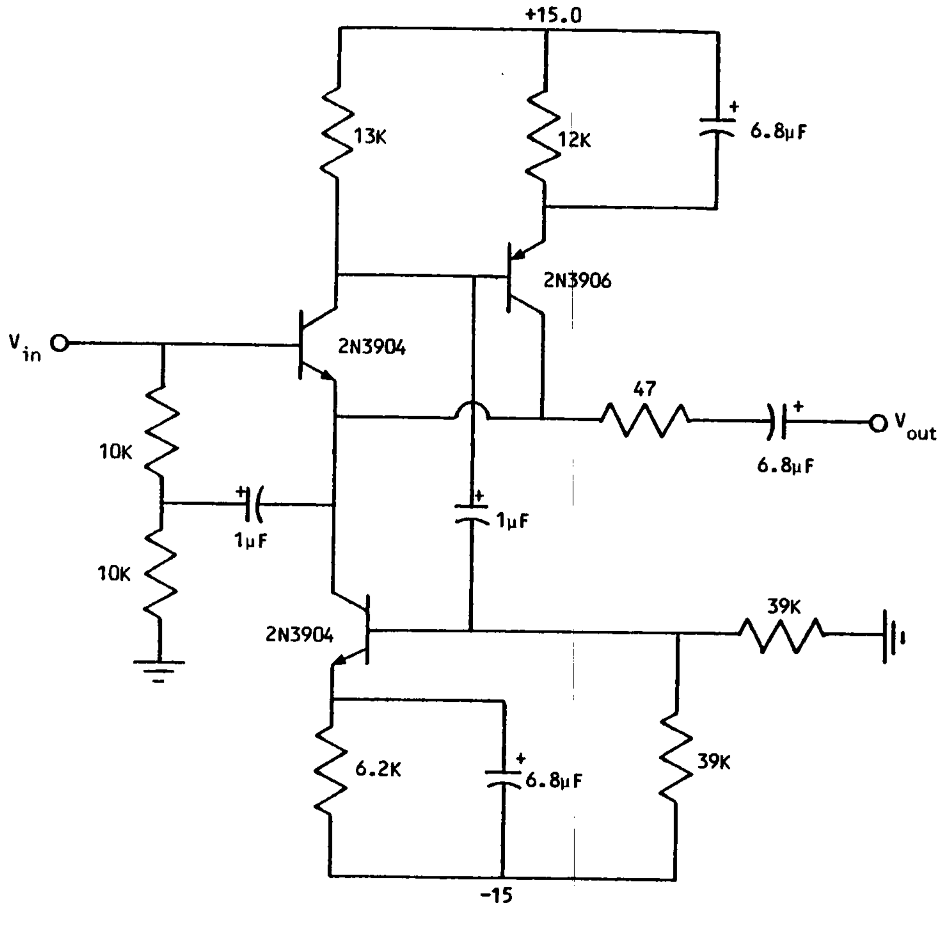

Figure A2.2. Schematic diagram of a noninverting unity-gain amplifier, numbered two.

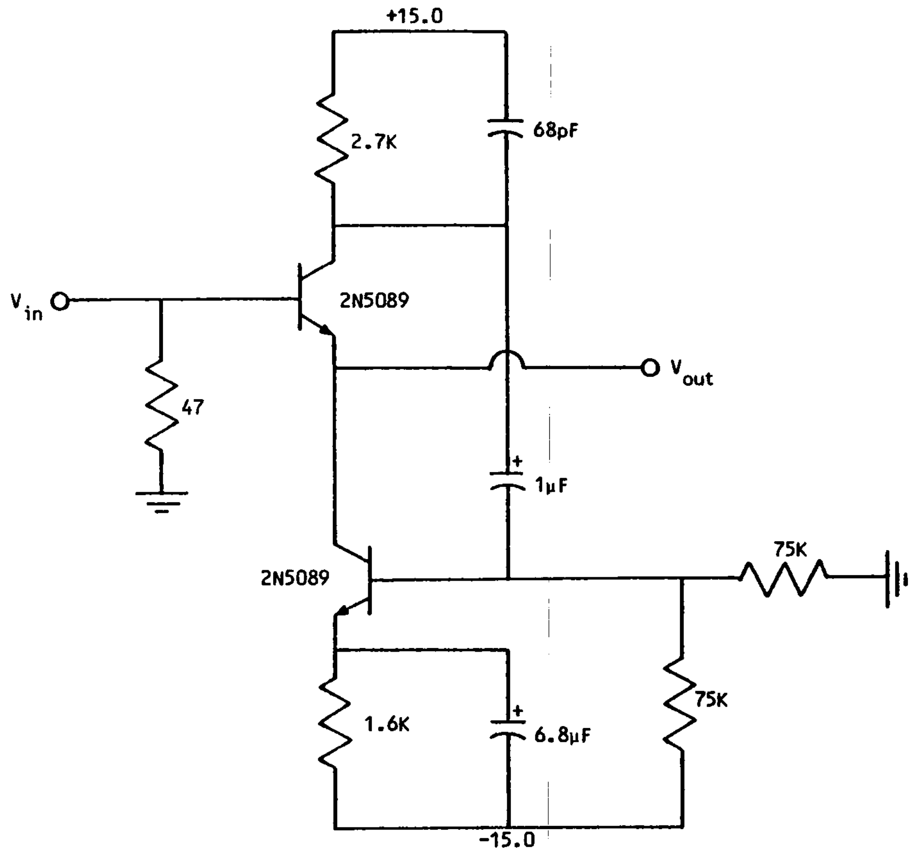

Figure A2.3. Schematic diagram of a noninverting unity-gain amplifier, numbered three.

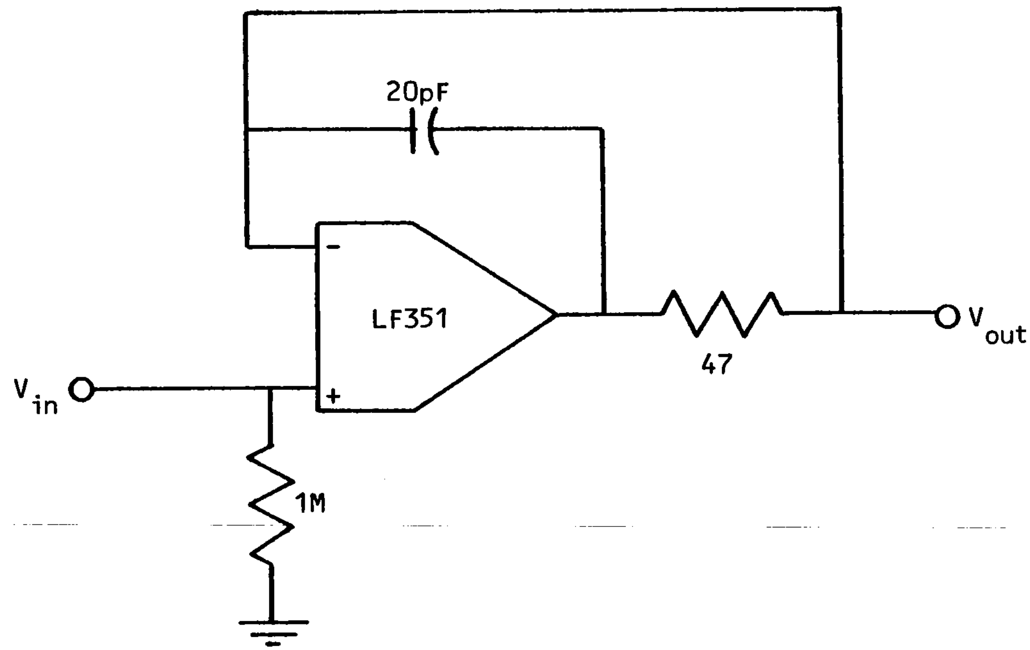

Figure A2.4. Schematic diagram of a noninverting unity-gain amplifier, numbered four.

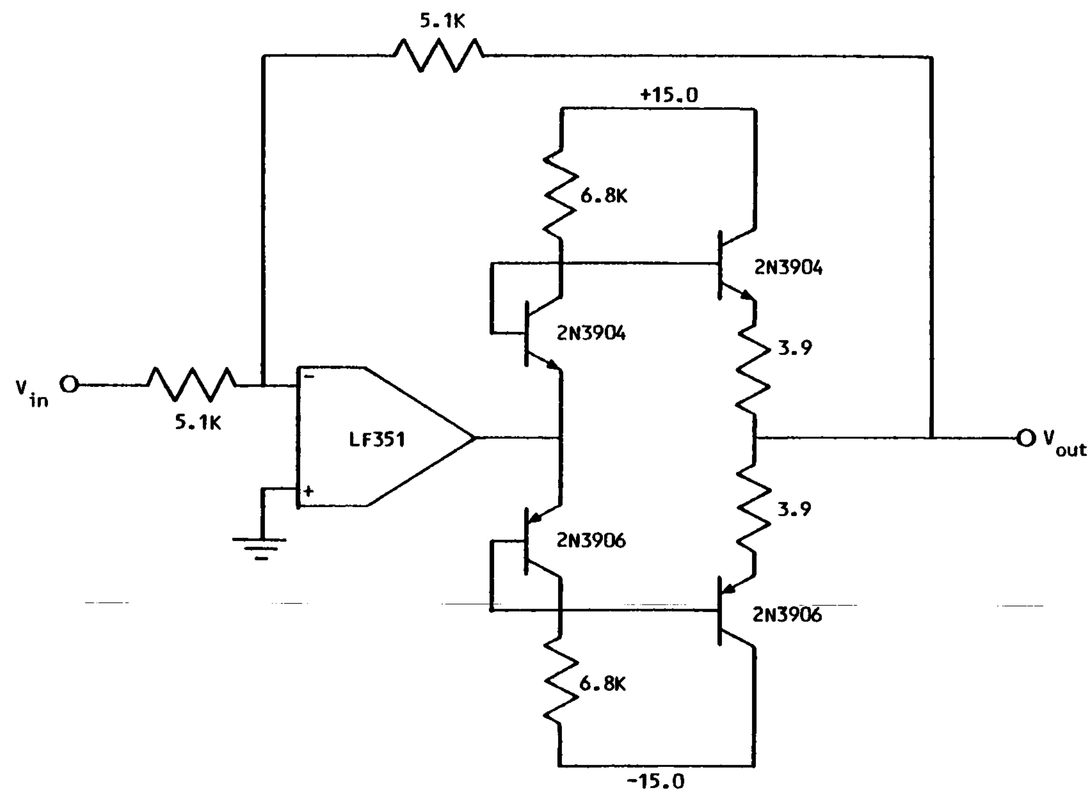

Figure A2.5. Schematic diagram of an inverting, unity-gain amplifier with a small output resistance.

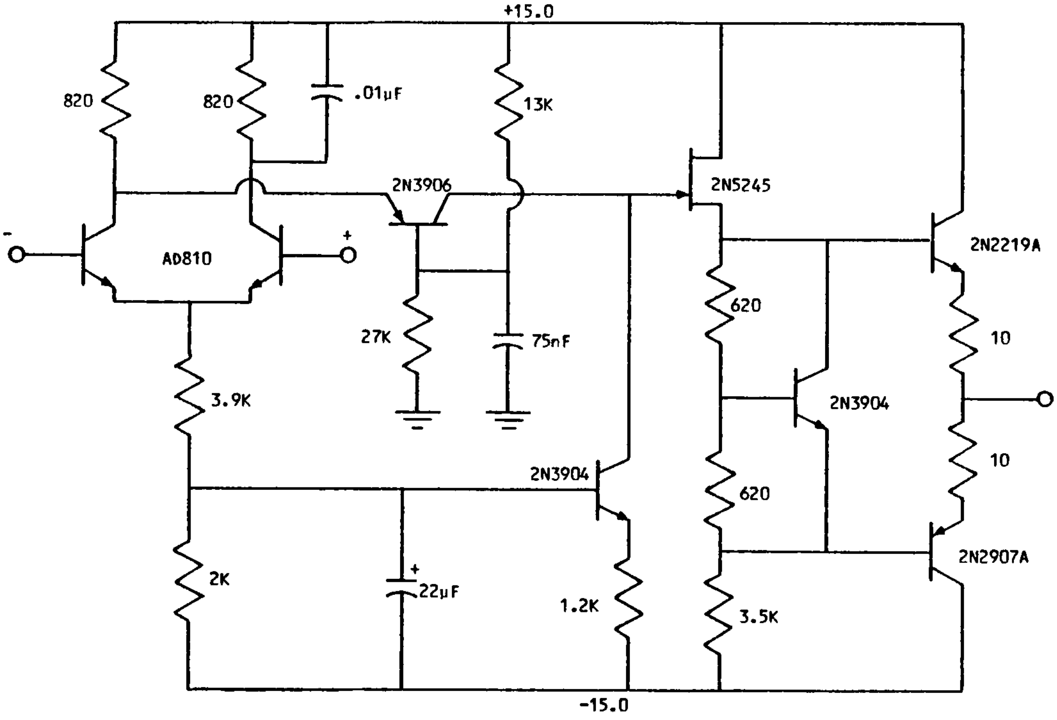

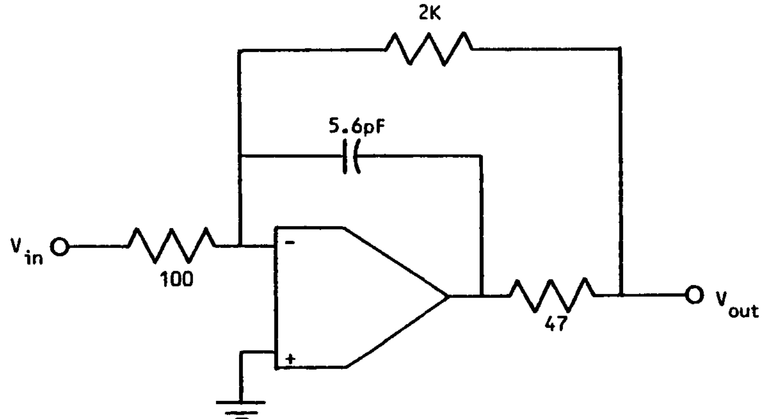

Figure A2.6. Schematic diagram and feedback configuration of an inverting, gain-of-twenty amplifier.

APPENDIX III

MEASUREMENT OF A JFET'S PARAMETERS

This appendix gives a description of the procedure used to determine three parameters of a JFET when modeled as a square-law device with some unbypassed source resistor. A schematic diagram of the model is shown in Figure A3.1. The transfer function of the JFET is given by

$$I_d = I_{dss}\left(1 - \frac{V_{gs}}{V_p}\right)^2. \tag{A3.1}$$

The resistor at the source terminal is internal to the device, and the value of the gate-to-source voltage, V_{gs}, cannot be measured directly because of the voltage drop across the resistor, R_s.

By including the effects of the unbypassed source resistor,

$$I_d = I_{dss}\left(1 - \frac{V_{in} - I_d R_s}{V_p}\right)^2, \tag{A3.2}$$

the square-law equation can be modified to

$$I_d = I_{dss}\left[\sqrt{\frac{V_{in} - V_p}{I_{dss}R_s} + \frac{V_p^{\,2}}{4I_{dss}^{\,2}R_s^{\,2}}} + \frac{V_p}{2I_{dss}R_s}\right]^2 \tag{A3.3}$$

where the variable I_d is isolated on the left side of the equation after completing the square. The three parameters of this model are the pinch-off voltage, V_p, the zero bias drain current, I_{dss}, and the unbypassed source resistance, R_s. The two variables are the drain current, I_d, and the input voltage, V_{in}.

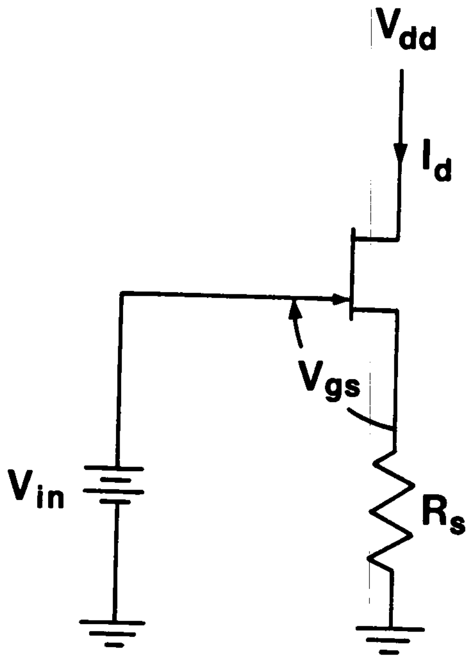

Figure A3.1. Schematic diagram illustrating the model of a JFET which includes some value of unbypassed source resistance.

The pinch-off voltage of JFETs were determined in this study by measuring the value of the gate-to-source voltage which reduced the drain current to 10 microamperes. This and other methods of determining the pinch-off voltage of JFETs have been summarized in a paper by Wedlock [33].

The value of the unbypassed source resistance can be determined by measuring two values of drain current, I_{d1} and I_{d2}, for two values of input voltage, V_{in1} and V_{in2} respectively. Substituting these measured values into Equation (A3.3) produces two equations with two unknowns. By eliminating the variable I_{dss} from the two equations gives

$$R_s = \frac{\dfrac{V_{in2}}{\sqrt{I_{d2}}} - \dfrac{V_{in1}}{\sqrt{I_{d1}}} + \left(\dfrac{1}{\sqrt{I_{d1}}} - \dfrac{1}{\sqrt{I_{d2}}}\right) V_p}{\sqrt{I_{d2}} - \sqrt{I_{d1}}} . \tag{A3.4}$$

Once the value of R_s is determined, the value of I_{dss} may be determined from Equation (A3.2).

For the JFET used in experimental measurements of the nonlinearity of several amplifiers in CHAPTER IV of this dissertation, the measured value of pinch-off voltage was -2.4531 volts. The measured values of input voltage and drain current are V_{in1} = 0.0 volts, I_{d1} = 7.909 mA, V_{in2} = -1.2264 volts, and I_{d2} = 2.450 mA. Inserting these values into Equation (A3.4) gives the value of the unbypassed source resistance is 71 ohms. From Equation (A3.2), the value of the unbiased drain current, I_{dss}, is 13.3 mA.

The drain voltage of the JFET was set at 5 volts for the above measurements. To avoid heating effects of the device, this drain voltage was pulsed. The duty cycle of the pulses was 2%.

APPENDIX IV

PROCEDURE FOR DETERMINING INPUT AT WHICH THE DEVIATION IS A MAXIMUM

In this appendix, a procedure is given for finding the value of the input variable at which the deviation of a nonlinear function is maximum. This procedure is valid for single-polarity integral nonlinearities. A third-order polynomial is used to approximate the deviation as a function of the input variable,

$$\mathrm{Del}(X) = G(1 - X)(X - Q)X, \tag{A4.1}$$

where X is the input variable, and where G and Q are constants. This function is zero when X equals zero and when X equals one, and is nonzero in between as shown in Figure A4.1.

The given criteria and function above guarantee the existence of a single maximum/minimum at a value of X between zero and one. This value of X may be found by setting the derivative of Del(X) equal to zero,

$$\frac{d\mathrm{Del}(X)}{dX} = G\left[-3X^2 + 2(1 + Q)X - Q\right] = 0, \tag{A4.2}$$

and then solving for X,

$$X = \frac{1 + Q \pm \sqrt{Q^2 - Q + 1}}{3}. \tag{A4.3}$$

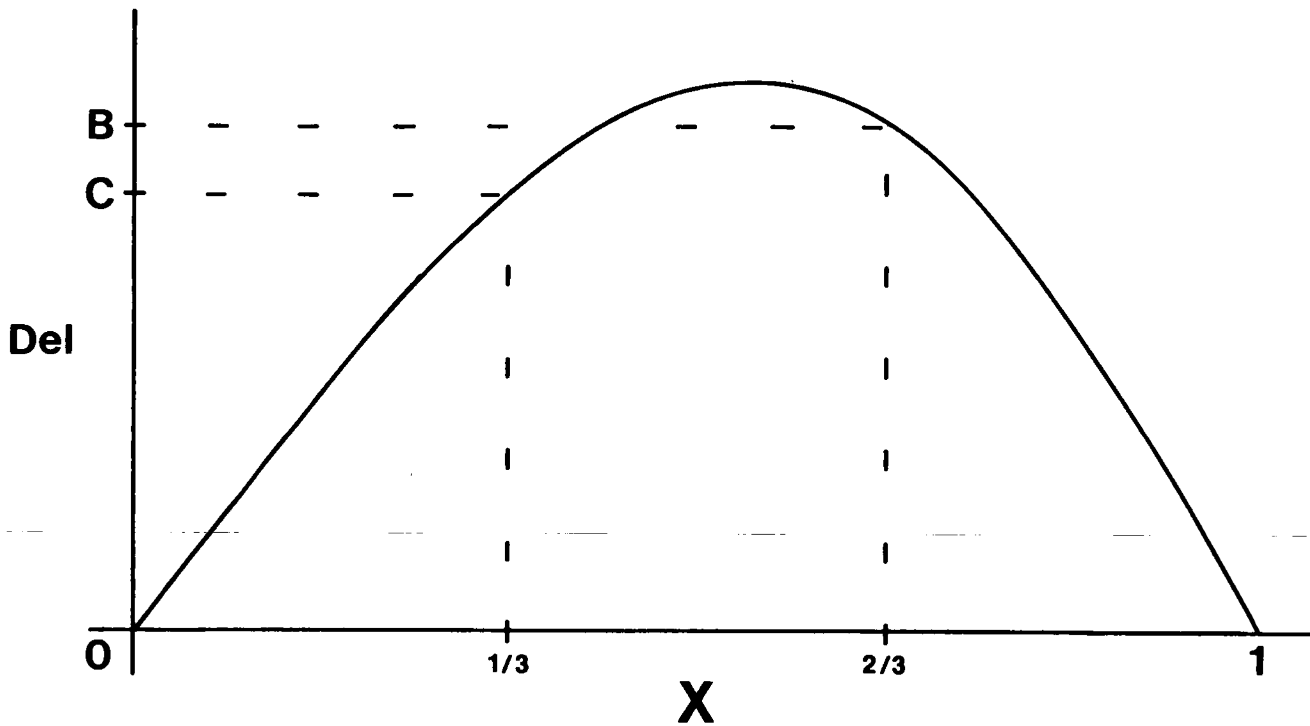

Figure A4.1. Deviation modeled as a third-order polynomial of the normalized variable X.

The value of the constant Q must be determined for any particular nonlinear function.

One method of determing Q is to determine Del(X) for values X equal to two thirds,

$$\mathrm{Del}\left(\frac{2}{3}\right) = B = G\left(1 - \frac{2}{3}\right)\left(\frac{2}{3} - Q\right)\left(\frac{2}{3}\right), \tag{A4.4}$$

and X equal to one third,

$$\mathrm{Del}\left(\frac{1}{3}\right) = C = G\left(1 - \frac{1}{3}\right)\left(\frac{1}{3} - Q\right)\left(\frac{1}{3}\right). \tag{A4.5}$$

Then Q may be found as a function of the values of deviations B and C,

$$Q = \frac{2C - B}{3(C - B)} . \tag{A4.6}$$

Substituting this value of Q into Equation (A4.3) gives two values for the variable X. The value between zero and one is the solution sought.

If the values of the deviations B and C are equal, then the value of the variable Q is undefined (i.e. infinite). In this case, the deviation is a second-order function whose maximum value occurs when X has a value of 0.5.

When the ratio of the variable B to the variable C is nearly unity,

$$\frac{B}{C} = 1 + Er \approx 1, \tag{A4.7}$$

then the value of X at which the maximum deviation occurs may be approximated by

$$X\Big|_{Delmax} \cong \frac{1}{2} + \frac{7}{18} \cdot Er. \qquad (A4.8)$$

The restrictions placed on the function Del(X) may be loosened some. This function can be allowed to have a value of zero at a single point between X equal zero and X equal one. For this case, Equation (A4.3) will give two values of X between zero and one. Both of these values of X must then be inserted into the nonlinear function to determine two values of deviation. The larger of the two values is the maximum deviation.

APPENDIX V

SAMPLE COMPUTER PROGRAMS USED TO SIMULATE

NONLINEAR SYSTEMS

```
$$$CONTINUOUS SYSTEM MODELING PROGRAM  III

      PARAM B = 0.00289352
      PARAM VN = 14.4

      PULSE = VN * (1.0-TIME) / EXP(TIME)
      HALF = PULSE / 2.0

      XY1 = PULSE + B*(PULSE**2)
      XY2 = HALF + B*(HALF**2)

      Y1 = INTGRL(0,XY1)
      Y2 = INTGRL(0,XY2)

      TIMER FINTIM = 1.1, PRDEL = 0.02
      PRINT PULSE, XY1, XY2, Y1, Y2

END
STOP
```

Figure A5.1. Computer program used to find the nonlinearity of a sample waveform before and after integration. Since a second-order two-term nonlinearity is used, both have their maximum deviations where the linear input is at half of its maximum amplitude. A block diagram of this system is shown in Figure 6.4 (page 110).

```
$$$CONTINUOUS SYSTEM MODELING PROGRAM  III

      PARAM A = 20.0

      PLSL = 2.718 * TIME / EXP(TIME)

      EL = PLSL - VL
      DVL = EL * A
      VL = INTGRL(0,DVL)

      PLSN = EL**2
      DVN = PLSN - (A * VN)
      VN = INTGRL(0,DVN)

TIMER FINTIM = 1.5, OUTDEL = 0.03
PRTPLT VN (VL)

END
STOP
```

Figure A5.2. Computer program which produced the output shown in Figure 7.7 (page 136). Simulation of the nonlinearity of a feedback system with an integrating stage in the forward path and a nonlinearity preceding the integrator.

```
$$$CONTINUOUS SYSTEM MODELING PROGRAM  III

       PARAM A = 20.0
       PARAM B = 0.2

       PLS = 2.718 * TIME / EXP(TIME)

       EL = PLS - VL
       AEL = EL * A
       DVL = REALPL(0, B, AEL)
       VL = INTGRL(0, DVL)

       PN1 = EL**2
       AEN1 = BAEN + PN1
       DVN1 = REALPL (0, B, AEN1)
       VN1 = INTGRL(0,DVN1)
       BAEN = (-VN1) * A

       PN2 = (VL**2) / 20.0
       VN2 = BVN + PN2
       AEN2 = (-VN2) * A
       DVN2 = REALPL (0, B, AEN2)
       BVN = INTGRL(0,DVN2)

  TIMER FINTIM = 1.5, OUTDEL = 0.03
  PRTPLT VN1 (VL)
  PRTPLT VN2 (VL)

  END
  STOP
```

Figure A5.3. Computer program which produced the nonlinearity output shown in Figure 7.8 (page 141). This system is the same as the system which produced the nonlinearity response shown in Figure 7.7 (page 136) except for a second high-frequency pole which reduced the phase margin to 28 degrees.

VITA

Bruce W. McNeill was born and reared in Oak Ridge, Tennessee. He is a graduate of Oak Ridge High School, and has received a Bachelor of Science degree and a Master of Engineering degree in Electrical Engineering from the University of Tennessee at Knoxville.